



MÁSTER EN INGENIERÍA INDUSTRIAL

TRABAJO FIN DE MÁSTER

Experimental analysis and modeling of magnetic
pumping for magnetic refrigeration applications

Autor: Ana de Cuadra Rabaneda

Director: Keerthivasan Rajamani

Madrid

Declaro, bajo mi responsabilidad, que el Proyecto presentado con el título
“Experimental analysis and modeling of magnetic pumping for magnetic refrigeration applications”

en la ETS de Ingeniería - ICAI de la Universidad Pontificia Comillas en el
curso académico 2019/20 es de mi autoría, original e inédito y

no ha sido presentado con anterioridad a otros efectos.

El Proyecto no es plagio de otro, ni total ni parcialmente y la información que ha sido
tomada de otros documentos está debidamente referenciada.

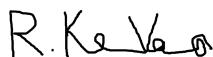


Fdo.: Ana de Cuadra Rabaneda

Fecha: ..23../ ..09../ ..202..
0

Autorizada la entrega del proyecto

EL DIRECTOR DEL PROYECTO



Fdo.: Keerthivasan Rajamani

Fecha: ..23../ ..09../ ..20..

AUTORIZACIÓN PARA LA DIGITALIZACIÓN, DEPÓSITO Y DIVULGACIÓN EN RED DE PROYECTOS FIN DE GRADO, FIN DE MÁSTER, TESIS O MEMORIAS DE BACHILLERATO

1º. Declaración de la autoría y acreditación de la misma.

El autor D. Ana de Cuadra Rabaneda

DECLARA ser el titular de los derechos de propiedad intelectual de la obra: “*Experimental analysis and modeling of magnetic pumping for magnetic refrigeration applications*”, que ésta es una obra original, y que ostenta la condición de autor en el sentido que otorga la Ley de Propiedad Intelectual.

2º. Objeto y fines de la cesión.

Con el fin de dar la máxima difusión a la obra citada a través del Repositorio institucional de la Universidad, el autor **CEDE** a la Universidad Pontificia Comillas, de forma gratuita y no exclusiva, por el máximo plazo legal y con ámbito universal, los derechos de digitalización, de archivo, de reproducción, de distribución y de comunicación pública, incluido el derecho de puesta a disposición electrónica, tal y como se describen en la Ley de Propiedad Intelectual. El derecho de transformación se cede a los únicos efectos de lo dispuesto en la letra a) del apartado siguiente.

3º. Condiciones de la cesión y acceso

Sin perjuicio de la titularidad de la obra, que sigue correspondiendo a su autor, la cesión de derechos contemplada en esta licencia habilita para:

- a) Transformarla con el fin de adaptarla a cualquier tecnología que permita incorporarla a internet y hacerla accesible; incorporar metadatos para realizar el registro de la obra e incorporar “marcas de agua” o cualquier otro sistema de seguridad o de protección.
- b) Reproducir la en un soporte digital para su incorporación a una base de datos electrónica, incluyendo el derecho de reproducir y almacenar la obra en servidores, a los efectos de garantizar su seguridad, conservación y preservar el formato.
- c) Comunicarla, por defecto, a través de un archivo institucional abierto, accesible de modo libre y gratuito a través de internet.
- d) Cualquier otra forma de acceso (restringido, embargado, cerrado) deberá solicitarse expresamente y obedecer a causas justificadas.
- e) Asignar por defecto a estos trabajos una licencia Creative Commons.
- f) Asignar por defecto a estos trabajos un HANDLE (URL *persistente*).

4º. Derechos del autor.

El autor, en tanto que titular de una obra tiene derecho a:

- a) Que la Universidad identifique claramente su nombre como autor de la misma
- b) Comunicar y dar publicidad a la obra en la versión que ceda y en otras posteriores a través de cualquier medio.
- c) Solicitar la retirada de la obra del repositorio por causa justificada.
- d) Recibir notificación fehaciente de cualquier reclamación que puedan formular terceras personas en relación con la obra y, en particular, de reclamaciones relativas a los derechos de propiedad intelectual sobre ella.

5º. Deberes del autor.

El autor se compromete a:

- a) Garantizar que el compromiso que adquiere mediante el presente escrito no infringe ningún derecho de terceros, ya sean de propiedad industrial, intelectual o cualquier otro.
- b) Garantizar que el contenido de las obras no atenta contra los derechos al honor, a la intimidad y a la imagen de terceros.
- c) Asumir toda reclamación o responsabilidad, incluyendo las indemnizaciones por daños, que pudieran ejercitarse contra la Universidad por terceros que vieran infringidos sus derechos e intereses a causa de la cesión.
- d) Asumir la responsabilidad en el caso de que las instituciones fueran condenadas por infracción

de derechos derivada de las obras objeto de la cesión.

6º. Fines y funcionamiento del Repositorio Institucional.

La obra se pondrá a disposición de los usuarios para que hagan de ella un uso justo y respetuoso con los derechos del autor, según lo permitido por la legislación aplicable, y con fines de estudio, investigación, o cualquier otro fin lícito. Con dicha finalidad, la Universidad asume los siguientes deberes y se reserva las siguientes facultades:

- La Universidad informará a los usuarios del archivo sobre los usos permitidos, y no garantiza ni asume responsabilidad alguna por otras formas en que los usuarios hagan un uso posterior de las obras no conforme con la legislación vigente. El uso posterior, más allá de la copia privada, requerirá que se cite la fuente y se reconozca la autoría, que no se obtenga beneficio comercial, y que no se realicen obras derivadas.
- La Universidad no revisará el contenido de las obras, que en todo caso permanecerá bajo la responsabilidad exclusiva del autor y no estará obligada a ejercitar acciones legales en nombre del autor en el supuesto de infracciones a derechos de propiedad intelectual derivados del depósito y archivo de las obras. El autor renuncia a cualquier reclamación frente a la Universidad por las formas no ajustadas a la legislación vigente en que los usuarios hagan uso de las obras.
- La Universidad adoptará las medidas necesarias para la preservación de la obra en un futuro.
- La Universidad se reserva la facultad de retirar la obra, previa notificación al autor, en supuestos suficientemente justificados, o en caso de reclamaciones de terceros.

Madrid, a 24 de septiembre de 2020

ACEPTA



Fdo: Ana de Cuadra Rabaneda

Motivos para solicitar el acceso restringido, cerrado o embargado del trabajo en el Repositorio Institucional:



MÁSTER EN INGENIERÍA INDUSTRIAL

TRABAJO FIN DE MÁSTER

Experimental analysis and modeling of magnetic
pumping for magnetic refrigeration applications

Autor: Ana de Cuadra Rabaneda

Director: Keerthivasan Rajamani

Madrid

ANÁLISIS EXPERIMENTAL Y MODELADO DE UNA BOMBA MAGNÉTICA PARA APLICACIONES DE REFRIGERACIÓN MAGNÉTICA

Autor: de Cuadra Rabaneda, Ana.

Supervisor: Rajamani, Keerthivasan.

Entidad colaboradora: ICAI – Universidad Pontificia Comillas

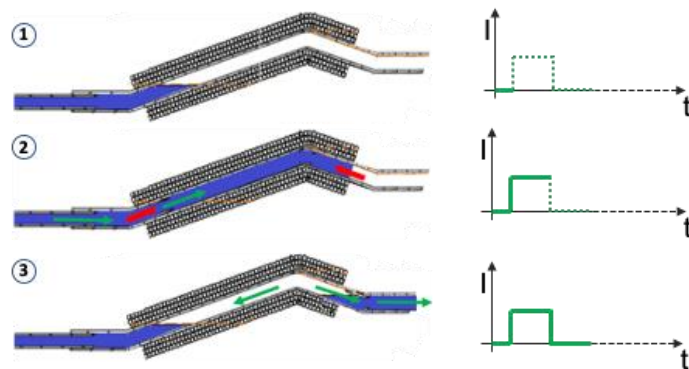
RESUMEN

Durante las últimas décadas se ha estado fomentado la investigación y desarrollo de tecnologías no contaminantes para combatir el avance del cambio climático. La refrigeración magnética a temperatura ambiente es un ejemplo, tratándose de una tecnología innovadora y segura para el medio ambiente. Se espera que, aun estando en fase de investigación y desarrollo, tenga el potencial para competir en el sector de la refrigeración. Su principal beneficio radica en el hecho de que, a diferencia de los sistemas convencionales de compresión de vapor, la refrigeración magnética cumple plenamente con la política internacional actual de limitación de gases de efecto invernadero ya que, al trabajar con materiales magnéticos, la posibilidad de fugas de gas o emisiones de CO₂ queda eliminada.

El principio de esta tecnología se basa en un fenómeno llamado efecto magnetocalórico. Se trata de una propiedad intrínseca de los materiales magnéticos que los hace capaces de calentarse y enfriarse en presencia de un campo magnético variable. Dicho fenómeno se explota integrando los procesos de magnetización y desmagnetización en un ciclo magnético – y por tanto térmico. No obstante, el poder de enfriamiento de la refrigeración magnética está limitado por el hecho de que las diferencias de temperatura que alcanza en el rango de la temperatura ambiente son relativamente pequeñas. Por esta razón, los refrigeradores magnéticos se basan en el ciclo de Regeneración Magnética Activa (RMA), en el que el material magnetocalórico funciona tanto como refrigerante como regenerador. De esta manera, el efecto magnetocalórico del material de trabajo se amplifica optimizando la capacidad de transferencia de calor, lo que convierte al sistema en apto para aplicaciones comerciales.

El siguiente trabajo forma parte del desarrollo de un innovador sistema de refrigeración magnética que se encuentra todavía en fase de investigación. El sistema trata de alcanzar

una mayor eficiencia, al menos desde el punto de vista del intercambio de calor. La novedad de este sistema se encuentra en el uso de nanofluidos magnéticos, que consiste en material magnético en forma de pequeñas partículas suspendidas en un fluido portador que circula por el sistema. De esta manera, no sólo el fluido trabaja como refrigerante y medio de refrigeración – RMA es el ciclo de referencia – sino también como vector de transferencia de calor. En particular, este proyecto se centra en la bomba magnética del sistema, que aprovecha las propiedades magnéticas del líquido magnético para impulsar el fluido mediante un campo magnético externo. La ausencia de componentes accionados mecánicamente le diferencia de otros sistemas, logrando una mayor fiabilidad y compacidad.



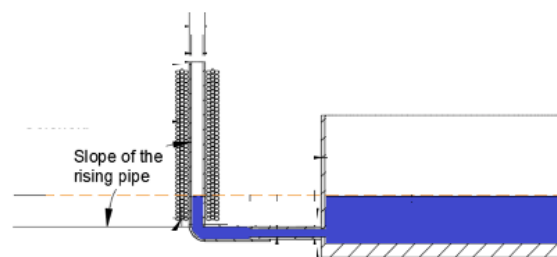
En la figura anterior se describe el diseño y funcionamiento de la futura bomba del sistema. Su configuración consiste en el conducto por el que circula el fluido magnético, una bobina enrollada a su alrededor y un sistema de alimentación de corriente continua que alimenta a la bobina con una señal cuadrada tal como se muestra en la figura. El fluido se encuentra inicialmente en la entrada de la bomba (1). Cuando la corriente se activa (2), se induce un campo magnético que atrae al fluido hacia el interior de la bobina, reteniéndolo, de manera que la región del solenoide se llena completamente. Las flechas rojas representan las fuerzas magnéticas de atracción responsables de este fenómeno, las cuales solo están presentes en los extremos – ya que dependen del gradiente magnético. Cuando la corriente se apaga de nuevo (3), las fuerzas de atracción desaparecen y el fluido sale hacia la salida por gravedad, lo que es posible gracias a la configuración de la bomba.

Distintos estudios y experimentos han demostrado que el bombeo magnético realizado de esta manera es posible. El nanofluido con el que se trabaja – tanto en los experimentos de

este proyecto como en anteriores – es el ferrofluido comercial *Ferrotec EFH1*, que a pesar de no tener un efecto magnetocalórico lo suficientemente fuerte a temperatura ambiente como para enfriar, resulta adecuado para el bombeo magnético en sí. Así pues, el presente trabajo parte de esos experimentos y resultados con el objetivo de seguir desarrollando el modelo de la bomba magnética del futuro sistema de refrigeración.

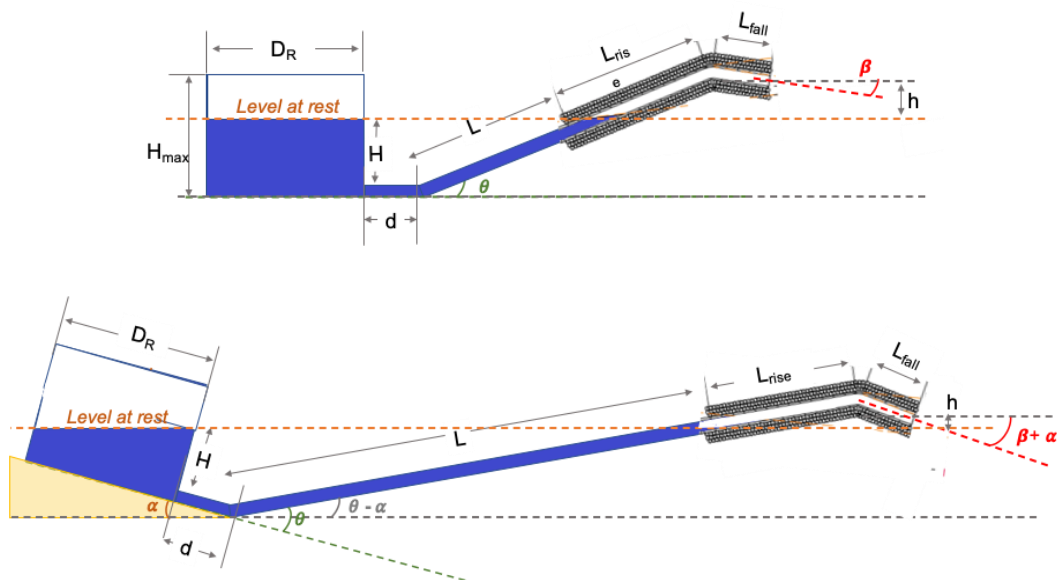
El Proyecto está estructurado en diferentes partes. Primero, se introduce y explica la tecnología de refrigeración magnética y el sistema de refrigeración en desarrollo. La siguiente sección introduce la bomba magnética y proporciona una visión general de los diferentes experimentos realizados hasta el momento. Tras una introducción a los procesos físicos que ocurren en el bombeo magnético, se pasa a explicar el estudio experimental.

Primero, se analiza el proceso en el que el fluido asciende por el conducto llenando la bomba, realizando distintos experimentos que tienen como objetivo final optimizar ciertos parámetros de la bomba. El nivel al cual el fluido está en reposo inicialmente es la variable protagonista en el estudio, ya que está directamente relacionado con la física del proceso y el tiempo de llenado. La fuerza magnética que aparece en la región del extremo inferior del solenoide es proporcional a la cantidad de fluido presente en su interior, por lo tanto, se obtienen respuestas más rápidas ante las entradas de corriente cuando el nivel del fluido es superior. La pendiente del conducto es otro factor importante. El uso de un tubo de plástico flexible permite realizar los experimentos para diferentes inclinaciones, y así determinar la configuración óptima. La teoría apunta a que la pendiente no afecta al aumento de altura – medida en dirección vertical – que es alcanzado por el fluido. Esto se debe a que la fuerza magnética que atrae y tira del fluido apunta siempre en dirección axial.



La corriente que se suministra a la bobina es también otra variable, tanto en la forma – que es un escalón en la mayoría de los experimentos – como en magnitud – que varía en un rango de [0 , 6] A. El cable que se usa para construir la bobina es también una opción de diseño. Se usan dos solenoides distintos que, al tener la misma longitud y número de capas, solo difieren en el número de vueltas por el uso de diferentes tamaños de cable. Por último está la temperatura, que es un factor que, sin ser punto de interés inicialmente, acaba cobrando un papel muy importante en los experimentos. Partiendo como base de la teoría y el estudio teórico realizado en la tesis de otro estudiante [13], el proceso que tiene lugar se modela en Matlab para proporcionar los datos teóricos sobre el comportamiento del fluido para unos ciertos parámetros. Dichos resultados son comparados con los resultados experimentales.

La segunda parte de la investigación se centra en la bomba. Sólo el diseño de su configuración y una estrategia propuesta para seguir en futuros experimentos, los cuales no pudieron realizarse por causas ajenas, son incluidos en este trabajo. La siguiente imagen muestra el esquema de la bomba en función de todos los parámetros.



El montaje de la bomba es prácticamente el mismo que los esquemas mostrados anteriormente, pero con un tubo rígido en vez de flexible, tal que el ángulo de inclinación no pueda ser variado manualmente. Para variarlo, se usa una cuña de alturas regulables,

por lo que ambas pendientes del “tubo de subida” y “tubo de bajada” se cambian simultáneamente. El resto de los elementos también pueden ser modificados, como la longitud de cada parte del solenoide con tan solo deslizarlo por el tubo o el nivel del fluido. Por último, el proyecto finaliza con las conclusiones extraídas del trabajo, además de un apartado que incluye la alineación de los objetivos de este proyecto con los de desarrollo sostenible de Naciones Unidas.

EXPERIMENTAL ANALYSIS AND MODELING OF MAGNETIC PUMPING FOR MAGNETIC REFRIGERATION APPLICATIONS

Author: de Cuadra Rabaneda, Ana.

Supervisor: Rajamani, Keerthivasan.

Collaborating Entity: ICAI – Universidad Pontificia Comillas

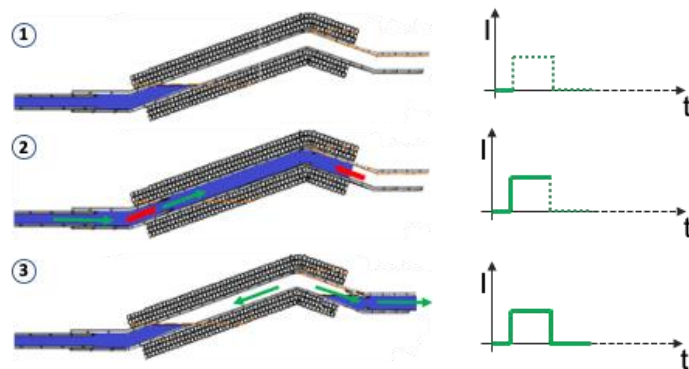
ABSTRACT

The research and development of non-polluting technologies has been encouraged during the last decades in order to fight global warming and ozone depletion. Magnetic refrigeration at room temperature is one such emerging, innovative and environment-safe technology. Still under research and development, it is expected to have the potential to compete in the heating and cooling sector in the near future. The most important benefit lies in the fact that, contrary to conventional Vapour Compression (VC) systems, magnetic refrigeration fully complies with the actual international policies of limiting the greenhouse gases emission. As it works with magnetic materials as refrigerant, there is no possibility of gas leakages or CO₂ emissions.

The working principle of this technology is based on a phenomenon called Magneto-Caloric Effect (MCE). It is an intrinsic property of magnetic materials, which makes them capable of heating and cooling when exposed to a varying magnetic field. The phenomenon is exploited by integrating these magnetization and demagnetization processes in a magnetic –and thus thermal– cycle. However, the cooling power of magnetic refrigeration is limited by the fact that the temperature differences reached in the range of room temperature are relatively small. For that reason, magnetic refrigerators are based on the active regenerator (AMR) cycle, in which the magneto-caloric material works both as refrigerant and as regenerator. This way, the magneto-caloric effect of the working material is amplified by optimizing the heat transfer capacity, making the system suitable for commercial applications.

This work contributes to the development of an innovative magnetic refrigeration system, still at a research stage, which aims to achieve a greater efficiency at least from the heat exchange point of view. The novelty of this technology relies on the use of magnetic nanofluids, which is a magneto-caloric material in the form of small particles suspended in

a carrier fluid circulating through the system. This way, not only the working fluid acts as refrigerant and regenerative medium –AMR is the reference cycle, but also as the heat transfer vector. In particular, this thesis focuses on the magnetic pump of the system, which exploits the magnetic properties of nanofluids to drive the fluid by the action of an external magnetic field. The absence of mechanically actuated components, in contrast with other systems, aims to achieve a more reliable and compact system.



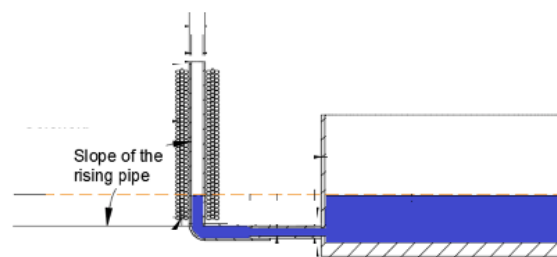
The figure above describes the design and performance of the future pump. The configuration comprises the duct containing the fluid, a coil wound around it and a DC power supply system which drives a square current input through the coil. The magnetic fluid rests initially at the inlet of the pump (1). When the current is ON (2), a magnetic field is induced in the tube, attracting the fluid inwards the coil and holding it inside, so that the solenoid region is completely filled. Red arrows represent the magnetic attractive forces responsible of the phenomenon, which are only present on the fluid present in the extremes (since they depend on the gradient of the magnetic field). When the current is OFF again (3), the attractive forces disappear and the fluid comes out through the outlet of the pump by gravity, which is possible thanks to the configuration of the tube.

Different studies and experiments have proven that the magnetic pumping is feasible. The nanofluid employed –also in this work– was the commercial ferrofluid *Ferrotec EFH1*, which despite not having a MCE strong enough at room temperature to produce a cooling effect, it proven to be suitable for magnetic pumping. Thus, the present work starts from those

experiments and results, aiming at the further development of the magnetic pump in the novel refrigeration system.

The thesis is structured in different parts. First, magnetic refrigeration technology and the proposed novel system are introduced and explained. The next part presents the magnetic pump element of the system and provides a literature overview of the different experiments performed so far. Then, after introducing the physics of magnetic pumping, the experimental study is explained.

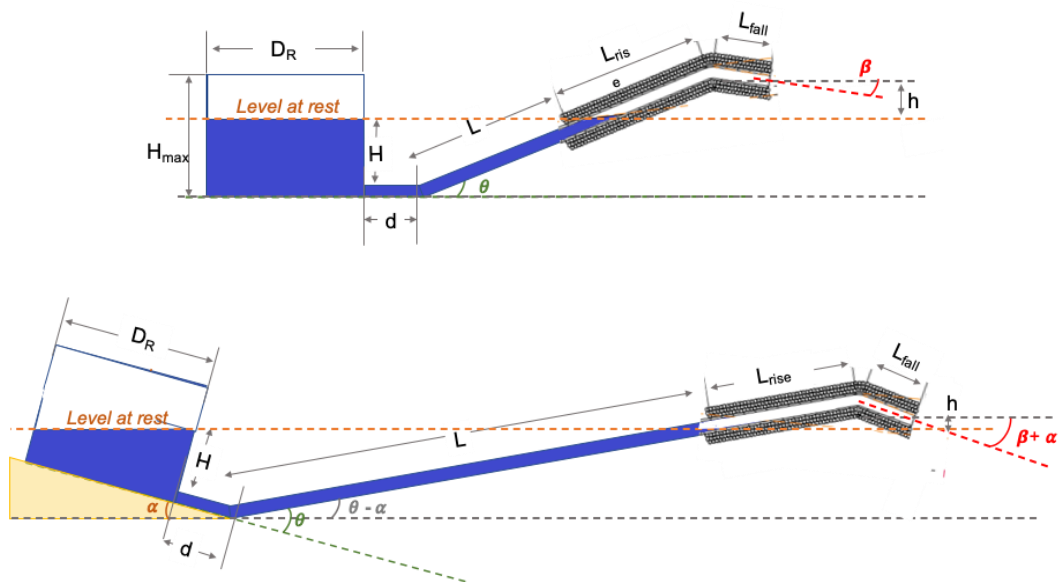
First, the rising process through which the magnetic pump is filled is analysed making use of the set-up represented in the figure below. The experiments conducted in this part are driven by different research questions and aim to optimize the parameters of the performance of the pump. The initial level of the fluid is initially is the factor on which more emphasis has been placed, as it is directly related to the physics of the process and the filling time. The magnetic force developed at the lower edge region of the coil is proportional to the amount of fluid present in such region. Hence, a faster response to the current input is obtained when the fluid starts at a higher level inside the solenoid. The slope of the pipe is another important factor analysed. The use of a flexible PVC pipe allows to test the performance for different inclinations, and thus to determine the optimal configuration. Theory suggests that the slope does not affect the height increase – measured in vertical direction – reached by the fluid in the pipe. This is because the magnetic force that pulls the liquid upwards is always pointing in axial direction.



The current supplied to the coil is also a variable, both the form – which is a single step in most of the experiments to simulate the square signal used for the pump – and the magnitude – which is varied within a range of [2 , 6] A. The wire of the coil is also a design option, which results in the use of two solenoids that only differ in the number of turns. Lastly, the temperature is another factor that, without being a point of interest at first, ends

up playing an important role. Based on the physics and the theoretical study conducted in another student Thesis [13], the process is modelled in *Matlab* to provide the theoretical results and compare them with the experiments. Such model explains the main characteristics of the behaviour of the fluid inside the pipe.

The second part of the research focuses on the pump. Only the design of the configuration and a proposed strategy to carry out the experiments is included. The experiments could not be completed because of external reasons. The first picture shows the set-up of the pump and the second, the scheme with all the parameters included.



The experimental set-up of the pump is practically the same as the schemes shown but with a rigid plastic pipe, so that the slopes cannot be changed manually. For that, a wedge with regular heights like the one represented in the last figure is placed below the reservoir, so that both the slope of the rising and falling pipe are changed simultaneously. The rest of the parameters may also be changed, like moving the solenoid along the pipes or modifying the level of the fluid in the reservoir. Lastly, the work ends with the conclusions extracted from the project, plus a section including the alignment of the project with the seventh goal of the United Nations: to ensure environmental sustainability.

Index

CHAPTER 1. INTRODUCTION	9
1.1 MCE AND MR CYCLES.....	11
1.2 PROJECT DEFINITION: THE MAGNETIC PUMP.....	17
CHAPTER 2. CURRENT STATE OF TECHNOLOGY	21
CHAPTER 3. THE PHYSICS OF FHD PUMP	27
3.1. THE MAGNETIC FIELD OF A COIL	27
3.1.1 Magnetic field on z axis.....	28
3.1.2 Magnetic field off z axis.....	29
3.2. THE KELVIN BODY FORCE	30
3.3. THE FLUID DYNAMICS.....	32
CHAPTER 4. THE EXPERIMENTAL SET-UP AND TECHNOLOGY USED	38
CHAPTER 5. THE RISING PROCESS.....	42
CHAPTER 6. INFLUENCE OF THE POSITION OF THE SOLENOID WITH RESPECT TO THE FLUID AT REST ...	44
<i>Analysis of the Kelvin force region</i>	<i>45</i>
▪ The level of the fluid is below the region.....	46
▪ The level of the fluid lies within the region.....	46
▪ The level of the fluid is at/beyond the end of the region	47
6.1 ANALYSIS OF DYNAMICS	51
6.2 INFLUENCE OF THE POSITION OF THE SOLENOID WITH RESPECT TO THE LEVEL OF THE FLUID AT REST	59
CHAPTER 7. INFLUENCE OF THE INCLINATION OF THE PIPE	65
CHAPTER 8. INFLUENCE OF THE TEMPERATURE	70
CHAPTER 9. INFLUENCE OF THE INPUT-CURRENT SHAPE	75
CHAPTER 10. SENSITIVITY ANALYSIS.....	79
9.1 DIAMETER OF WIRE	79
9.1 LENGTH OF THE COIL.....	81

CHAPTER 11. THE MAGNETIC PUMP SET-UP	84
CHAPTER 12. CONCLUSIONS	88
CHAPTER 13. MAGNETIC REFRIGERATION AND SUSTAINABLE DEVELOPMENT	90

Index of figures

Figure 1. Magnetic Carnot cycle [10].....	12
Figure 2. Comparison between magnetic and conventional Brayton cycle [3].....	14
Figure 3. Step 1 [3].....	15
Figure 4: Step 2 [3].....	15
Figure 5: Step 3 [3].....	15
Figure 6: Step 4 [3].....	16
Figure 7: Current OFF.....	18
Figure 8: Current ON.....	18
Figure 9: Current OFF.....	18
Figure 10: Example of ferrofluidic plugs manipulation [16].	21
Figure 11: Micropump developed in [17].....	22
Figure 12: Microfluidic pump developed in [18]	23
Figure 13: Experimental set-up and working principle from [14].....	23
Figure 14: Experimental set-up and working principle from [15].....	25
Figure 15: Magnetic field created by a coil.....	28
Figure 16: Magnetization curve of EFH1 [12]	31
Figure 17: Representation of a certain moment during transient state	33
Figure 18: a) The fluid is initially at rest. b) The fluid is rising and gravity (yellow arrow) acts on the column of ferrofluid	34
Figure 19: Solenoid of 150 mm of length, 3 mm of radius and 2 mm of wire diameter. Solenoid centered at $z = 0$ m with the bottom at $z = -0,05$ m. $I = 20$ A	35
Figure 20: Body force acting on the fluid when the level is within the region	36
Figure 21: Body force acting on the fluid when the level is above the region	36
Figure 22: Set-up of the pump developed in [12].....	38

Figure 23: Set-up used in the experiments conducted on the rising process	39
Figure 24: Scheme of the measuring system set-up	40
Figure 25: Performance of the pump	42
Figure 26: Position of the solenoid respect to the fluid at rest	44
Figure 27: The level of the fluid is below the Kelvin force region	46
Figure 28: The level of the fluid is within the Kelvin force region	47
Figure 29: The level of the fluid is above the Kelvin force region	48
Figure 30: Scheme of the experiment conducted	50
Figure 31: calculated Kelvin force region for the range of currents	51
Figure 32: Comparison between $z = 8$ mm and $z = -4$ mm of distance to the bottom of the solenoid.....	52
Figure 33: Height increase in the pipe when the level of the fluid at rest is at $z = -12$ mm	54
Figure 34: Height increase in the pipe when the level of the fluid at rest is at $z = -8$ mm..	54
Figure 35: Height increase in the pipe when the solenoid is supplied with 2 A	55
Figure 36: Height increase in the pipe when the solenoid is supplied with 6 A	56
Figure 37: Height increase in the pipe when the solenoid is supplied with 3 A	57
Figure 38: Height increase in the pipe when the solenoid is supplied with 3 A	57
Figure 39: Height increase in the pipe when the solenoid is supplied with 4 A	58
Figure 40: Steady state value for each experiment (each initial starting level) for the range of currents.....	59
Figure 41: Magnetic field measured on-axis	60
Figure 42: Comparison between the magnetic field measured and the theoretical magnetic field.....	61
Figure 43: Scheme of the experiment conducted	62
Figure 44: Final height increase in the pipe when the level of the fluid at rest is at different points for the whole range of currents	63
Figure 45: Theoretical evolution of the steady state for the range of currents	64
Figure 46: Comparison between vertical and inclined pipe	65
Figure 47: Final height increase reached in the pump for different initial levels and for the whole range of currents	67

Figure 48: Final height increase reached in the pump for different initial levels and for the whole range of currents	67
Figure 49: Distribution of the fluid in both configurations	68
Figure 50: Height increase in the pipe for different initial levels. Comparison between the minimum and maximum value of current within the range. Solenoid of 0,8 mm of wire diameter.	70
Figure 51: Schematic set-up of the experiment	71
Figure 52: Height increase in the pipe, Voltage and current supplied to the coil. $I = 5 \text{ A}$..	72
Figure 53: Temperature dependency of magnetic susceptibility [22]. It should be noted that only the ferromagnetic region is of interest, as the Curie temperature is never exceeded (T_c).	73
Figure 54: Set-up of the experiment	75
Figure 55: a) Current input comparison. b) Height increase in the pipe comparison.....	76
Figure 56: a) Current input comparison. b) Height increase in the pipe comparison.....	77
Figure 57: Comparison of fluid behavior for a) 0.8 mm of wire diameter and b) 1 mm of wire diameter	80
Figure 58: Final height increase for a) Solenoid of 0.8 mm of wire diameter. b) Solenoid of 1 mm of wire diameter.....	81
Figure 59: Kelvin body force comparison for different coil lengths	82
Figure 60: Dynamic response comparison	83
Figure 61: Scheme of the experimental set-up of the pump.....	84
Figure 62: Design of the experiments.....	86
Figure 63: Model TSX1820 [28]	94
Figure 64: PicoScope2205A [26]	95
Figure 65: Connection scheme of the teslameter.....	96
Figure 66: Working principle of the confocal sensor	97
Figure 67: Confocal sensor	97
Figure 68: Experiments conducted for selecting a sensor	100
Figure 69: Set-up with the pipe in vertical position. Solenoid 1 mm	101
Figure 70: Different initial levels of the fluid respect to the solenoid.....	102

Figure 71: Set-up with the pipe in vertical position. Solenoid 0.8 mm.....	102
Figure 72: Set-up with the pipe in inclined position. Solenoid 0.8 mm	103
Figure 73: Initial levels of ferrofluid. Pipe in inclined position. Solenoid 0.8 mm.....	104
Figure 74: Wounding process of the solenoids	105
Figure 75: Solenoid 1 mm. 6 layers. 15 cm.....	106
Figure 76: Solenoid 0.8 mm. 6 layers. 15 cm.....	106
Figure 77: Solenoid 2 mm. 3 layers. 15 cm.....	107
Figure 78: Measuring set-up.....	108
Figure 79: Height increase in the pipe for $I = 2$ A.....	109
Figure 80: Height increase in the pipe for $I = 3$ A.....	110
Figure 81: : Height increase in the pipe for $I = 4$ A.....	110
Figure 82: : Height increase in the pipe for $I = 5$ A.....	111
Figure 83: : Height increase in the pipe for $I = 6$ A.....	111
Figure 84: Experiment conducted in Chapter 9. Current input at intervals. The experiment is repeated twice in terms of repeatability	112
Figure 85: Experiment conducted in Chapter 9. Current input at continuous input. The experiment is repeated twice in terms of repeatability	112
Figure 86: Height increase in the pipe for $I = 2$ A. a) Pipe in 90° b) Pipe in 37°	113
Figure 87: Height increase in the pipe for $I = 3$ A. a) Pipe in 90° b) Pipe in 37°	113
Figure 88: Height increase in the pipe for $I = 4$ A. a) Pipe in 90° . b) Pipe in 37°	114
Figure 89: Height increase in the pipe for $I = 5$ A. a) Pipe in 90° . b) Pipe in 37°	114
Figure 90: Height increase in the pipe for $I = 6$ A. a) Pipe in 90° . b) Pipe in 37°	115
Figure 91: Measured magnetic field on- axis. Solenoid 1 mm.....	116
Figure 92: Measured magnetic field on- axis. Solenoid 0.8 mm.....	117
Figure 93: Measured magnetic field on- axis. Solenoid 2 mm.....	117
Figure 94: Expression for $E(k)$ by polynomial approximation.....	123
Figure 95: Expression for $K(k)$ by polynomial approximation	123

Tabla 1. Tabla de datos 5

Chapter 1. Introduction

Global climate change is one of the most important threats that humanity has ever confronted and the world seems to have finally taken it seriously. Over the last years, governments and international organizations have been taking actions to meet the challenge and curb the alarming situation.

One relevant example is the adoption of measures to reduce the emission of ozone-depleting substances to the atmosphere. The Montreal Protocol, signed in 1987, has been the most important agreement in this regard. The statement imposes the limit of the use of chlorofluorocarbons (CFC), a chemical substance that has been traditionally used as refrigerant of cooling systems, and that has proven to be one of the causes of the ozone-depletion. In this context, scientist and engineers have been encouraged to develop non-polluting technologies. There are many studies and applications that have been aimed to improve the traditional systems as well, for example, by replacing the polluting refrigerants with natural and environmentally friendly ones [9]. However, traditional technology –as Vapour Compression (VC)– is still very inefficient and has limited room for further improvements.

Magnetic refrigeration at room temperature is an innovative and promising technology that emerges as an environment-safe alternative to conventional systems. Still under development, it shows a real potential to compete in the heating and cooling sector in the coming years. The greatest benefit of this technology lies in the fact that there is no possibility of gas leakages or greenhouse gases emissions, as it works with magnetic materials as refrigerants. There is no combustion or chemical reactions either, only the action of magnetic fields. In addition, magnetic refrigeration technology overcomes some current technical constraints. For example, the elimination of the compressor allows more

reliable and efficient designs, as it is the most power-consuming and inefficient element of conventional systems.

The working principle of magnetic refrigeration is based on the so-called Magneto-Caloric Effect (MCE), an intrinsic property of magnetic materials that makes them capable of absorbing and emitting heat when exposed to an external magnetic field. The awareness of this phenomenon dates back to more than 100 years ago and has been attributed to different authors [11]. However, it was not until 1917 that the physicist Weiss and his collaborator Piccard discovered it experimentally, identifying the thermodynamic relation between the temperature change in the sample – of nickel – and the magnetic field applied. The discovery led to the first application of MCE to arise, consisting of a magnetic refrigeration cycle capable of reaching extremely low temperatures in the magnetic refrigerant, so that heat could effectively be picked up from the cooling load. Such applications are maturely used in cryogenics and gas liquefaction.

The feasibility of magnetic refrigeration operating at room temperature was later introduced by Brown in 1976. Since then, numerous studies and publications have explored further designs of suitable prototypes for commercial applications. The present work forms part of the development of an innovative system that, contrary to the prototypes developed so far, uses both refrigerant and heat-transfer vector together in a same working magnetic fluid. This way, a higher efficiency, at least from the heat transfer point of view, can be achieved. Moreover, the design of the system does not include mechanically actuated components, which improves reliability and reduces maintenance. Instead, the fluid is driven by the exclusive action of an external magnetic field generated in a magnetic pump. Within the novel refrigeration system, this work is centred on the magnetic pumping development. Preceding research and experiments successfully proved the feasibility of magnetic pumping and proposed a configuration design. The working nanofluid was

Ferrotec EFH1, a commercial ferrofluid suitable for pumping in small-scale experiments, although its MCE is not good enough for commercial heat-transfer processes.

In summary, this project contributes to the further development of magnetic pumping, defining the dynamics of the process through experimental results in order to obtain an optimized prototype of the pump of the system.

1.1 MCE AND MR CYCLES

The MCE can be defined as the thermal response that all magnetic materials present when exposed to a changing magnetic field. Such response is the result of internal entropy changes in the material. In general, the total entropy of a magnetic element is the sum of three terms: the lattice entropy caused by the vibrations of crystal lattice, electronic entropy of the material's free electrons and the magnetic entropy of the magnetization of the material [10].

$$S_T(T, H) = S_L(T) + S_E(T) + S_M(T, H)$$

When a ferromagnetic material is exposed to an external magnetic field, the magnetic dipoles of the atoms align in the field direction and reach a higher magnetic order, which reduces the magnetic entropy. The process is reversed when the magnetic field is removed. The magnetic moments of the atoms return to have a random orientation and the magnetic order decreases, thereby increasing the magnetic entropy. Depending on the conditions in which the magnetic field is applied and removed, MCE is manifested in two ways. When magnetization and demagnetization are undergone at a constant temperature, MCE is measured as the reversible change of entropy in the material, manifested as absorbed or emitted heat. Alternatively, if the process takes place under adiabatic conditions so that no energy is allowed to be transferred –the total entropy remains constant, the variation of

magnetic entropy is translated into a reversible change of temperature in the material caused by the entropy rebalance.

Both effects are exploited in magnetic refrigerators by integrating adiabatic (or isothermal) magnetization and demagnetization processes into different thermodynamic cycles. Carnot cycle can be considered as the reference, as it includes the two manifestations of MCE [10]. It consists of two adiabatic processes in which the magnetic refrigerant is magnetized and demagnetized to attain a temperature range (1-2 and 3-4 in Figure 1), and two isothermal processes in which the heat exchange is produced by the heat transfer fluid (2-3 and 4-1).

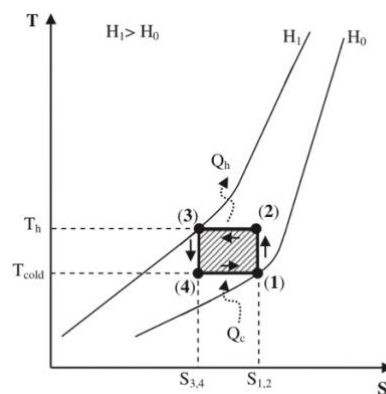


Figure 1. Magnetic Carnot cycle [10]

However, the applications based on this cycle are very limited by the temperature range achieved in the material through adiabatic MCE, which at room temperature is not large enough to be used directly for cooling. In fact, the search of magnetocaloric materials capable of producing a suitable cooling effect is one of the focus points of research in magnetic refrigeration.

This technical barrier is overcome with the integration of a regenerator in magnetic refrigeration systems, through which the effective MCE and thus the temperature span obtained are amplified. Here, magnetic Brayton and Ericsson cycles integrating regeneration are suitable for room temperature operation, consisting both of very similar processes that only differ in the way of producing MCE –isothermally in the case of Ericsson and adiabatically in Brayton cycle.

In particular, magnetic Brayton cycle is analogous to that of conventional systems. Figure 2 shows how both comprise the same stages but replacing the adiabatic compression and expansion of the gas with the material magnetization and demagnetization (step 1 and 3). The external magnetic intensity remains constant during steps 2 and 4, just as the corresponding isobaric stages of the gas Brayton cycle.

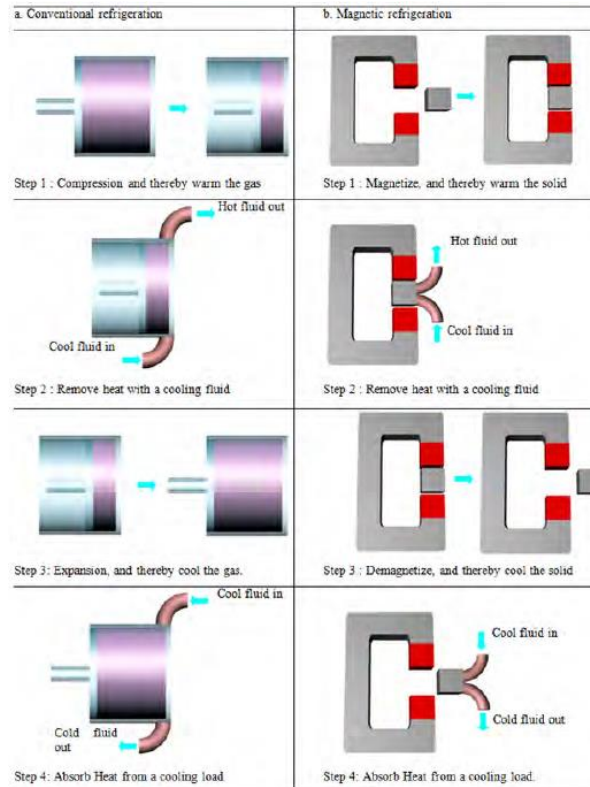


Figure 2. Comparison between magnetic and conventional Brayton cycle [3]

So far, most used technologies are based on the Active Magnetic Regenerative (AMR) cycle, which compared with the abovementioned ones, presents the best performance. The working principle of such cycle is the same as that of Brayton, since both produce MCE in adiabatic conditions and execute the heat transfer with the applied magnetic field remaining constant. The difference and main advantage that AMR presents lies in the use of the magnetic material both as refrigerant and regenerative medium, which is immersed into the heat transfer fluid flow so that each particle undergoes the thermodynamic cycle.

AMR cycle comprises four basic stages. In the first one the working material that is initially at room temperature is adiabatically magnetized and thus heated (Figure 3). In next step,

the heat transfer fluid is flown through the solid refrigerant –which is built in a porous body– from the cold to the hot source of the heat exchanger, absorbing the heat generated.

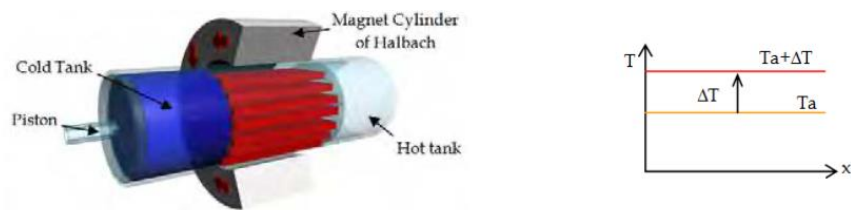


Figure 3: Step 1 [3]



Figure 4: Step 2 [3]



Figure 5: Step 3 [3]



Figure 6: Step 4 [3]

During this process, a temperature gradient is produced in the regenerator as a consequence of the contact between the immersed refrigerant and the fluid (Figure 4). In the third stage, the magnetic material is brought again to adiabatic conditions and the magnetic field is removed, which reduces the temperature in all the refrigerant particles by MCE (Figure 5). In the final step, the heat transfer fluid enters in the regenerator at the hot source temperature, flows through the material again and rejects the heat. The cycle is repeated until reaching the maximum temperature span – gradient – in the steady state (Figure 6), only limited by the hot and cold sources of the heat exchanger [3].

The refrigeration system presented in this project performs a Brayton cycle as well. However, the greatest benefit that makes it different from AMR lies in the use of the magnetocaloric material not only as refrigerant and regenerative medium, but also as the heat transfer fluid. This is achieved by the use of nanofluids, which are colloidal suspensions made out of magnetic nano-sized particles in a base fluid. The magnetocaloric material is thus presented in the form of nanoparticles suspended in a carrier fluid that carries out the transfer of the heat. The heat-transfer performance is improved because the refrigerant stays the whole time in contact with the transfer fluid. On the other hand, the elimination of a secondary fluid can avoid the use of mechanical devices in the system. This way, rather than creating the flow by means of pistons, the magnetic nanofluid can be dragged by magnetic attraction forces generated by a magnetic field in a magnetic pump – the focus point of this work.

1.2 PROJECT DEFINITION: THE MAGNETIC PUMP

The horizontal closed loop that forms the magnetic refrigeration system of this project requires external work to create the flow in the system. As mentioned, the nature of the magnetic refrigerant makes it possible to carry it out without the need for mechanical moving parts. Instead, a magnetic field external to the fluid acts on it to push it through the system, in a so-called magnetic pump. Depending on the nature of the magnetic field and fluid interaction, the magnetic pump may be (1): magnetohydrodynamic (MHD), or (2) ferrohydromagnetic (FHD). In the first group, Lorentz forces are developed between the external field and a magnetic fluid conducting electricity. In the second group, i.e. the FHD pumps, the interaction appears when the magnetic field varies over time and/or space, presenting a gradient. Then, the ferromagnetic nanoparticles of the fluid are attracted to the magnetic field and drag the carrier fluid with them. The phenomenon is called magnetophoresis. The magnetic pump of this project is of the FHD type. The magnetic field is created by a coil –subject to DC but intermittent current- wrapped around the duct carrying the magnetic fluid. This way, magnetic attractive forces are developed along the flow direction. The magnetic attraction force density receives the name of Kelvin force (or magnetophoretic force) [11], and can be expressed as [12]:

$$F_{Kelvin} = \mu_0 (\vec{M} \cdot \vec{\nabla}) \vec{H}$$

As shown in the equation, the Kelvin force is only developed when the fluid lies under the presence of an external magnetic field gradient, which will depend on the distribution and form of the magnetic field created by the coil. In the previous work [11], different models of the pump were built at small-scale and analysed before getting to the most efficient set-up. Both the final prototype and its working principle are shown in Figures 7, 8 and 9.

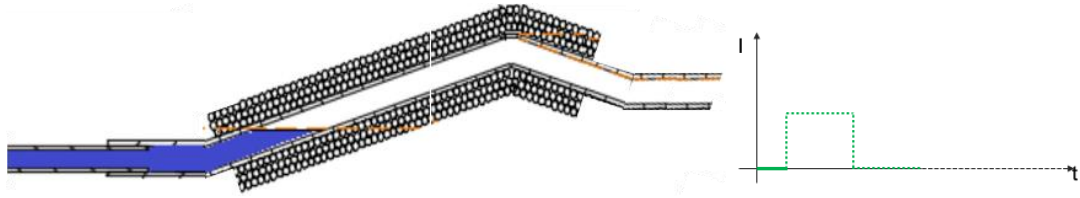


Figure 7: Current OFF

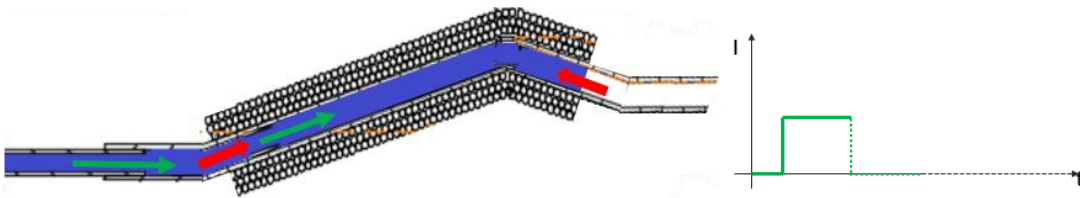


Figure 8: Current ON

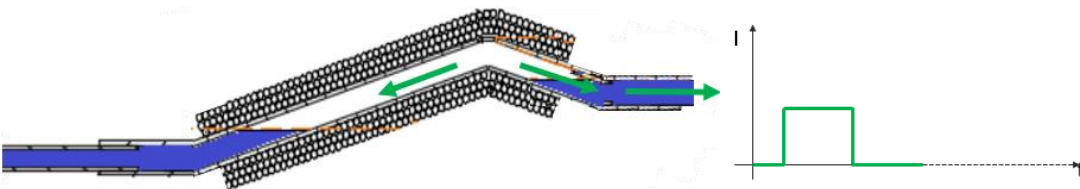


Figure 9: Current OFF

The pump is formed by a coil made of copper wire wound around a duct through which the fluid is driven. The duct –and therefore the solenoid– is bent in such a way that the ferrofluid enters the pump flowing upwards and leaves it flowing downwards. This is achieved by the following process.

The solenoid is supplied with DC current in the form of a square wave signal. During the intervals at which the current is ON, a magnetic field is induced on the axis of the solenoid. Considering the dimensions of the coil – which is long enough when compared to the radius

– the magnetic field can be assumed constant in the centre [12], while at the extremes it decreases abruptly to zero, and outside the solenoid the field is neglectable. This way, the gradient present at the ends of the coil attracts the fluid approaching such regions towards the centre of the solenoid. Figure 7 shows the initial state at which the current is OFF and the fluid at rest. When the current is ON (Figure 8), the magnetic field is induced and Kelvin forces –represented by red arrows– are developed at the bottom, pulling the fluid upwards. When the fluid reaches the end of the solenoid, Kelvin forces pointing in the opposite direction prevent the fluid from falling, holding the fluid inside the pipe. The current is then OFF and the attractive forces disappear, releasing the fluid by gravity (Figure 9). The process is repeated obtaining a discontinuous flow – represented by green arrows.

The performance of the pump depends on different parameters. Some of them are constructive, such as length and position of the solenoid respect to the bent part, section of the duct or inclination of the inlet and angle of the outlet duct; others are electrical, like the amplitude and frequency (of interruption) of the current supplied to the coil. The final objective is to determine the parameters that optimize the model of the pump to achieve the highest flow rate and thus the efficiency of the whole system.

The development of the magnetic pump towards its optimization is carried out by Jeroen in his Bachelor Thesis [12] through a theoretical model of the pump, which is focused on the physics behind the FHD pumping. In the present project, the study is carried out experimentally. This experimental work is described in chapters 5 and 6.

In chapters 6 to 9 the physics of the FHD pump are studied focusing on the rising process of the fluid. The section is oriented and driven by certain research questions previously stated. This way, the theory is taken into practice, in order to determine to what extent the expectations are met by the experimental results.

Chapter 10 moves forward to the magnetic pumping process itself. Here, starting with the optimal design of the pump that is proposed by the theoretical model, pumping is to be

tested with respect to different sets of parameters. Only the design of the experiments are included in this section, as unfortunately, they could not be finished.

The rest of the document is organized as follows. Chapter 2 is devoted to the State Of the Art review about FHD pumping. A brief theoretical basis is given in Chapter 3, in order to put this work in context. In Chapter 4, the experimental set-ups used for the experiments are introduced, together with the measuring system technology, which is one of the core topics of this project. Finally, different annexes at the end of the document provide additional details about the project, such as the data obtained in the experiments and the descriptions of the equipment.

Chapter 2. Current state of technology

Since their first appearance 60 years ago, ferrofluids have attracted a significant attention. Their magnetic composition allows them to be manipulated externally by magnetic actuators, such as permanent magnets and electromagnets. In addition to magnetism, ferrofluids possess unique properties such as biocompatibility – depending on the carrier fluid [19] – or the ability to transfer heat that make them suitable for different applications, as in the Medicine field.

Over the last years, the main focus of research has been the miniaturization of biochemical analysis systems, which typically use ferrofluidic micropumps. At milli- and micro-scales, the techniques of pumping a fluid present certain advantages over other methods. For example, the possibility to circulate a secondary non-magnetic fluid by making use of ferrofluids that is immiscible in them. This is normally achieved by the configuration of valves and plugs of ferrofluid that can only exist in very narrow channels, where capillarity and surface tension can be used to maintain cohesion. The circulation of the secondary fluid is produced when these ferrofluid plugs are dragged along the duct by an external field applied, acting as a piston.

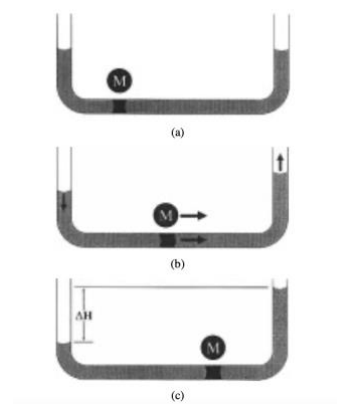


Figure 10: Example of ferrofluidic plugs manipulation [16].

Many of these micropumps make use of permanent magnets to manipulate the ferrofluid, as in [16]. Figure 10 shows the basic usage of this technique. Others, instead, employ electromagnets to induce space and/or time-varying magnetic fields to move the ferrofluid without mechanical moving parts, thus creating FHD pumps, on which this project focuses. There are many studies that have been carried out about FHD pumps, from which interesting novel systems have come out. In [17], for example, the ferrofluid is used in combination with a permanent magnet as a piston, and its movement is induced by an oscillating magnetic field created in the coil (Figure 11).

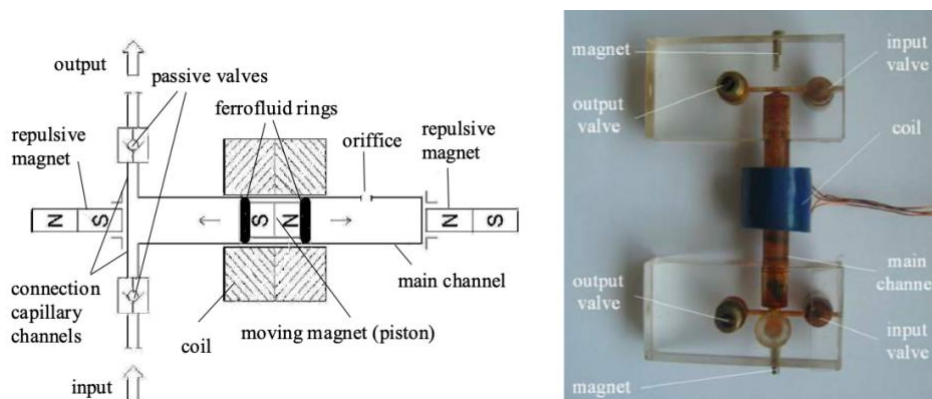


Figure 11: Micropump developed in [17]

A different strategy is applied in [18]. In this case, the ferrofluid is separated from the secondary fluid to be pumped – water in the experiment – by a thin rubber. The pump effect is performed by connecting different sets of coils in a certain sequence. The fluid exposed to the connected coils is attracted towards the magnetic field, deforming the rubber and creating the configuration represented in Figure 12.

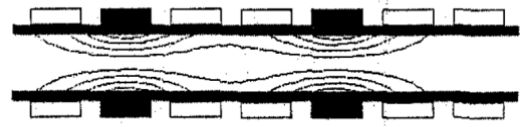
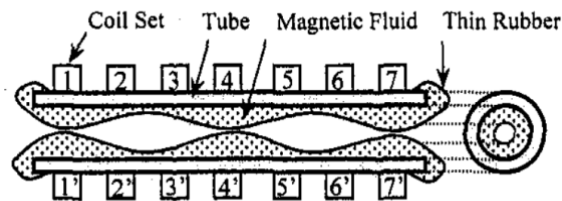


Fig. 4 Examples of the magnetic fluid shape

Figure 12: Microfluidic pump developed in [18]

So far, most of the examples given consist of experimental set-ups of pumps whose potential applications are limited to lab-on-a-chip devices, as they only work within the micron- or millimetre-scale channels. Thus, while they can serve as inspiration, they cannot be scaled to industrial applications such as the magnetic refrigeration system of this project.

Direct body – FHD – pumping of ferrofluids has been experimentally proven for the first time in [14]. This means that the techniques used to create the flow are not based on surface tension effects, and therefore they can be scaled to both microfluidic devices and industrial-scale applications.

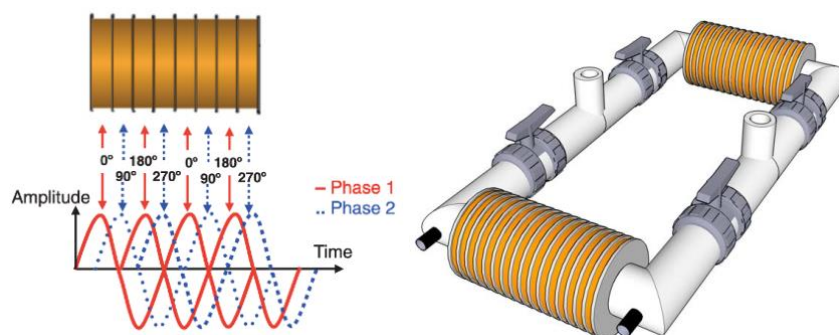


Figure 13: Experimental set-up and working principle from [14]

Figure 13 schematizes the experimental set-up used. The pump channel is configured as a closed loop made of PVC tubes of 15.4 mm of inner diameter and 2.8 mm of thickness. The external magnetic field directing the fluid consists of a space-traveling wave generated by the electromagnets – only one of the extremes shown in the figure is used – in a similar way to a motor stator. The coils are supplied with AC current in such a way that a full period of the travelling magnetic field is formed by four balanced phases with differences of phase of 90° among them (0° , 90° , 180° and 270° as the left of Figure 13 shows). For that, a total of 8 electromagnetic slots were used, each one formed by 70 turns of 7.9 mm copper-tape.

In [15] a different FHD pumping technique, also scalable – and therefore of interest – is presented. It is a novel magnetic-pumping system that creates a discontinuous and unidirectional flow by means of an electromagnet supplied with pulsating DC. The working principle is based on the variable reluctance concept. It studies the evolution or transient state of the magnetic flux density induced in the ferrofluid when it is magnetized by the external field. It is related with how the ferromagnetic nanoparticles are distributed in the fluid, whose concentration is increased as it approaches the electromagnet region. An increase in particle density results in a reduction of magnetic path reluctance. Thus, the highest concentration of particles corresponds to the minimal reluctance position, and this is the state to which the fluid will naturally tend.

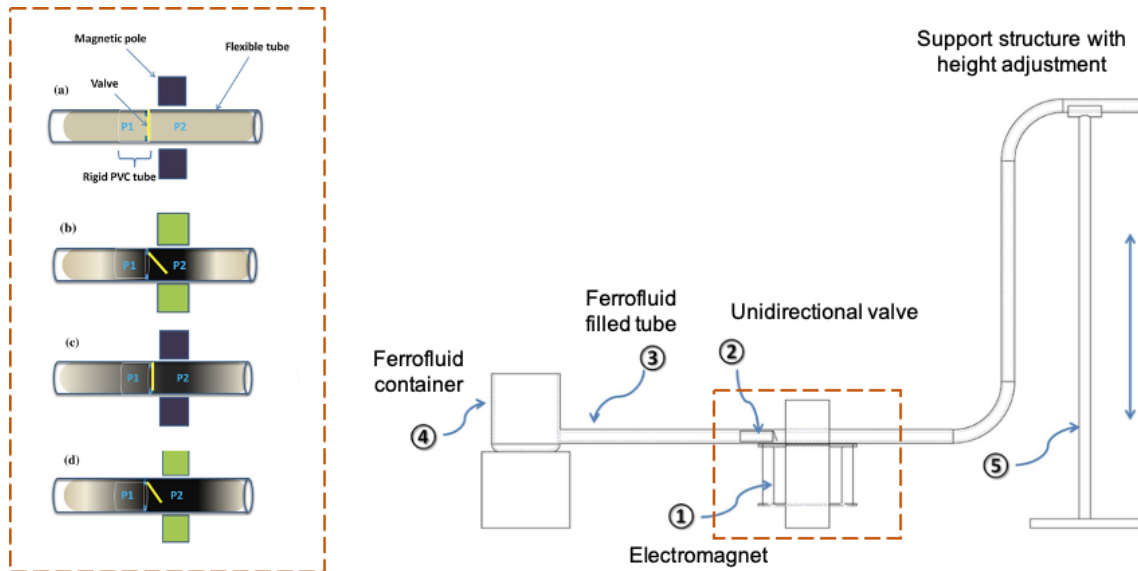


Figure 14: Experimental set-up and working principle from [15]

The working principle of the variable reluctance pump is represented in Figure 14 at the left, in the zoom of the electromagnet component. The electromagnet configuration consists of a coil wrapped around a rigid tube filled with ferrofluid. The unidirectional flow is obtained by the action of a valve incorporated in the tube, which is placed at the left – inlet – of the coil.

The first figure (a) shows the initial state of the pump, in which the current of the coil is switched OFF and the ferrofluid presents a homogeneous concentration. When the coil is switched to ON in (b), the magnetic nanoparticles from both sides of the valve are attracted to the coil in order to reduce the magnetic path reluctance. The axial pressure created from P1 towards P2 region as a result of the attractive forces produces the opening of the valve, creating a flow. When the coil is switched to OFF in (c), the concentration of particles decreases on the left side in the absence of magnetic field and the pressure that was

keeping the valve open is no longer enough, so it closes. The process is repeated when the coil is switched ON again in (d), creating a discontinuous flow.

The fluid used for both two last studies is EFH1, just the same as in the present project. Considering this, and since microfluidic applications are discarded as they cannot be scaled, only these two models can be compared to our model.

Chapter 3. The physics of FHD pump

This chapter describes the physics behind FHD pumping, with the aim of providing a theoretical background for the experimental research conducted in the project. Specifically, the focus is placed on the filling process of the pump that takes place when the magnetic field is induced in the coil – i.e., when the current is ON.

The study conducted by Granelli [12] provided the baseline for this process; in this work, the steady state was expressed as the maximum height to which the magnetic forces can lift the fluid upwards. The transient state was afterwards analysed by Boerma [13], in which a mathematical model was developed to describe the dynamics of the process. This section is based on such model to determine the theoretical behaviour of EFH1 in the pump, in order to compare it later with the experimental results obtained.

In this Chapter, the equations defining the dynamics of magnetic fluids are introduced and explained. In Chapter 4 those equations are applied to the small-scale set-ups that are used for the experiments. This way, the results obtained from experiments can be compared with the theoretical behaviour of the ferrofluid.

3.1. THE MAGNETIC FIELD OF A COIL

The magnetic field used in the FHD pump is generated through a coil that is supplied with DC current. As the solenoid is wound around the duct through which the flow is created, it is important to determine the magnetic field strength value at any local point of the core – both in and out the solenoid.

Considering z as the position along the axis of the coil and r the position along the radius of the coil, the magnetic field expressions for both on axis and off axis of the solenoid are presented as a function of these two variables.

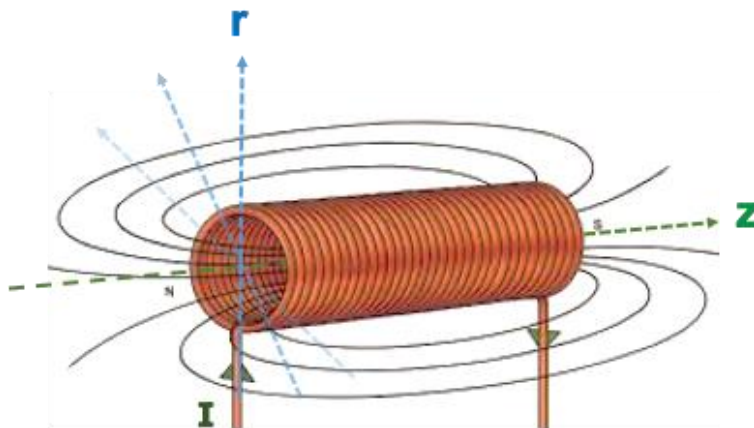


Figure 15: Magnetic field created by a coil

3.1.1 MAGNETIC FIELD ON Z AXIS

When a DC current circulates through a coil that is long enough when compared to the radius, a quasi-uniform magnetic field is created inside the solenoid. The value is proportional to the current and the density of turns, expressed as the number of turns divided by the total length of the coil and multiplied by the number of layers:

$$H = nl$$

with

$$n = \frac{N}{L}k$$

where L is the length of the solenoid, N is the number of turns per layer and k is the number of layers. When moving outwards the solenoid the magnetic field decreases abruptly to zero, thereby creating a gradient that will develop Kelvin forces when the fluid approaches such regions.

The following equation shows the magnetic field strength on axis created by a solenoid that is centred on $z = 0$:

$$H(z) = \frac{nI}{2L} \left(\frac{z + \frac{1}{2}L}{\sqrt{\left(z + \frac{1}{2}L\right)^2 + R^2}} - \frac{z - \frac{1}{2}L}{\sqrt{\left(z - \frac{1}{2}L\right)^2 + R^2}} \right)$$

being R the average radius of the coil – note that we are considering more than one layer.

3.1.2 MAGNETIC FIELD OFF Z AXIS

As the fluid flows through the core, it is important to have defined the magnetic field along the cross section of the tube. However, a more complex expression than that of on z -axis is required. The following expressions define the magnetic field strength for a point located at (z, r) in cylindrical coordinates [12]:

$$B_r = \frac{\mu_0 I}{2\pi R} \frac{\xi}{\rho \sqrt{(1 + \rho)^2 + \xi^2}} \left(-K(k) + \frac{1 + \rho^2 + \xi^2}{(1 - \rho)^2 + \xi^2} E(k) \right)$$

$$B_\phi = 0$$

$$B_z = \frac{\mu_0 I}{2\pi R} \frac{I}{\rho \sqrt{(1 + \rho)^2 + \xi^2}} \left(K(k) + \frac{1 - \rho^2 - \xi^2}{(1 - \rho)^2 + \xi^2} E(k) \right)$$

with

$$\rho = \frac{r}{R}$$

$$\zeta = \frac{z}{R}$$

$$k^2 = \frac{4\rho}{\zeta^2 + (1 + \rho)^2}$$

$E(k)$ and $K(k)$ equations can be found in Annex VI.

3.2. THE KELVIN BODY FORCE

The magnetic attraction force density developed in a magnetic fluid receives the name of Kelvin force (or magnetophoretic force) [12] and can be expressed as:

$$F_{Kelvin} = \mu_0(\vec{M} \cdot \vec{\nabla})\vec{H}$$

where M is the magnetization of the fluid and H is the magnetic field strength. The force – expressed in pressure units – points in the magnetic field direction and depends on the angle between M and H as the equation shows. The magnetization is in turn a function of the magnetic field strength, given by the magnetization curve of the ferrofluid. The characteristic curve for EFH1 is shown in Figure 16.

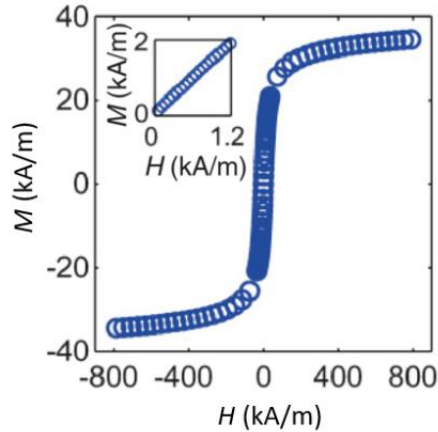


Figure 16: Magnetization curve of EFH1 [12]

Considering Figure 16 and the fact that the magnetic moments of ferromagnetic materials align with the external field when magnetized – so that both H and M always have the same direction for the frequency used – the expression of the Kelvin force at a local point can be expressed as:

$$F_{Kelvin} \left[\frac{N}{m^3} \right] = \mu_0 \chi H \nabla H$$

Thus, this force is active on the regions where both a magnetic field gradient and the ferrofluid itself are present. These regions – which will be called Kelvin force regions from now on – are located around the extremes of the solenoid and, considering the symmetry of both sides, the density force must have the same value while the directions points to the centre of the solenoid. As only the rising process is of interest in this section, the only Kelvin force region considered is that of the inlet of the pump – the bottom of the solenoid. This is the case in which the level of the fluid is always far from the highest end.

In the same way as the magnetic field off-axis, the Kelvin force is a function of both the radial and axial direction. However, the model describing the fluid dynamics assume that forces are constant over the cross section of the tube, so an average value is taken. This value can be calculated by integrating the density force along the cross section (the radius variable) of the tube:

$$\bar{F}_{body} \left[\frac{N}{m} \right] = \frac{S}{R} \int_0^R F_{Kelvin}(r) dr$$

where S is the cross-section area and R is the inner radius of the tube. Since Kelvin force consists of a force density, the term “body force” is used to define the force that acts on the section of the tube.

3.3. THE FLUID DYNAMICS

The dynamics of the fluid can be defined through the increase of height of the level of the fluid in the pipe – which is initially at rest – over time. For this analysis, let us simplify and assume that the tube through which the fluid rises is in vertical position. Let us also assume that the fluid is incompressible, and that all the points of the fluid move in the same direction at the same velocity, behaving as a rigid and solid body. Finally, let us assume that the latter is only applied to the fluid flowing through the pipe and horizontal tube but not to the fluid contained in the reservoir, which is assumed to be at rest given its wide section.

When the current flows through the solenoid, a body force is developed on the fluid attracting it towards the centre of the coil. As a result, the fluid is accelerated and the level starts to rise, filling the tube. From that moment on, the gravity and the friction between the fluid in motion and the walls of the tube start to act in the opposite direction of the

flow. To analyse the behaviour of the fluid during the rising process, the following volume of control is considered:

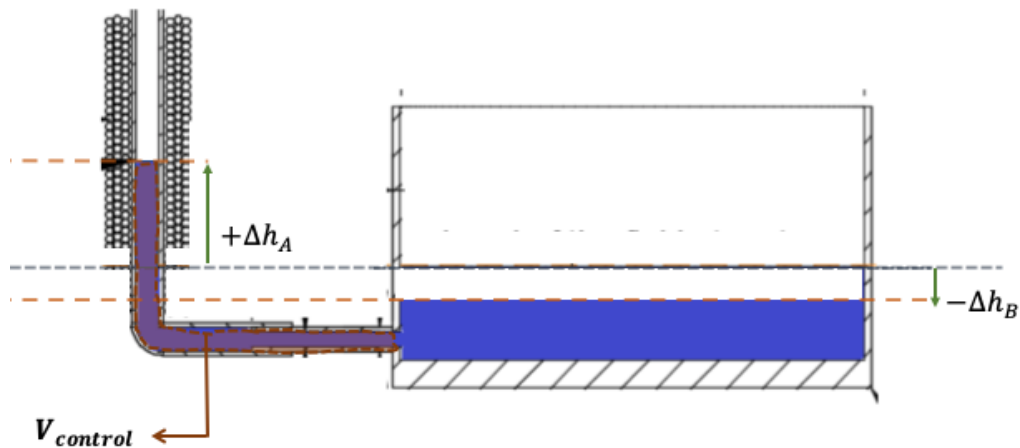


Figure 17: Representation of a certain moment during transient state

$$V_{control} = S_A L_{filled\ pipe}$$

where S_A is the cross-section of the pipe and $L_{filled\ pipe}$ is the total length of the pipe that the fluid has filled, including the tube welded to the reservoir as shown in Figure 17. The scheme represents a “picture” taken during the rising process in order to analyse the conjunction of forces acting in a certain moment.

$$F = F_{body} - F_{gravity} - F_{friction}$$

where the friction force can be expressed for a certain time as

$$F_{friction} = \frac{1}{2} C_f \rho A \Delta h U^2$$

being C_f the dimensionless friction coefficient, A is the area of contact between the fluid in movement and the walls of the channel, and U is the velocity of the fluid. The gravity force is calculated as the weight of the column of fluid above the reservoir level. Figure 18 helps to picture it.

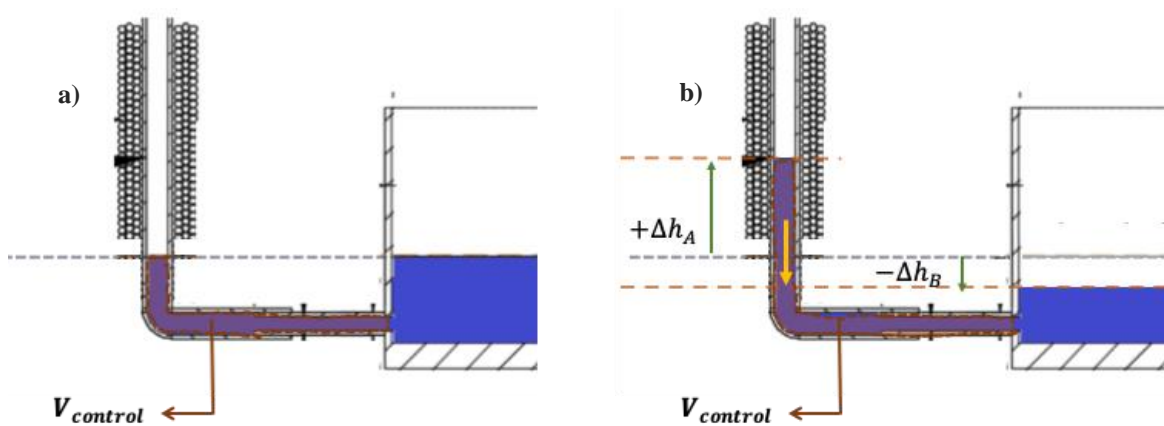


Figure 18: a) The fluid is initially at rest. b) The fluid is rising and gravity (yellow arrow) acts on the column of ferrofluid

Figure 18.a shows the initial state, wherein the fluid is distributed in such a way that the free surface of both the pipe and the reservoir are at the same level. Since there is not fluid above the reservoir level, the gravity is not acting. On the other hand, Figure 18.b represents a moment in which the fluid is rising, and the level in the pipe has increased a certain height (Δh_A). The gravity acts in the column of fluid above the reservoir level, which has decreased in turn to conserve the same amount of fluid in the set-up. Hence, the gravity force is expressed for a certain moment as:

$$F_{gravity} = S_A(\Delta h_A + \Delta h_B) \rho g$$

While gravity and friction only depend on the amount of fluid displaced in the tube – which increases over time – the body force is also a function of the position on z axis. Figure 19 shows the body force calculated with the model for certain parameters, as an example to show the shape of the function.

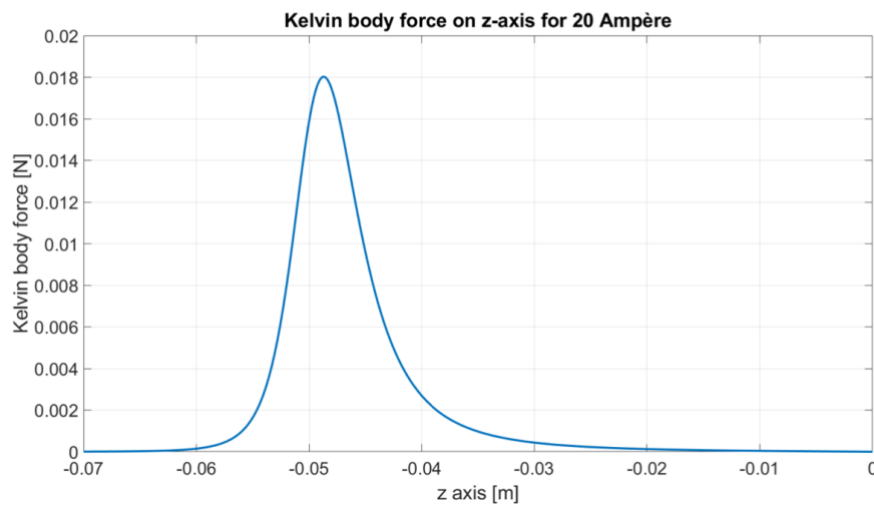


Figure 19: Solenoid of 150 mm of length, 3 mm of radius and 2 mm of wire diameter. Solenoid centered at $z = 0$ m with the bottom at $z = -0,05$ m. $I = 20$ A

The body force is therefore calculated as:

$$F_{body} = \int_{z_0}^{z_f} \bar{F}_{body} dz$$

where z_0 and z_f limit the Kelvin force region filled with magnetic fluid and \bar{F}_{body} is the average value calculated for the body force across the section.

Figures 20 and 21 depict how the value of the body forces increases as the fluid rises and fills the Kelvin force region:

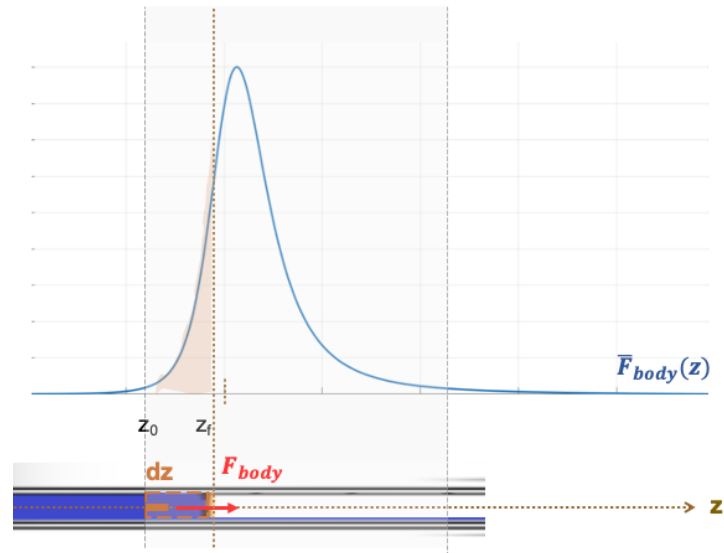


Figure 20: Body force acting on the fluid when the level is within the region

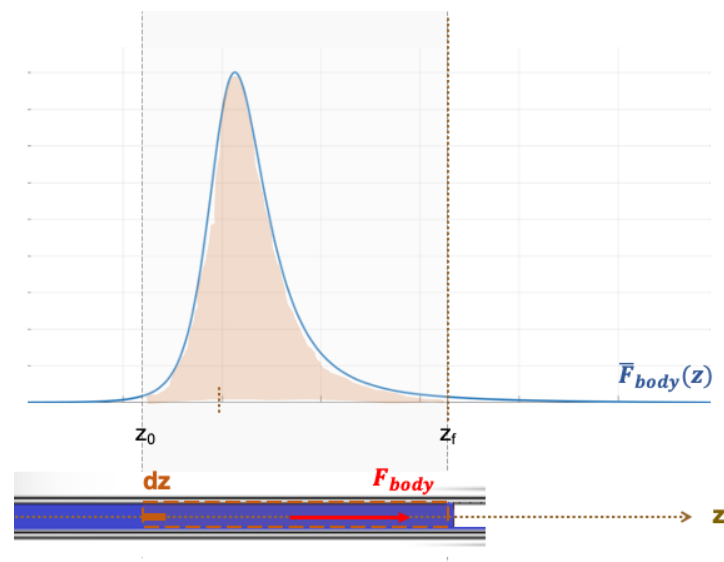


Figure 21: Body force acting on the fluid when the level is above the region

This way, the body force remains at a constant value after the fluid passes the Kelvin force region (Figure 21).

The model developed in [12] assumes that the initial level is above the Kelvin force region. This way the model is simplified by using a constant body force during the whole process. With the aim of deepening on the rising process, the model is extended to the cases in which the level of the fluid is inside the Kelvin force region and therefore, the body force increases over time (Figure 20).

On the other hand, when the transient period ends and the fluid stops rising, only the body force and weight of the volume displaced remain in equilibrium.

$$F_{body} = F_{gravity}$$

Thus, the final increase of height inside the pipe can be obtained from the steady state equation:

$$F_{gravity} = \rho g S_A (\Delta h_A + \Delta h_B) \quad \rightarrow \quad \Delta h_A = \frac{F_{body}}{\rho g S_A + \frac{S_A}{S_B}}$$

The results from the analysis of the dynamics of the fluid are included in Chapter 6 together with the experimental results, in order to contrast them.

Chapter 4. The experimental set-up and technology used

The physical set-up used to conduct the experimental research in this project is similar to the set-up employed during the first project [12]. The scheme of the design of the set-up constructed for the pump is shown below.

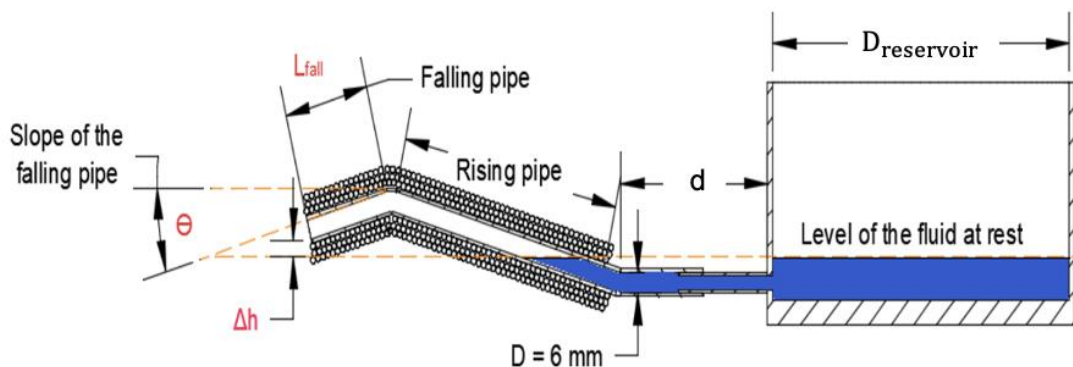


Figure 22: Set-up of the pump developed in [12]

The set-up represented shows at the left a small-scale prototype of the pump that is built with a folded plastic-PVC pipe, and a coil made out of copper wire wound around it, that is connected to a current source, to be used as electromagnet. A cylindrical stainless-steel container is connected to the inlet of the pump through a tube that is welded to the reservoir, shown in the right side of the figure.

The different set-ups used are based in this configuration, adjusting it according to the type of experiment conducted. As mentioned in previous chapters, the experimental research

of this project is divided in two parts. The object of the experiments conducted in the first group is to analyse the rising process described in the theoretical model previously developed, and to try to answer certain research questions.

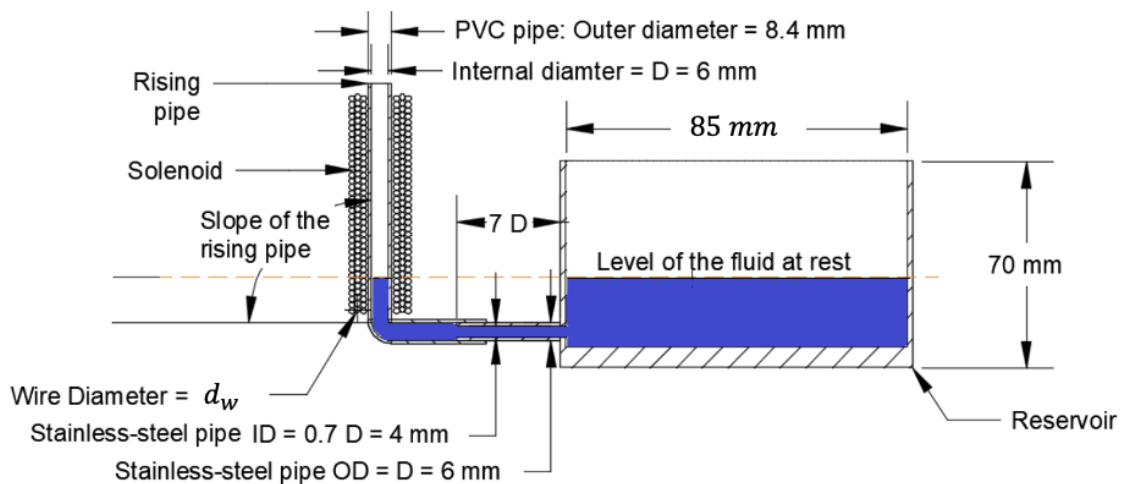


Figure 23: Set-up used in the experiments conducted on the rising process

The set-up used for the first set of experiments, the rising part, is shown in figure 23.

The PVC pipe used in this case is chosen to be flexible, in order to adjust easily the slope of the rising pipe (in vertical position in the picture, as an example).

Two different solenoids were built. Both have the same length and same number of layers, differing only in the diameter of the wire (d_w), that are 0.8 mm and 1 mm respectively. The reason for using two different thickness of wire was flexibility, as when the solenoid is wound over the folded area the creation of gaps can be reduced. On the other hand, thicker wires stand higher values of current and therefore can induce higher values of magnetic field. A higher number of layers is required to build these solenoids, which also might affect the uniformity of the magnetic field.

The element that is new with respect to the previous work is the use of a sophisticated measuring system used to monitor the rising process in the pipe: the confocal-chromatic sensor. A description of the working principle of the technology will be provided in an annex. In fact, the search of a suitable sensor to conduct the experiments turned out to be an important part of the workload. The search was focused on finding a reliable device capable of measuring the height increase inside the pipe directly from the top (spot A). Unfortunately, such system was not found. Instead, a suitable device was found to measure the height increase indirectly from the reservoir (spot B).

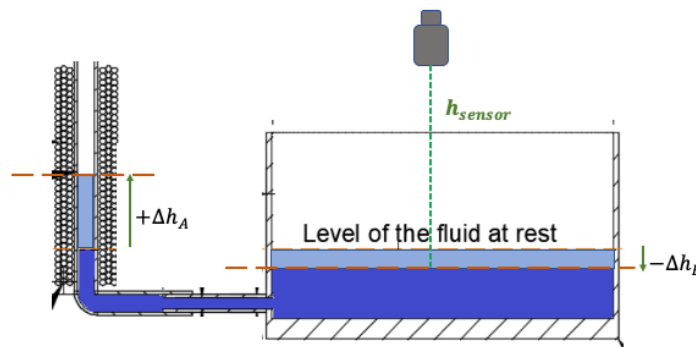


Figure 24: Scheme of the measuring system set-up

Figure 24 represents the method used to conduct the measurements. The sensor is arranged at the top of the reservoir and positioned in perpendicular direction with respect to the level of the fluid, in order to measure the correct distances. Then, the height increase in the pipe is calculated considering the following relation:

$$\frac{\Delta h_A}{\sin \theta} S_A = \Delta h_B S_B$$

where θ is the slope of the rising pipe, S_A is the section of the pipe and S_B is the diameter of the reservoir. This equation is based on the assumption that the volume displaced in both spots is the same, which is true provided that the fluid is incompressible and that no suction forces are acting on the hole of the reservoir. Both facts are assumed.

The experiments conducted as well as a more detailed description of their corresponding set-ups are included in next chapter.

Chapter 5. The rising process

One of the factors involved in the modelling of the magnetic pump is the time that the pump takes to be filled with the magnetic fluid. For example, to determine the ON/OFF ratio of the current input and the frequency used, or the length of the rising pipe.

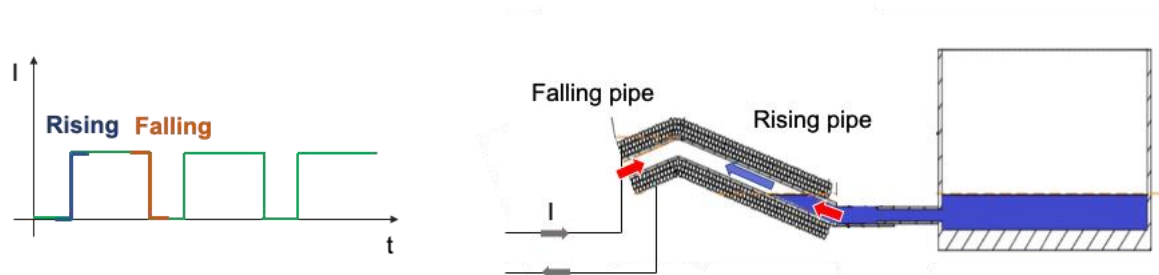


Figure 25: Performance of the pump

With the aim of obtaining experimental results which contribute to the optimization of the pump performance, the rising process is separated to thoroughly analyse it in the set-ups described in the previous chapter. The sets of experiments dedicated to the rising process are designed to pursue different objectives or research questions, all with the same target of optimizing the efficiency of the pump through the definition of its parameters.

The mathematical model describing the physics of the FHD pump and the behaviour of the fluid is experimentally investigated to provide knowledge about the real processes.

The main research question that has motivated the experiments starts with determining the optimum level at which the fluid should start. The results from these experiments provide not only an answer to the question, but also reliable data about the real behaviour

of the fluid in the FHD pump prototype tested. These experiments together with the expected results from the model are treated in the next chapter.

On the other hand, the previous work draws certain conclusions and assumptions from the experiments that are repeated and analysed in detail. As the measuring technology available in this project is very accurate, better results can be obtained. Two questions that belong to this group are: (1) the influence of the position of the solenoid with respect to the fluid, and (2) the influence of the inclination in the pipe.

All these experiments are carried out for a step current input that is repeated for different values – in separate experiments. The dynamic response to different current inputs is also studied to see the influence of the form of the signal supplied to the coil and compare it with the single-step behaviour.

Finally, the effect of temperature is analysed. In this case, the question came after the results, when unexpected behaviours of the fluid were observed and attributed to this factor. This is explained in Chapter 8.

Chapter 6. Influence of the position of the solenoid with respect to the fluid at rest

The influence of the position of the solenoid was studied for the first time in [12]. In that experiment, a solenoid of 4 cm of length was used to create the magnetic field. The level of the fluid at rest was then changed along the axial direction through the experiment, so that different starting points were taken to measure the height increase after switching the current to ON.

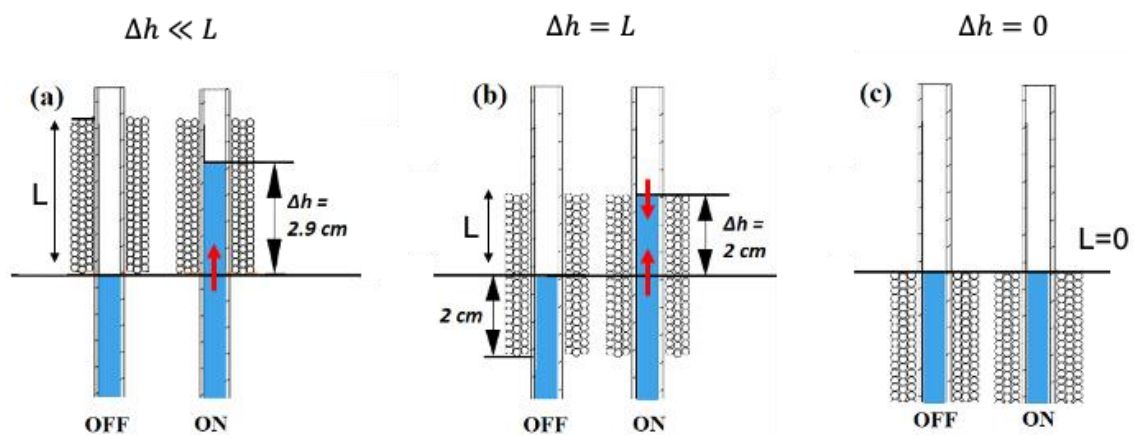


Figure 26: Position of the solenoid respect to the fluid at rest

From the results, three extreme cases represented in Figure 26 can be described. Figure 26.a shows how the height increase occurs when the fluid is near the bottom of the solenoid due to the presence of an upward gradient. As the level of the fluid at rest is increased inwards the solenoid, and the top of the solenoid is approached, the fluid does not rise beyond the solenoid region because of the presence of the downward gradient.

This case is represented in Figure 26.b and 26.c, being the latter the extreme case of no height increase.

This experiment is taken as a baseline for the further analysis of the position of the fluid at rest with respect to the solenoid. For that, only the case corresponded to Figure 26.a is considered, assuming that $L \gg \Delta h$, so that the downward gradient present at the top does not affect. As explained in Chapter 3, the final height increase reached in static conditions depends only on the body force acting on the fluid. From theory, it is assumed that for any level of liquid above the bottom of the solenoid, the height increase for a given magnetic field will be the same. This assumption constitutes one of the research questions analysed

ANALYSIS OF THE KELVIN FORCE REGION

As the fluid approaches the solenoid region, it is expected that a body force starts to act on the fluid, attracting it inwards the solenoid. The issue here is to determine at what distance from the solenoid this phenomenon starts to happen. The boundaries and location of the Kelvin force region can be estimated from the mathematical expression of the Kelvin force density, which is dependent on the magnitude of both magnetic field and magnetic field gradient for the same fluid (susceptibility).

However, as explained in Chapter 3, the body force responsible of the rising of the fluid depends on the amount of fluid that is present within the region. Thus, according to the position of the fluid at rest with respect to the Kelvin force region, three different cases are identified for a same given magnetic field in the coil (below, inside and above):

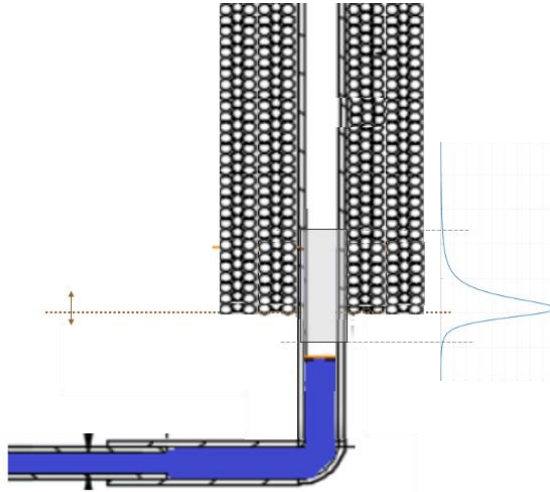


Figure 27: The level of the fluid is below the Kelvin force region

- ***The level of the fluid is below the region***

In this case, the rising does not happen as the fluid is too far from the magnetic field to be affected.

- ***The level of the fluid lies within the region***

The Kelvin force starts to be active on the portion of the fluid present in the region as soon as the coil is switched to ON. As the fluid starts to rise and fills the pipe, the force increases as well because more volume of fluid is being affected.

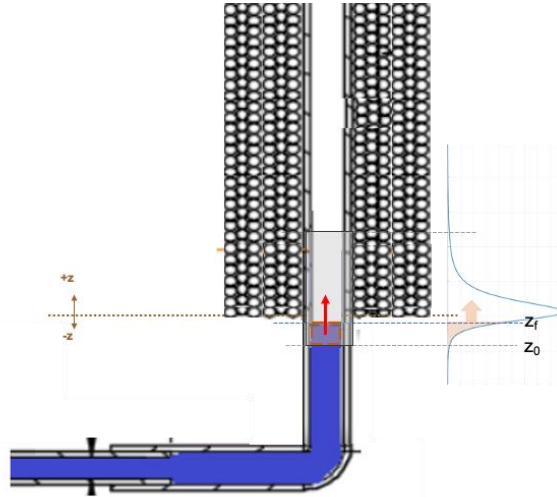


Figure 28: The level of the fluid is within the Kelvin force region

Within this section, two different sub-cases can be found:

- a) *The fluid rises over the end of the region.*

The body force increases until the fluid reaches the end of the region, moment at which the force remains constant at its maximum value.

- b) *The final level reached by the fluid is still within the region*

The final value that the body force reaches, when the fluid stops rising, is under the maximum value corresponded to the given magnetic field.

- ***The level of the fluid is at/beyond the end of the region***

The total body force in that case takes its maximum value from the moment in which the coil is turned ON, as the amount of fluid present in the region does not change

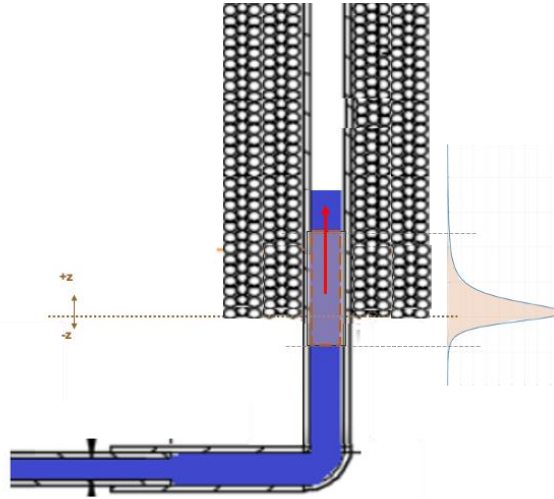


Figure 29: The level of the fluid is above the Kelvin force region

The last classification is important when it comes to analyse the transient period of the rising process of the fluid, which will present different dynamics according to the case. Newton's second law defines the evolution of the height increase inside the pipe over time. From equations presented in Chapter 3 [12]:

$$\sum F = F_{body} - F_{friction} - F_{gravity} = m_{V_c} a$$

where a is the acceleration of the fluid over time and m_{V_c} is the mass of the volume of control taken.

As said in Chapter 3, the dynamics of the fluid are first analysed through a mathematical model, developed as an extension of the previous project [13]. In this case, the equations that govern the rising process are extended to the cases in which the magnetic force is not constant over time – which was considered as simplification – but increasing as the fluid fills the pipe. The parameters used for the simulation correspond to the experimental set-up described in this chapter:

- Solenoid
Diameter of the wire: 1 mm
Number of turns: 150
Number of layers: 6
Length: 150 mm
Inner diameter: 8.4 mm
- Rising pipe
Slope of the rising pipe: 90°

The description of the experiment is as follows. The initial level of the fluid is set at different distances from the solenoid, taking as a reference the bottom (0 mm). At each starting point, currents within the range of 2 to 6 A are supplied to the coil in separate experiments, so that each one corresponds to a different current step input. The starting points taken along the axis vary from -12 to 8 mm.

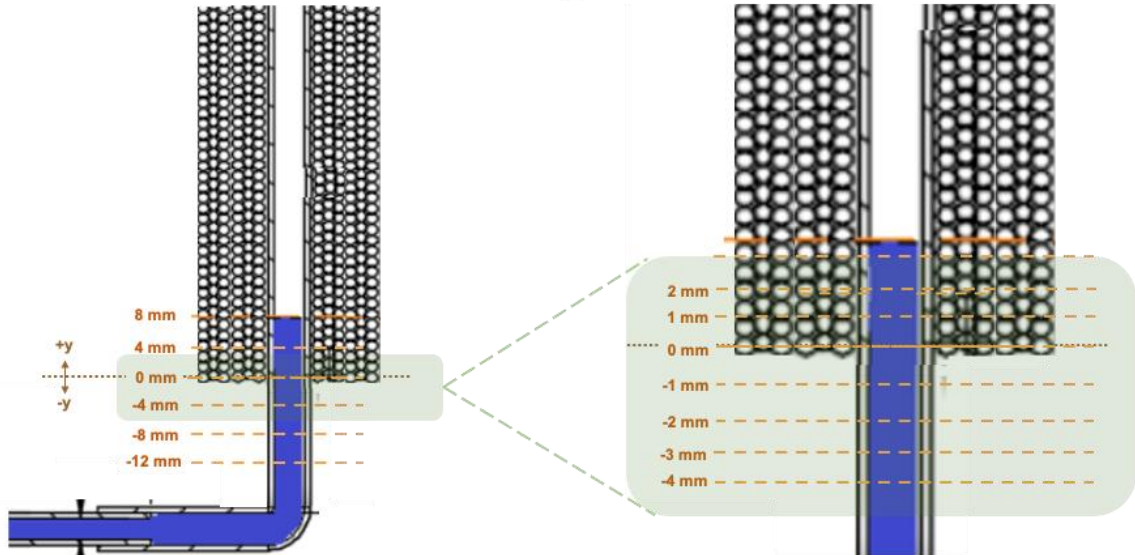


Figure 30: Scheme of the experiment conducted

As Figure 30 depicts, the increment between successive points is 4 mm, except for the region that is closer to the bottom – green area in Figure 29- that indicates the region around which the Kelvin force density is higher. In that critical region (interval between -4 and 2 mm), trials are carried out in steps of 1 mm.

The sensor, which measures the level of the reservoir, starts to record when the fluid is stable at rest, before switching to ON the electromagnet. The current step is introduced at some point and the variation in the reservoir level is measured over time, until the signal stabilizes reaching the static condition. The same process is repeated for each one of the experiments. The height increase in the pipe is then calculated – according to the relation given in Chapter 4 – and represented over time.

Each one of the experiments is simulated using the developed analytical model. Theoretical and experimental results are analysed and compared in the next subchapters. Section 6.1 takes up the previous classification – Figures 27, 28 and 29 –and analyses the transient

state. On the other hand, Section 6.2 focuses on the steady state with the aim of verifying the initial statement of this chapter– see Figure 26.

6.1 ANALYSIS OF DYNAMICS

The Kelvin force region over the z-axis is calculated and represented in Figure 31 for the range of [2 , 6] A used in the experiments. Only the lower half is represented, as the fluid does not rise beyond such region.

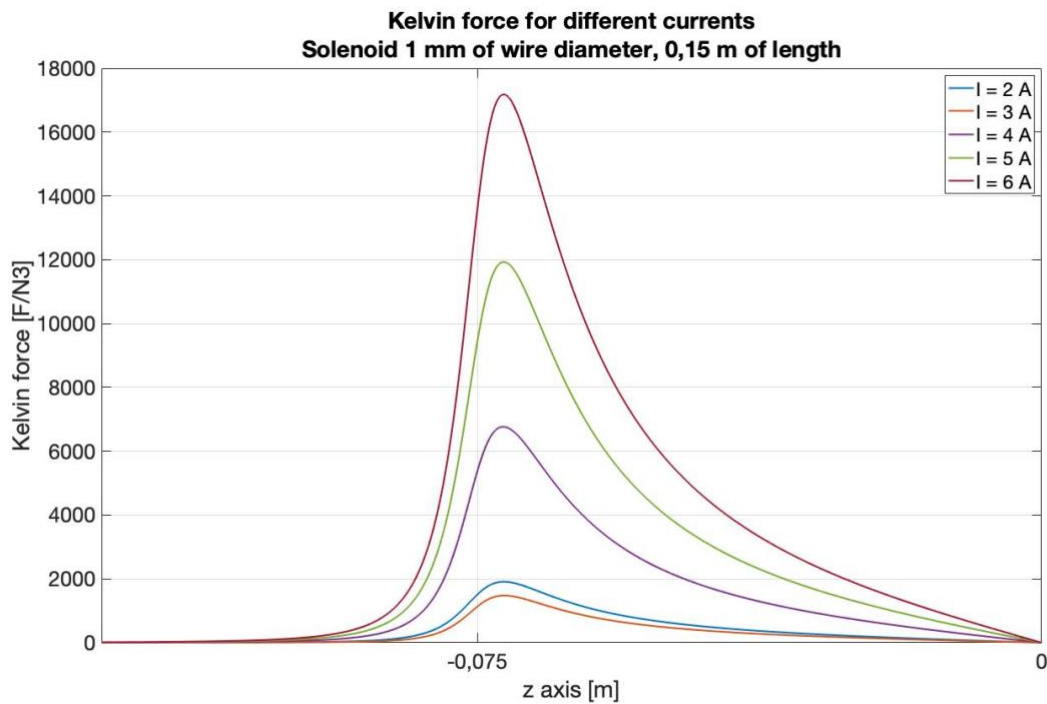


Figure 31: calculated Kelvin force region for the range of currents

In the Figure, $z = 0$ m corresponds to the middle point of the coil and -0.075 m is the bottom of the solenoid. It is shown how not only the magnitude of the force is proportional to the current, but also the extension of the Kelvin force region. Hence, it is expected that the distance in which the fluid is attracted by the coil is larger for higher currents. For a given magnetic field – i.e. for a given current– the strength with which the fluid is pulled up depends on the position of the fluid in the pipe and the volume of fluid within the region. This fact, which is already predicted in the previous classification, is demonstrated in the following results.

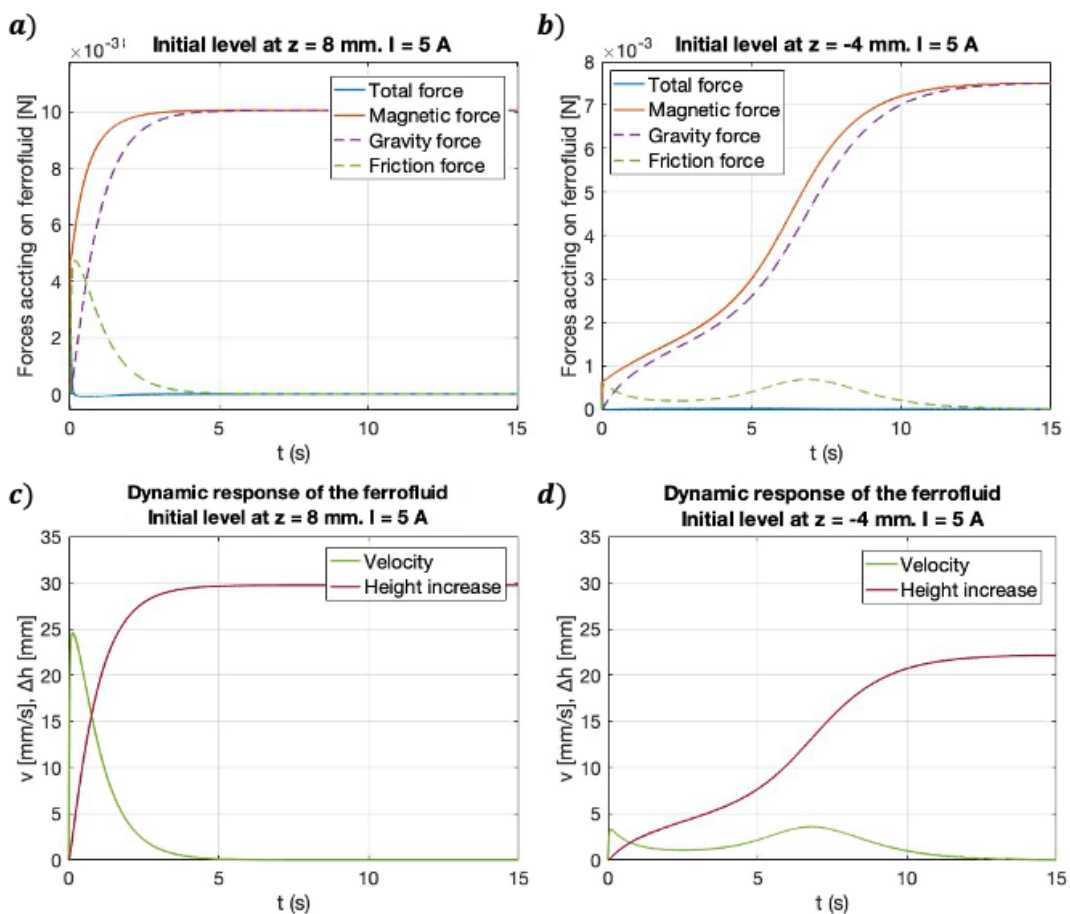


Figure 32: Comparison between $z = 8$ mm and $z = -4$ mm of distance to the bottom of the solenoid.

Two extreme points are taken to contrast the behaviour of the fluid for the cases in which the fluid initially lies under the coil – Figure 32.b and 32.d – and for those in which the fluid is initially within the coil – Figure 32.a and 32.c. It should be clarified that the locations of the different starting points along the pipe are taken from the bottom of the coil as a reference – $z = 0$ mm – just as Figure 31 represents. The current is supplied to the coil at $t = 0$ and has the value of 5 A.

The dynamic response of the fluid is significantly different in both cases, which is explained by the amount of fluid that is initially within the Kelvin force region. This becomes clear when the magnetic forces simulated for each case are compared, observing how the initial body force is greater for Figure 32.a than for Figure 32.b. This results in a faster response of the fluid in the case of higher initial levels, which is clear in the example given – Figure 32.c vs Figure 32.d. Hence, it will be preferable to have the fluid inwards to reduce the filling time of the rising pipe, considering the pump optimization. As a last remark, it is interesting to highlight the non-linearity that both the magnetic force and the height increase present in the case of $z = -4$ mm, which is due to the irregular trend that Kelvin force presents around the extreme of the solenoid.

The experimental results shown below are presented in two ways. On one hand, the height increase over time is represented for the whole range of currents in the same plot when the fluid rests initially at a given point. This way, the influence of the magnitude of the magnetic field can be represented. On the other hand, the height increase of the fluid for a given magnetic field is represented in the same graph for the range of different initial levels. This can be useful to show how the previous classification affects – the influence of the position. In the annexes all the results are included. Here, only the most representative ones are shown.

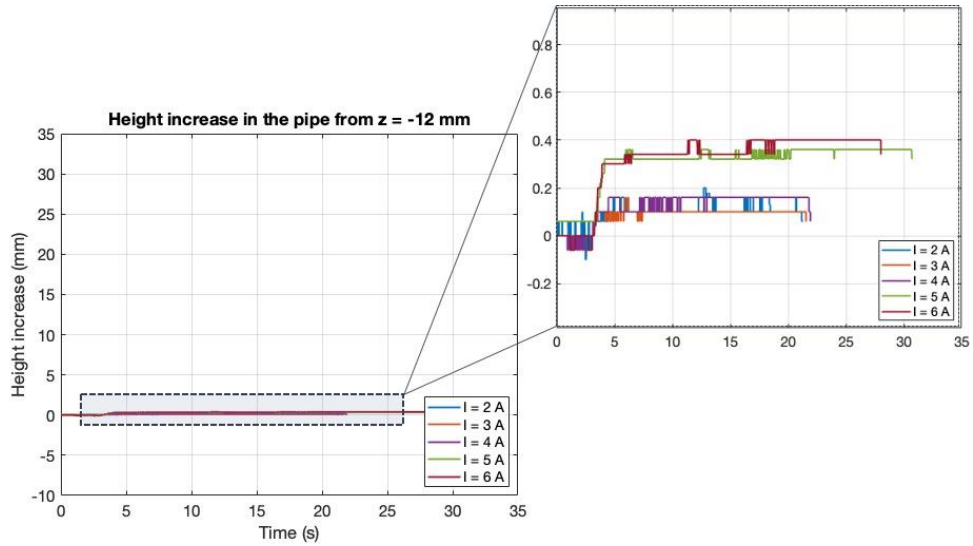


Figure 33: Height increase in the pipe when the level of the fluid at rest is at $z = -12$ mm

Figure 33 shows how the fluid is too far from the solenoid to present a significant height increase, which corresponds to the first case of the classification.

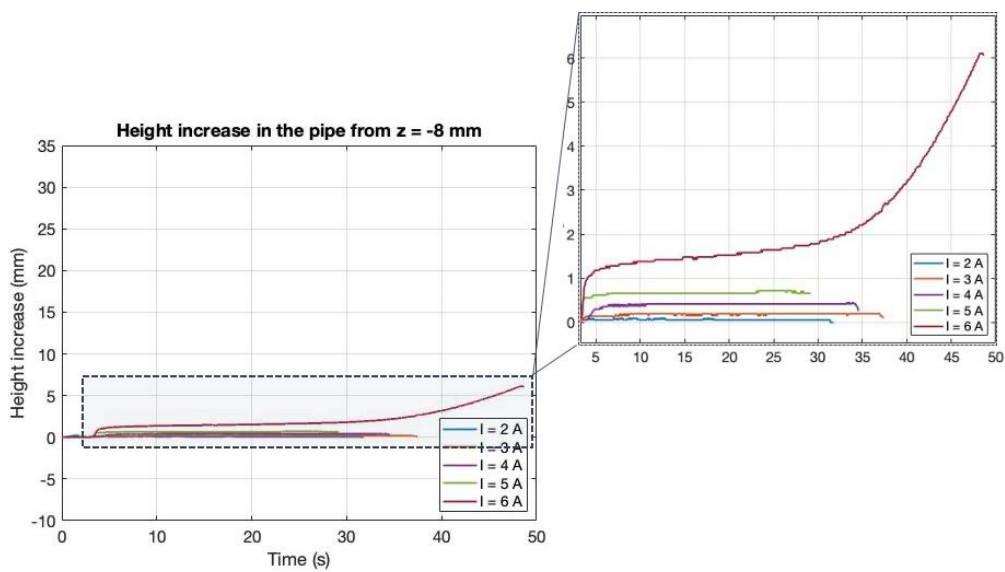


Figure 34: Height increase in the pipe when the level of the fluid at rest is at $z = -8$ mm

Figure 34 shows how at -8 mm the height increase is still not significant for most of the current values. For $I = 6 A$, however, the fluid presents a change in acceleration as it approaches the solenoid, which is a proof of how the body force varies according to the distribution of the Kelvin force density along z , which presents a more irregular form around the bottom of the coil – as remarked from Figure 31.

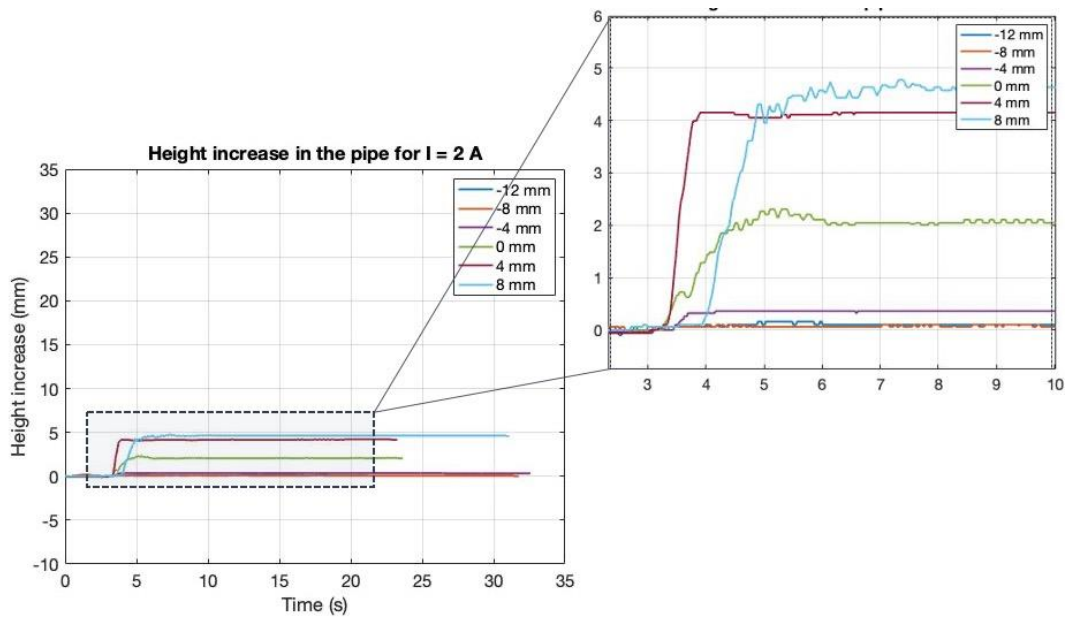


Figure 35: Height increase in the pipe when the solenoid is supplied with 2 A

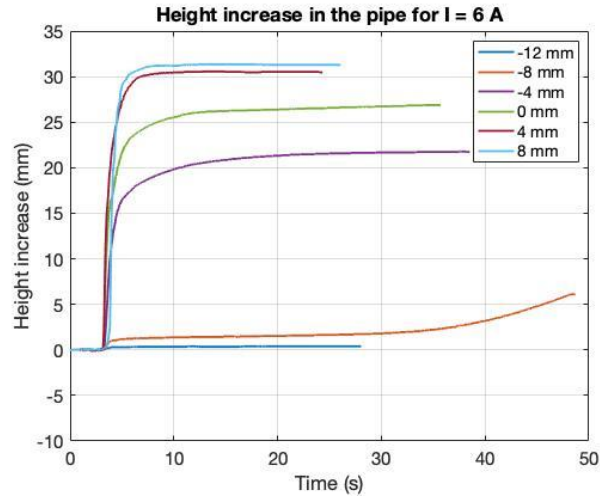


Figure 36: Height increase in the pipe when the solenoid is supplied with 6 A

Figures 35 and 36 aim to show how the boundaries of the Kelvin force region depend on the magnitude of the magnetic field. Thus, when the coil is switched to ON with $I = 2 A$, the level of the fluid does not undergo a significant increase until it is not at 0 mm. In contrast, when $I = 6 A$ the height increase starts at -4 mm.

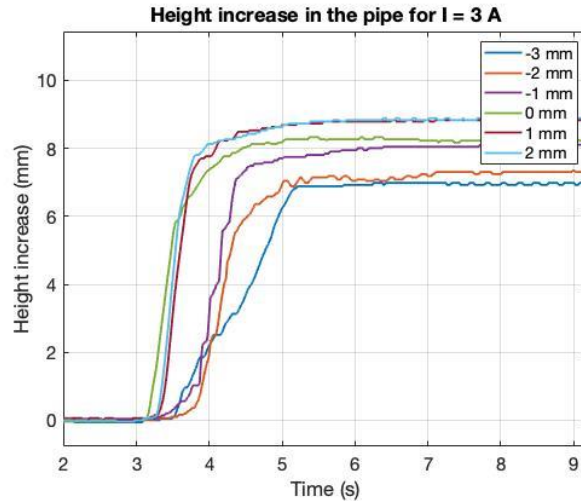


Figure 37: Height increase in the pipe when the solenoid is supplied with 3 A

Figure 37 shows an example of how the slope of the height increase over time depends on the initial position at rest respect to the solenoid. As the initial height of the fluid approaches the interior of the solenoid, the slope gets steeper and the time taken to stabilize is reduced. This is a proof of, as earlier suggested, the optimal initial level is inwards the solenoid.

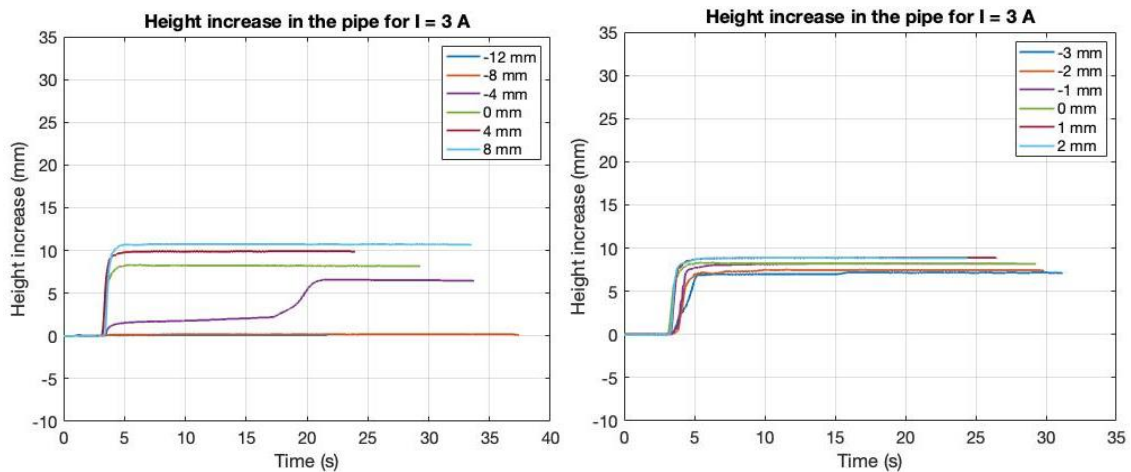


Figure 38: Height increase in the pipe when the solenoid is supplied with 3 A

Figure 38 contributes to the last conclusion. The significant difference between the initial point -4 mm and the rest of points above it suggests that, while the first case could belong to the second group in the classification – since the fluid undergoes a change of slope that suggests that is crossing the Kelvin force region – the points above present a more uniform and steep response to the body force. This can be a sign of the fact that, as the fluid rests at a higher height inwards the solenoid, the amount of fluid inside the region remain practically constant along the process.

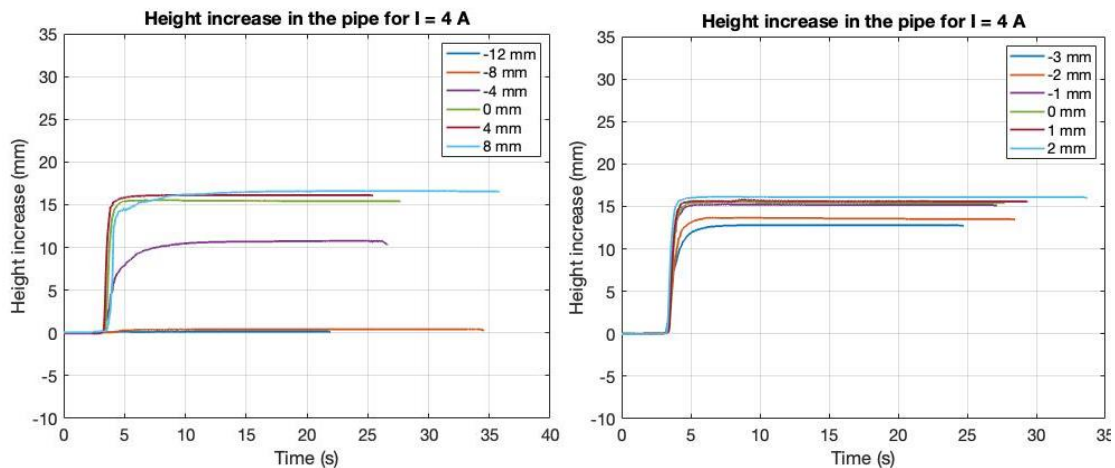


Figure 39: Height increase in the pipe when the solenoid is supplied with 4 A

Finally, Figure 39 is included as an example of the third case of the classification conducted, as it shows how for points higher than 4 mm, the height increase remains practically constant.

6.2 INFLUENCE OF THE POSITION OF THE SOLENOID WITH RESPECT TO THE LEVEL OF THE FLUID AT REST

The latter conclusion is related to the initial assumption made in this section: For a given magnetic field, the final height increase should be the same for the cases in which the level rests above the Kelvin force region.

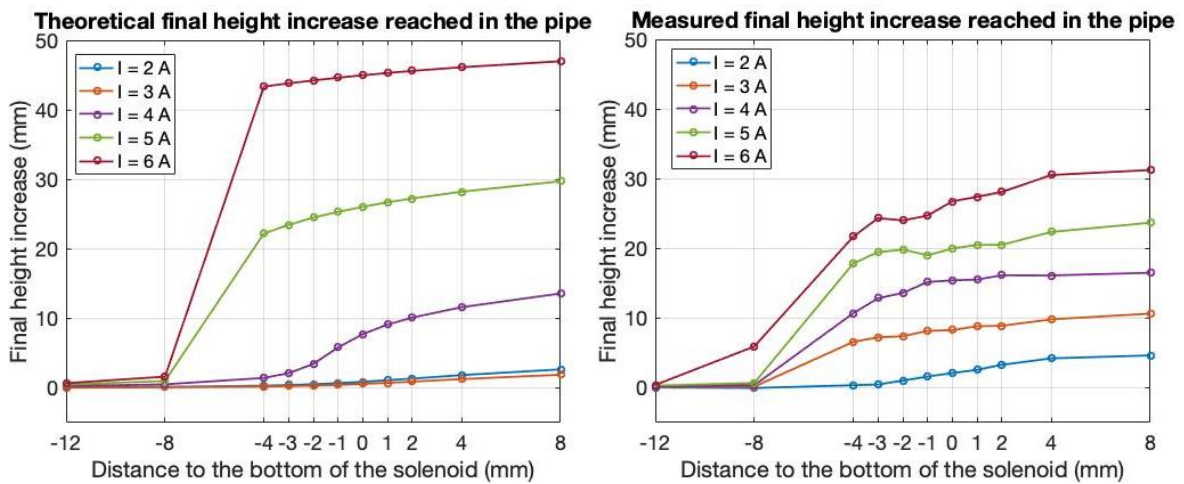


Figure 40: Steady state value for each experiment (each initial starting level) for the range of currents.

Figure 40 presents the evolution of the final height increase of the fluid along the different starting points for both the simulations and the experimental results. The behaviour of the fluid meets expectations in a qualitative way, as the value of the steady state tends to stabilize for the points approaching the end of the Kelvin force region. Quantitatively, however, the experimental results are far from meeting the simulations. There are many possible reasons behind it. Some of them are related to measurement inaccuracies, in which case, an error interval can be estimated – Annex V. For others, however, it is not easy to assign a value.

The latter is the case of the magnetic field. The real magnetic field induced by the coil – in empty core – is measured with the aim of better estimating the real Kelvin force value.

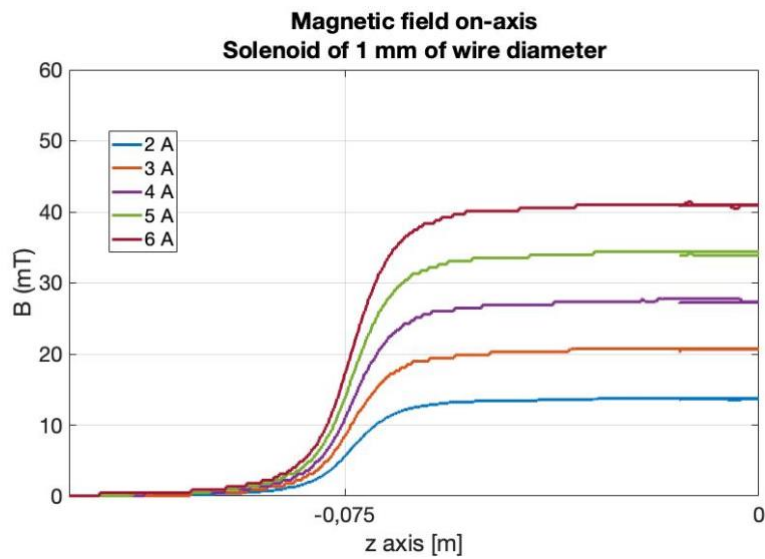


Figure 41: Magnetic field measured on-axis

Figure 41 presents the magnetic field measured for the coil used for the experiments – the extended results are included in Annex IV. With respect to the model, the measured field results to be around 10% smaller than expected

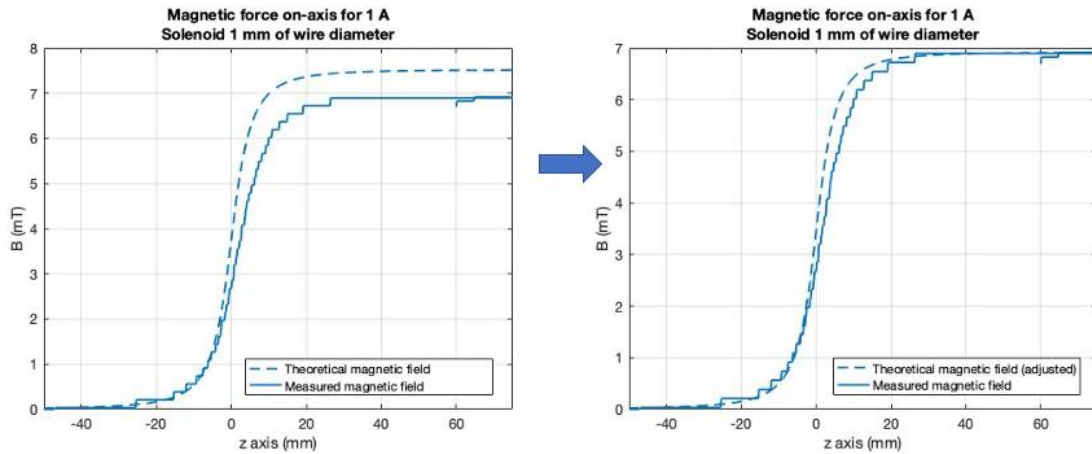


Figure 42: Comparison between the magnetic field measured and the theoretical magnetic field.

The left graph of Figure 42 shows the comparison between the magnetic field calculated and the one measured. The first observation is that the magnetic field is a 10 % smaller than the expected one. For that, the curve is scaled with the aim of comparing the gradients (right graph). The result from such comparison reveals that the magnetic field from the model is steeper than the real magnetic field used in the laboratory. This conclusion proves the need for actual measurements of the force rather than theoretical estimations.

In order to further analyse the steady state, the following experiment is conducted on the same set-up.

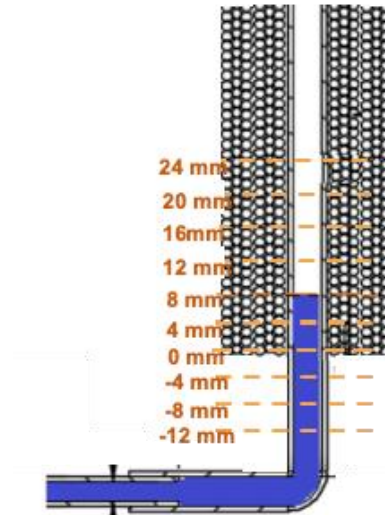


Figure 43: Scheme of the experiment conducted

The difference lies in an extension of the trials, with is aimed to analyse the last statement. Figure 44 represents the steady state evolution through the different starting level for each given. It is expected that the trend remains constant from a certain point within the solenoid.

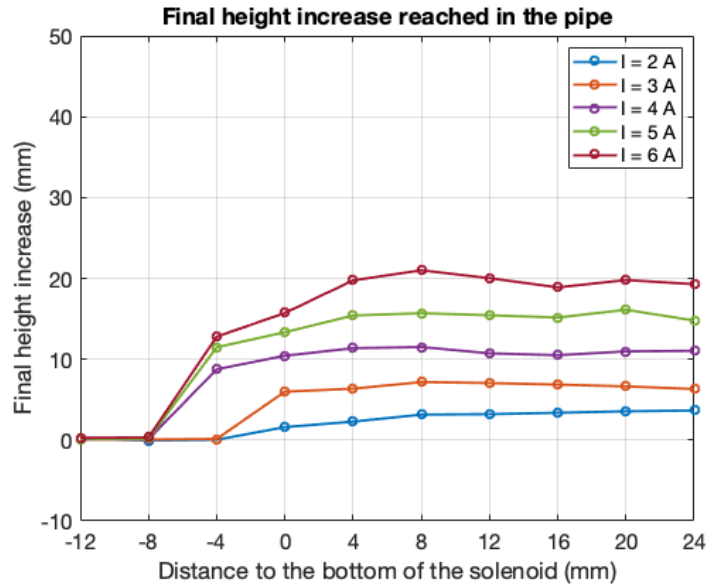


Figure 44: Final height increase in the pipe when the level of the fluid at rest is at different points for the whole range of currents

It is observed that the final height reached increases over the bottom of the solenoid – Kelvin force region – while beyond 4 mm, it remains constant. It is important to point out that the results from this experiment present a significant measurement error, which we noticed later on: the position of the sensor was not fully perpendicular to the liquid surface. Therefore, the height increases shown in Figure 44 are not numerically reliable in full. Nevertheless, the position of the sensor was not changed during the experiment, so the results are valid qualitatively.

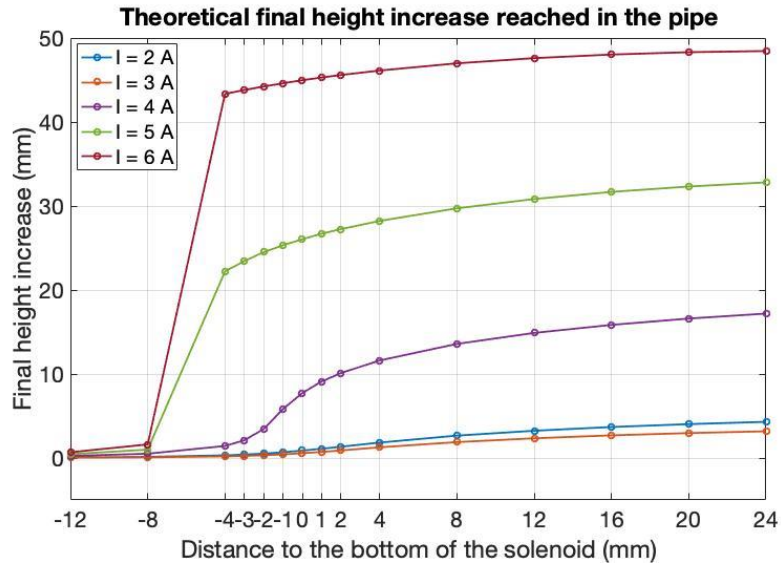


Figure 45: Theoretical evolution of the steady state for the range of currents

Although it is assumed that the height increase is constant beyond a certain level inside the solenoid, the simulations predict otherwise. Instead, the model shows in Figure 45 that even if the trend tends to stabilize, it is never constant. This is due to the fact that the Kelvin force region does not present zero value at any point, which can be observed in Figure 31. Hence, it is checked how the final height increase tends to stabilize while the obtained is totally flat. As in this experiment there was no time of cooling of the coil between experiments, it is assumed that the coil overheated and heated up the ferrofluid, which decrease its magnetization and therefore the final height increase. This fact could be behind the smaller height increase when the fluid rests at higher points.

Chapter 7. Influence of the inclination of the pipe

The previous experiments have been carried out in a vertical pipe in order to simplify calculations. However, the rising pipe of the pump is actually at inclined position. Either way, the same results should be valid for both configurations as the – vertical - height increase is independent from the slope. The physical explanation behind this statement is shown below:

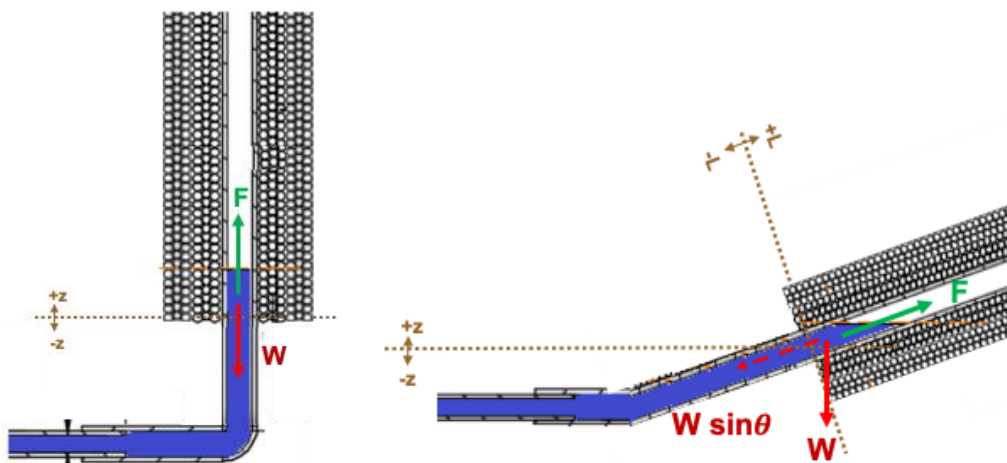


Figure 46: Comparison between vertical and inclined pipe

In the steady state, the body force acting on the fluid is in equilibrium with the weight of the amount of fluid displaced:

$$F = W$$

where both body force and weight are expressed in N/m² This equity is expressed for the vertical pipe as:

$$F_m = \pi r^2 \rho g (\Delta h_A + \Delta h_B) \rightarrow \text{if } \Delta h_A \gg \Delta h_B \rightarrow F_m \approx \pi r^2 \rho g \Delta h_A$$

While for the inclined position:

$$F_m = r^2 \rho g L \sin \vartheta = \pi r^2 \rho g \Delta h_A$$

As one of the main research questions, the following experiment is conducted. The parameters of the set-up are listed below:

- Solenoid
Diameter of the wire: 0.8 mm
Number of turns: 188
Number of layers: 6
Length: 150 mm
Inner diameter: 8,4 mm
- Rising pipe
Slope of the rising pipe: 90° and 37°

The experiments are conducted in the same way as in the previous section. The fluid is positioned at different starting points with respect to the solenoid – in a range of [-12, 8] mm in steps of 4 mm – supplying at different experiments current single steps within the range of [2, 6] A. The steady state of both configurations is studied.

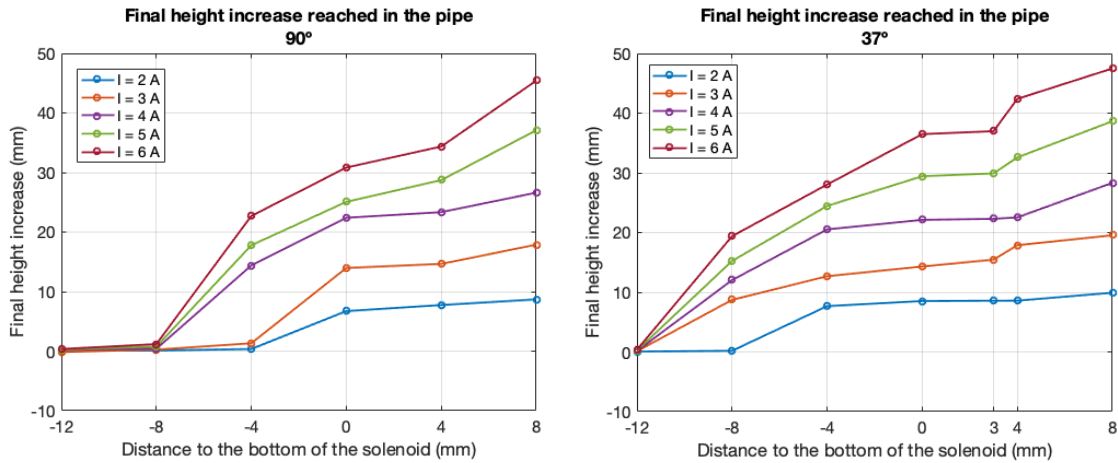


Figure 47: Final height increase reached in the pump for different initial levels and for the whole range of currents

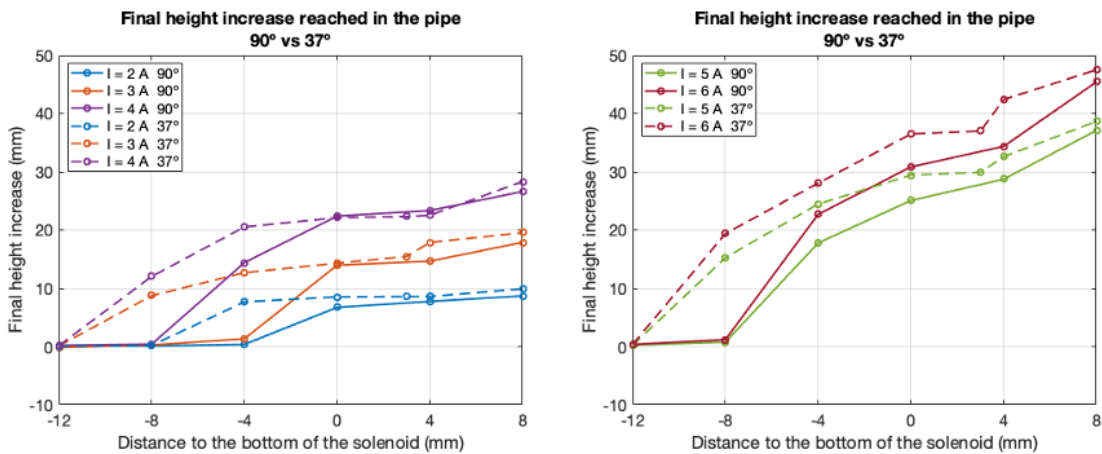


Figure 48: Final height increase reached in the pump for different initial levels and for the whole range of currents

Figure 47 shows the final height increase reached by the fluid in the pipe in both configurations separately, while Figure 48 shows them overlapped with the aim of comparing them.

The graph has been split in turn in two groups. The first one shows the range of currents from 2 to 4 A. On one hand, it can be observed how the height increase in the inclined pipe takes place earlier – at a lower point – than in the vertical configuration. This is explained by the fact that the Kelvin force along the axis is the same for both, but the distribution of the liquid in the pipe is not.

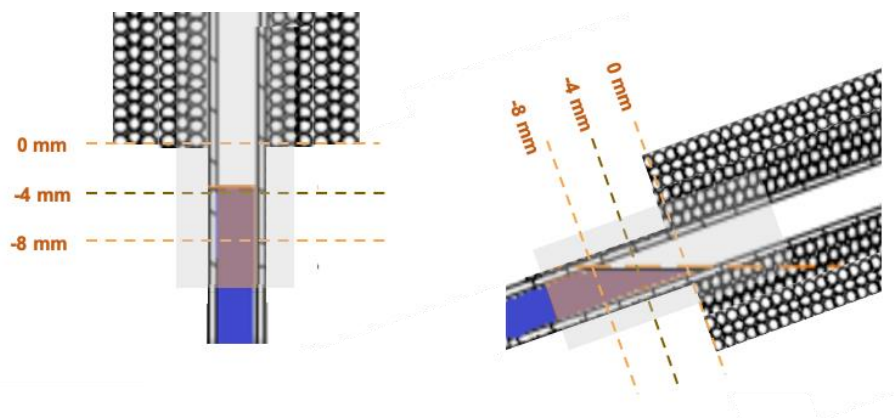


Figure 49: Distribution of the fluid in both configurations

Figure 49 is given to illustrate the case in which both are at -4 mm. When the pipe is vertical, the volume of fluid inside the region – and therefore affected by the gradient – is confined to that point. In the case of inclined position, however, the fluid distribution takes also further points, so the fluid is actually closer to the solenoid. This implies that for the same Kelvin force region – the same given magnetic field – the rising occurs before in the inclined position when compared to the vertical one. In terms of final height increase reached, in the graph we can see a sort of delay of the vertical pipe with respect to the inclined

configuration. As the end of the gradient region is approached – further points above the bottom of the solenoid – the final height increase tends to converge.

It is to be noted, however, that the results carry certain measuring errors as the position of the sensor respect to the liquid surface, or measurement of the slope of the rising pipe.

Chapter 8. Influence of the temperature

According to the theory, the fluid rises upwards the pipe until a point in which the Kelvin body forces cannot support a higher column of ferrofluid. From then on, both forces – body force and weight of the fluid risen – remain in equilibrium on a new level within the pipe. Given a time invariant current source, both the body force and height increase reached in the steady state are expected to remain constant. However, while results verify this in most of the experiments, there is a small portion of cases presenting an unexpected behaviour.

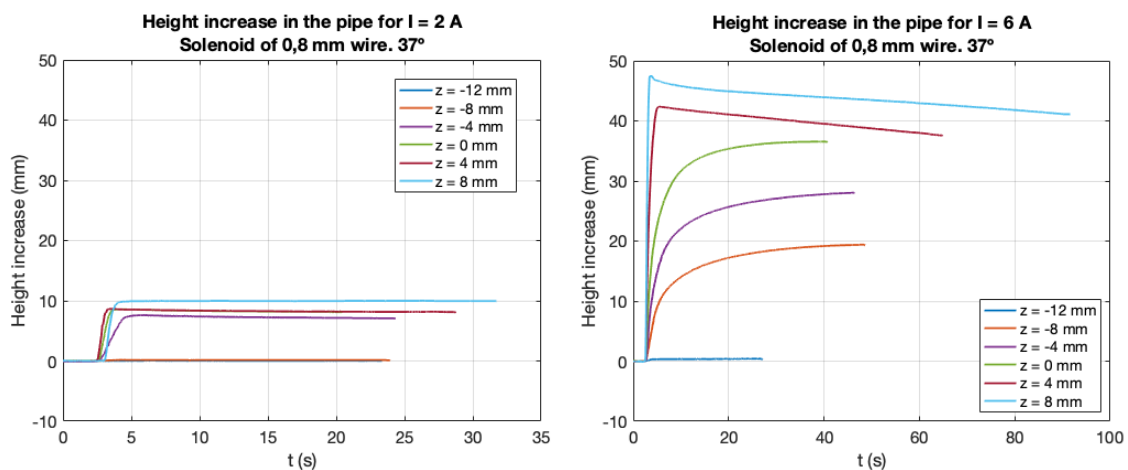


Figure 50: Height increase in the pipe for different initial levels. Comparison between the minimum and maximum value of current within the range. Solenoid of 0,8 mm of wire diameter.

Figure 50 provides an example. It belongs to previous experiments conducted on the pipe in inclined position and the solenoid made of 0.8 mm of wire diameter. The graphs correspond to the minimum and maximum value within the range of current supplied to the coil. It is observed how the height increase reduction takes place for $I = 6 \text{ A}$ and not for $I = 2 \text{ A}$ – the graphs for the rest of values are included in Annex IV. Moreover, the

effect is observed when the fluid rests initially at the highest points. These two factors appear as the common denominator of all the experiments presenting this effect.

A third observation, however, provided the definitive clue of the origin of the phenomenon. The clue consisted of an increase observed in the electrical resistance of the circuit and the cause, its temperature.

In order to analyse this effect separately, an additional experiment is conducted with the thinnest conductor (0.8 mm).

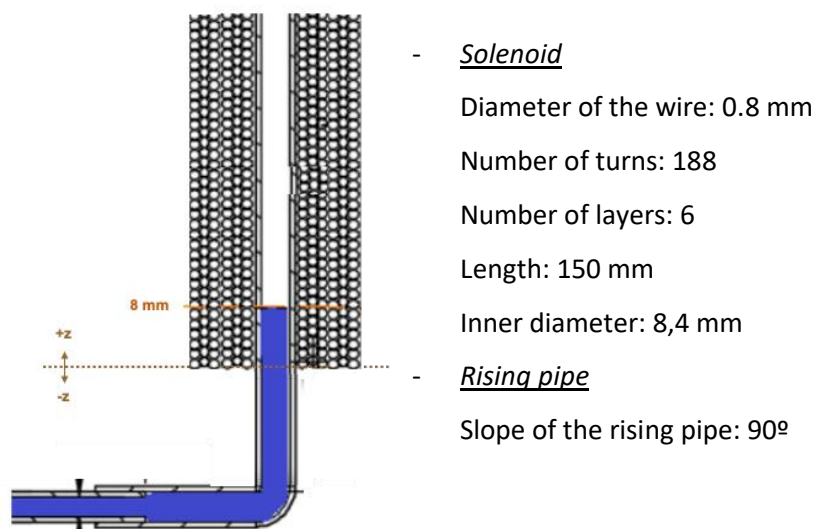


Figure 51: Schematic set-up of the experiment

The experiment takes place right after a whole set of measurements carried out in the same coil – 30 experiments in concrete – between which the coil was not allowed to cool down. In addition, the duration of each measurement is extended in order to observe the evolution.

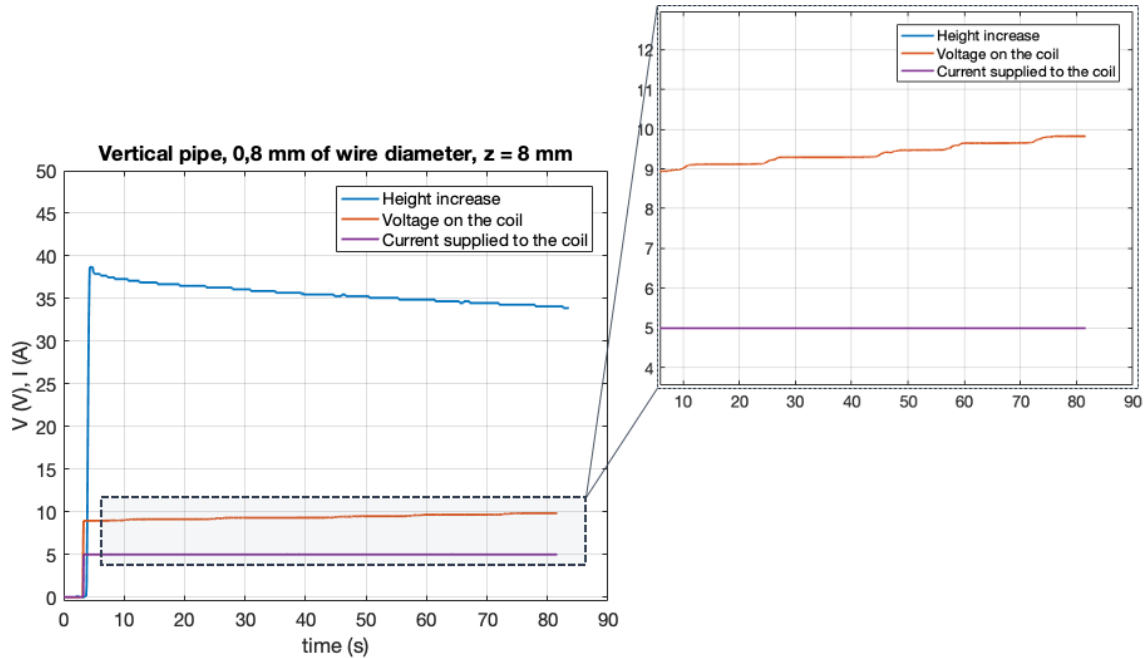


Figure 52: Height increase in the pipe, Voltage and current supplied to the coil. $I = 5 A$

In Figure 52 the case for which $I = 5 A$ is provided as example. The resistance of metallic wires is sensitive to their temperature of operation. This is a result of a faster movement of the electrons inside the conductor, which collide with each other hampering the passing of the current. Figure 52 shows how while the current supplied is fixed, the voltage drop in the circuit increases continuously over time, which is a proof of the temperature dependency of the electrical resistance:

$$(\uparrow)V_{circuit} = I \cdot (\uparrow)R_{circuit}$$

where $R_{circuit}$ is the resistance of the coil and the rest of elements connected to it, and $V_{circuit}$ is the voltage measured at the entrance of the circuit.

When the current exceeds the thermal capacity of the wire for a long while, the insulation cover is not enough and the heat generated inside the conductor is dissipated [20], [24]. The wire current capacity – also called ampacity – is limited by the size of the conductor,

which in the case of the solenoids used in the experiments – 0,8 mm and 1 mm of wire diameter – is pretty low, rounding the 2 A in both cases [21].

As the experiments are planned to have a short duration, this restriction is ignored and values up to 6 A are taken in experiments that had not interruptions. Thus, the effect is more noticeable at higher currents and higher starting levels because of the order of experiments conducted.

Since some heat is transferred to both the plastic pipe and the ferrofluid, their temperature rise. The height increase reduction observed in the ferrofluid is a result of the inverse relationship between temperature and magnetization [22], [23].

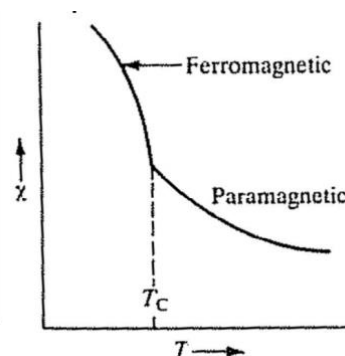


Figure 53: Temperature dependency of magnetic susceptibility [22]. It should be noted that only the ferromagnetic region is of interest, as the Curie temperature is never exceeded (T_c).

where χ is the magnetic susceptibility and T_c the Curie temperature, above which ferromagnetic materials lose their magnetic properties. Hence, the overheating of the coil produces a temperature increase in the ferrofluid which weakens the body forces and therefore, the height increase in the pipe.

The problem of temperature rise may affect not only the final phase of a particular

experiment; it may also alter the conditions of successive experiments.

During the subsequent experiments, the phenomenon was taken into account and prevented by allowing the coil to cool down between the measurements with the help of a fan at times, during a period that was previously estimated according to the wire characteristics.

Chapter 9. Influence of the input-current shape

The height increase reduction over time observed for high current values suggested a possible overshoot in the movement of the fluid, which could be related to a high step value in the magnetic field generated in the coil. There are significant evidences to attribute the phenomenon to a temperature increase in the fluid. Nevertheless, different time-varying current signals are supplied to the coil with the aim of exploring how the step input affects to the rising process.

Two similar experiments are conducted in the following set-up (Figure 54).

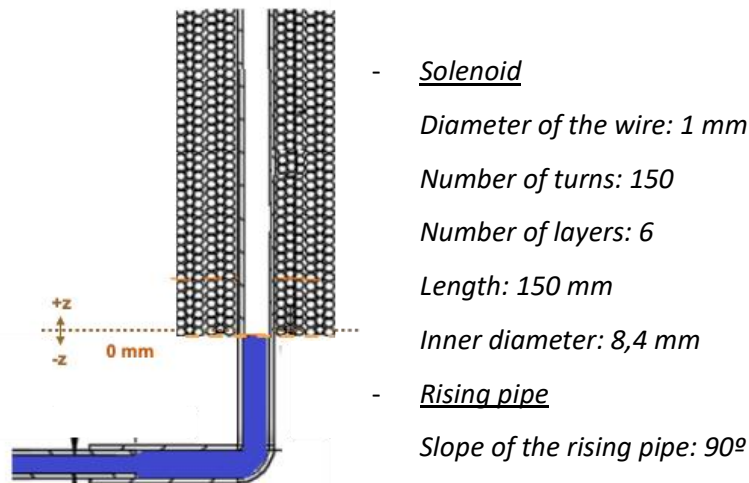


Figure 54: Set-up of the experiment

As Figure 54 shows, the fluid begins at rest right at the bottom of the solenoid level ($z=0$) and the range of current values used do not exceed 6 A. However, rather than applied a

single step value at a time, a time-varying current that goes from 0 A to 6 A is used. In the first experiment, the current is kept constant at 1 A steps, in order to reach the steady state at each current value just as previous experiments. Figure 55 shows both input and output of the experiment – represented by the black lines – in contrast to those conducted for each step current separately at the same spot ($z=0$).

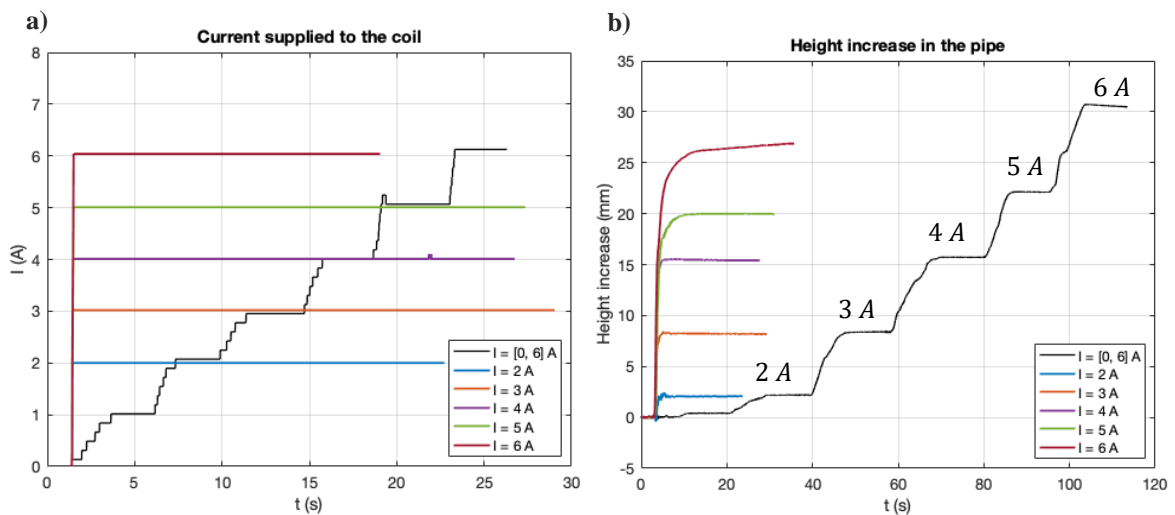


Figure 55: a) Current input comparison. b) Height increase in the pipe comparison

It is observed in Figure 55 how the steady states reached at each interval meet the values obtained for the corresponding single steps only for $I = [2, 4]$ A interval. For $I = 5$ A and $I = 6$ A, however, a higher final height increase is reached in the pipe.

The next experiment provides similar results. The current supplied to the coil is varied from 0 A to 6 A again, but without the intermediate steps. Only the final value remains constant.

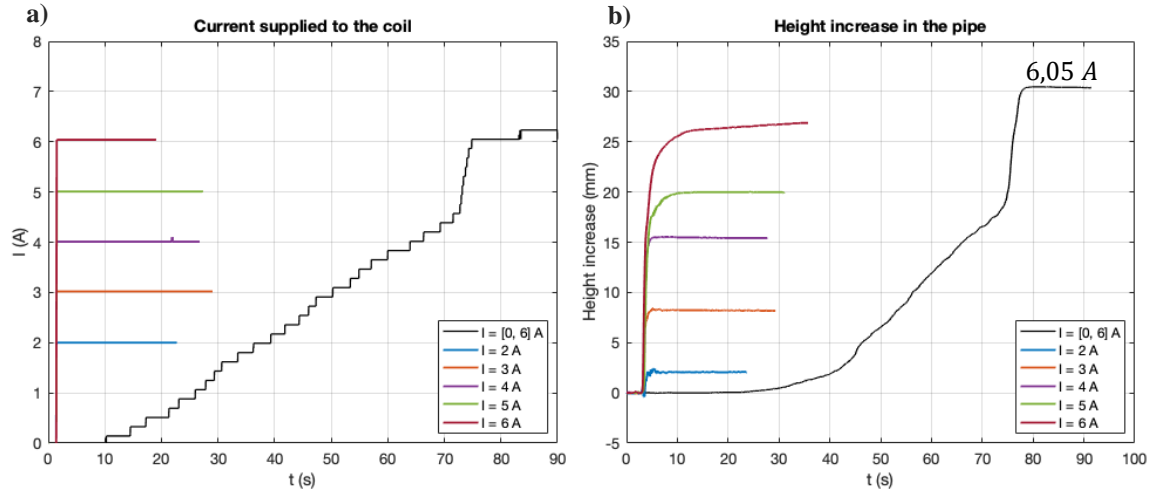


Figure 56: a) Current input comparison. b) Height increase in the pipe comparison

Figure 56.b shows how the final height increase is higher than expected when compared to the corresponding 6 A step input.

It is not easy to find a logical explanation. On one hand, the fact that the steady state from both time invariant and variant current inputs match is expected if the final body force acting on the fluid is the same – the final height increase is only dependant on the magnetic body force in the steady state. On the other hand, a time-varying current induces a magnetic field presenting a time dependence. Therefore, the magnetic field gradient with respect to a new variable is a new factor subject to influence the ferrofluid behaviour in the final steady state. The fact that the mismatch is only given for the highest currents is what results to be surprising. Especially considering that the temperature effect is a controlled parameter in this section – measures against overheating were taken – which could be involved in the difference in behaviour observed for lower and highest currents.

The fact that the non-linearity given only for high values of currents results when comparing both inputs might be related to a non-linear magnetization. The saturation magnetic field in EFH1 is 44 mT, which is less than the expected magnetic fields given for

high currents in that solenoid – see Annex IV. It is assumed that only the linear part of the magnetization curve is used [12], hence this factor could be playing a role.

Chapter 10. Sensitivity analysis

The main factors affecting the rising process have already analysed and compared experimentally. These factors consist of the current supplied to the coil – in magnitude and form – and the initial position of the fluid respect to the solenoid. Others, as the angle of inclination of the rising pipe are theoretically compared in previous research work [13], which used a model to study the sensitivity of the outcomes to those variables. Maintaining the focus on the Kelvin force region and transient state of the fluid, this chapter studies the sensitivity of the ferrofluid to different magnitudes: density of turns in the coil – which has a direct impact on magnetic field magnitude – and the length of the solenoid, aiming at studying the its influence on the Kelvin force region boundaries.

The base-line case takes the parameters from the experiments conducted in Chapter 6, in which the wire of the coil has 1 mm of diameter and the length of the coil is 15 cm – this parameter is kept constant through the experiments. Here, the effects of varying the diameter of the wire and the length of the coil are studied.

9.1 DIAMETER OF WIRE

The solenoids used in the experiments are both of the same length and number of layers, but a different size of wire – 1 mm and 0.8 mm. This fact results in a different total number of turns that will induce a greater magnetic field in the case of the thinnest wire. Both coils are used in similar experiments, in which the fluid level at rest is changed to variate the distance to the solenoid and the values of current applied are the same. This is also reproduced in this section in a theoretical way, in which the separate effect of increasing the coil density is to be analysed when the rest of factors remain constant.

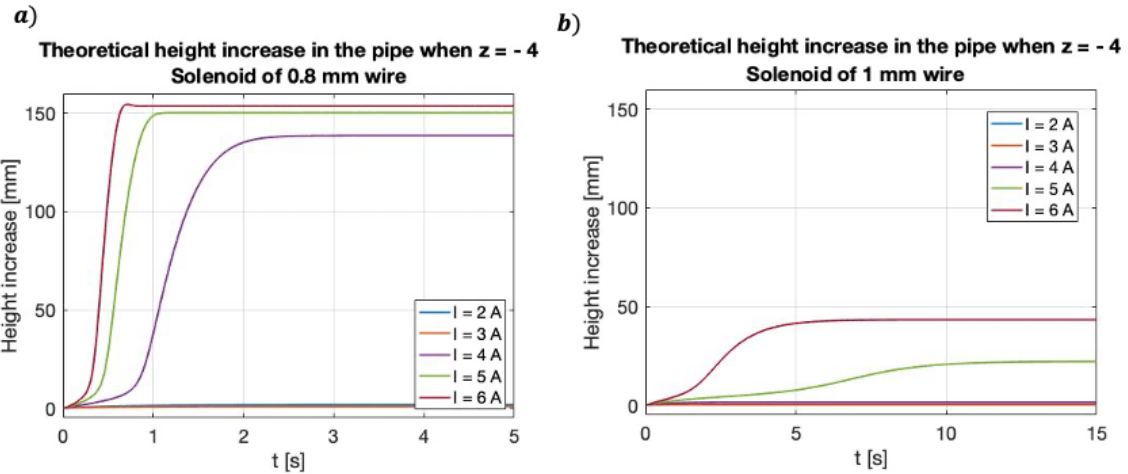


Figure 57: Comparison of fluid behavior for a) 0.8 mm of wire diameter and b) 1 mm of wire diameter

The number of turns changes from 150 to 188 when using the 0.8 mm of wire diameter solenoid instead of that of 1 mm. This results in a 25 % higher magnetic field intensity.

$$\frac{H_{d_w=0.8\text{ mm}}}{H_{d_w=1\text{ mm}}} = \frac{N_{d_w=0.8\text{ mm}}}{N_{d_w=1\text{ mm}}}$$

Figure 57 shows, however, how the fluid response significantly exceeds that value, and reaches a three times higher level at least for $I = 4\text{ A}$, $I = 5\text{ A}$ and $I = 6\text{ A}$, presenting a high sensitivity.

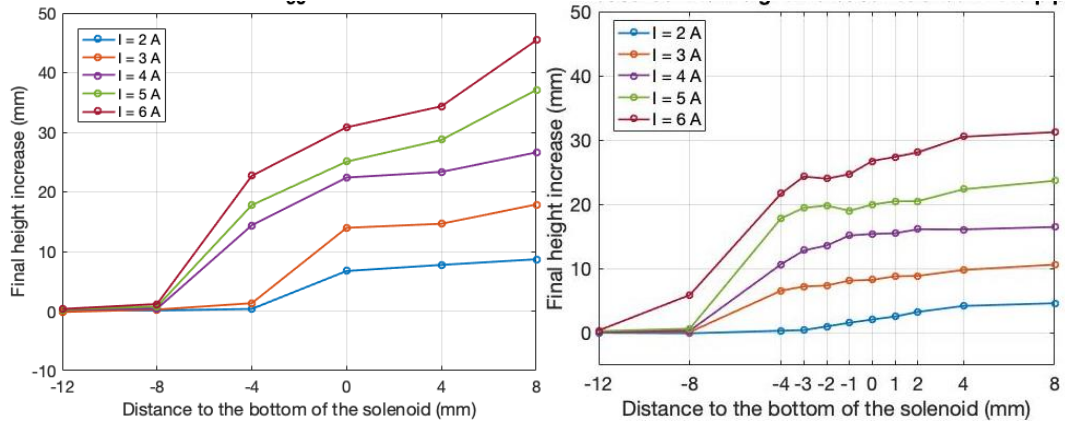


Figure 58: Final height increase for a) Solenoid of 0.8 mm of wire diameter. b) Solenoid of 1 mm of wire diameter.

As shown in Figure 58, when compared the static conditions for both solenoids, higher levels are reached for the 0.8 mm wire. However, it is not a significant difference. It must be taken into account that in the case of 0.8 mm, the quantitative results might be incorrect because of the sensor position.

9.1 LENGTH OF THE COIL

The length of the rising pipe is one of the factors analysed in the previous theoretical research [13], as it is one of the design parameters to be optimized. In this case, the focus is put on the fluid dynamic response to this parameter, which is only theoretically analysed as in the experiments did not change.

It is studied as an example the case in which the current has a value of 5 A and the fluid is initially resting right in the bottom. The only parameter changing is the length of the coil which takes (a) the half and (b) the double of the base-line case value.

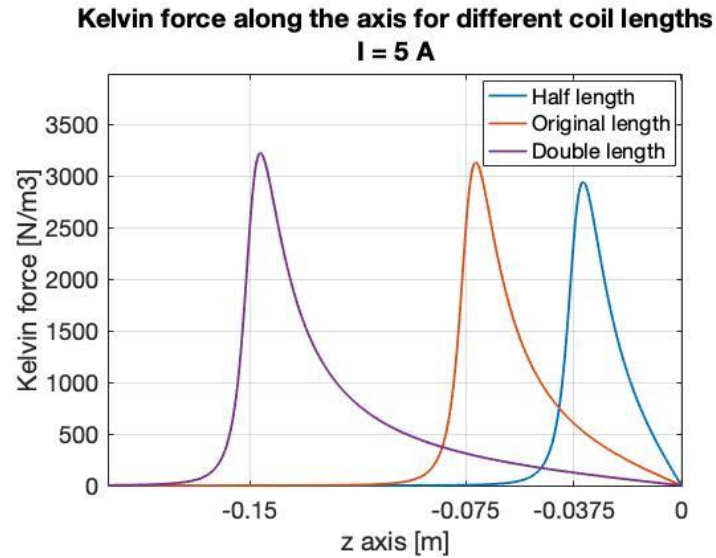


Figure 59: Kelvin body force comparison for different coil lengths

In Figure 59 it is shown how the length of the solenoid practically only affects to the extent of the Kelvin force region – the magnitude comparison is not that significant. To analyse the effect that this can have on the dynamic response, the fluid is positioned at the same distance from the bottom of the coil in all cases. Graphs below present the outcome for this factor.

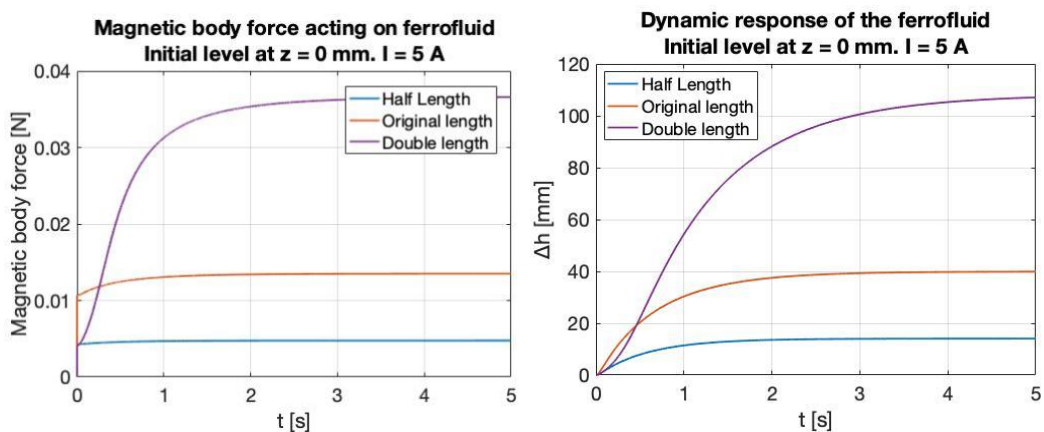


Figure 60: Dynamic response comparison

Figure 60 shows how, although the Kelvin force magnitudes are not that different, the height increase in each one of them increase with the length of the solenoid as the area of the region increases as well.

Chapter 11. The magnetic pump set-up

So far, the aim of the research has been focused on the analysis of the real processes taking place when the magnetic field is active. Thus, the influence that certain parameters have on the rising are explored with the aim of determining the values that optimizes the process. In the target system, the pump, there are more factors involved in performance. The final goal is to optimize the design, which has been carried out theoretically [13] and experimentally in the first research conducted [12]. Despite the fact that experiments on the pump could not be performed for external reasons, the design of the set-up as well as the experiments planning are introduced with the aim of contributing to the further work.

The pump construction is similar to the previous configurations but with some exceptions. The first one is obviously the presence of the falling pipe. The other lies in the pipe used, which in contrast to the previous experiment is rigid, so that a change of inclination is not possible.

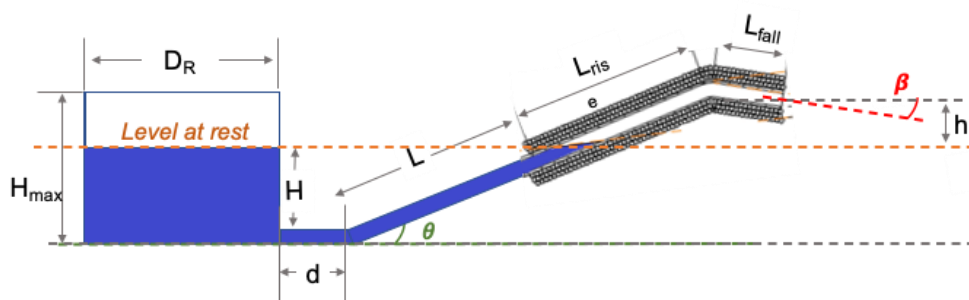


Figure 61: Scheme of the experimental set-up of the pump

All the parameters are included in Figure 61. D_R and H_{max} represent the diameter and height of the reservoir, d is the length of the horizontal tube connecting the pipe to the

reservoir, and θ and β are the slopes of the rising and falling pipe respectively. L is the length of the area of the rising pipe without coil and L_{rise} and L_{fall} are the respective proportions of the total length of the solenoid placed on both pipes.

$$L_{solenoid} = L_{rise} + L_{fall}$$

Finally, h represents the difference of height between the level of the fluid and the outlet of the pump, which must be present to have a real pumping effect – otherwise the fluid would come out due to siphoning effect.

What is pursued here is to find the combination of all of these parameters – together with the electrical variables – that obtain the best performance of the pump, which is quantified through the flow rate.

Thus, the idea is to take a range of values for all these variables and apply them in multiple experiments just as done previously when varying the initial level and the current supplied. While the latter is included as a variable, the initial level of the fluid is decided to rest inwards the solenoid – from the rising pipe. There are two reasons behind this. It should be taken into account that the volume of ferrofluid in this case is not constant, as it is supposed to come out through the outlet during the pumping. The level at the inlet is hence expected to be reduced during the experiments, which will end up resulting in a weaker magnetic attraction. On the other hand, previous results proved that the higher the level in the pipe, the faster the response of the fluid when rising. The solenoid used has the same length of 15 cm but is made of a wire of 2 mm of diameter and 3 layers. For the coil length fixed, the lengths of both the rising and falling pipe depend on each other according to last equation. Given also that the structure of the set-up is practically fixed, the possible combination of parameters turns out to be quite limited. Figure 62 shows a possible solution.

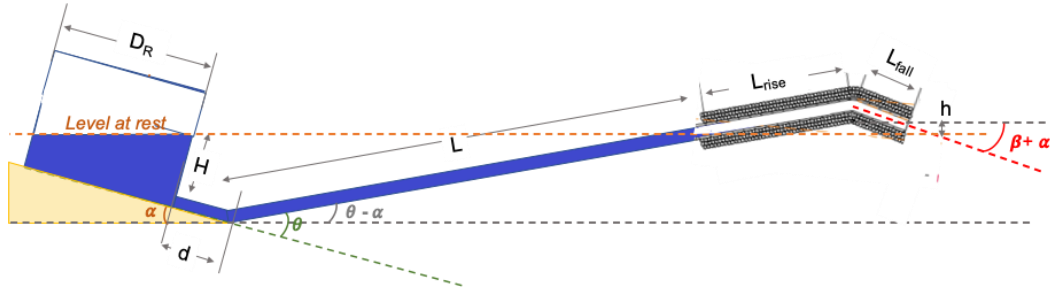


Figure 62: Design of the experiments

As the tube of the pump in this case is chosen to not be flexible, the slope of both rising and falling pipe is varied by means of a wedge that can be adjusted in inclination, represented by α in Figure X. The length of the total rising pipe L can be also varied with the level of the fluid – variable H in the scheme – and the position of the solenoid – and hence L_{rise} and L_{pipe} variables. The length of the pipe can be estimated according to the following equations.

$$L = \frac{\sin \alpha}{\sin(\theta - \alpha)} d + \frac{H \cos \alpha}{\sin(\theta - \alpha)}$$

$$L_{fall} = L_{solenoid} \cdot \frac{\sin(\theta - \alpha)}{\sin(\theta - \alpha) + \sin(\beta + \alpha)} + \frac{h}{\sin(\theta - \alpha) + \sin(\beta + \alpha)}$$

where:

$$\theta > \alpha, \quad h > 0, \quad H \leq H_{max}$$

The interdependence of the variables in the design, however, make it a very constrained problem. For example, the lengths of rising pipe are required to be excessively long to obtain a proper range of values of its inclination. H , in turn, is limited by the minimum amount of fluid needed in the reservoir. It should be considered that the level of the fluid

is measured in the reservoir. When it is inclined, the height increase relationship between the pipe and the reservoir is no longer valid. For this reason, a new reservoir is built, which is designed to be deeper below the tube, easing some of the limitations.

There can be different alternatives to the presented experimental set-up. For example, a set of pipes presenting different slopes can be built to eliminate the constant dependence of θ and β . Nevertheless, it is preferable to keep the same set-up in terms of repeatability of results.

Chapter 12. Conclusions

An experimental research on the magnetic pump of a novel magnetic refrigeration system is conducted in this Thesis. Previous studies [12] proved the feasibility of the pump and provided a base-line model from which a more careful analysis has been conducted. Such analysis has been done in two ways: theoretically, by defining the equations governing the fluid and the physics of FHD pumping in [13], and experimentally in this project, by measuring the real process in the pump taking the theory into practice. Both studies are conducted simultaneously in such a way that both works are complemented sharing the ultimate goal of defining and optimizing the model of the pump in view of a future implementation. The project was structured in two parts. First the analysis of the rising process and the internal processes in the fluid. Second, was to put the same level of detail on the pump, also compared with previous analysis. This last part, however, could not be finished, although Chapter 10 includes the experimental design done.

All the experiments carried out in this thesis are relevant in qualitative terms and help understanding the behaviour of the pump. However, only the ones described in Chapter 6 provided fully reliable results, because all the set-up mistakes (or inconsistencies) detected in the previous experiments were already solved. In addition, this work includes an extension from the previous model to obtain more realistic processes, as shown in results. The adjusting and correction of the experimental methods allowed not only reliable results, but also the identification and analysis of actual unexpected effects, which were also subject to affect the magnetic pump.

With respect to future developments, the project makes clear the need for a careful and strict way of performing the experiments. It is worthy to include elements of high precision – as the sensor used – and mostly elements that are not obviously important at first. For example, reliability could be improved by assuring the strict inclination required for the

pipe. Another key issue is to assure the strict repeatability of experiments, in order to identify measuring or set-up errors. It is always worth to devote enough time and thinking to the design and specification of experiments (set-ups, devices, cases, method), stressing on their quality instead of their quantity. Every detail counts specially when working at such small scale and with such a small resolution. Factors and details that seem to be neglectable end up being crucial.

Chapter 13. Magnetic refrigeration and sustainable development

Renewable energy resources are one of the most powerful long-term solutions to face the environmental problems that we are currently facing. It is well-known that global warming and the pollution of the environment are mainly caused by the human activities. The refrigeration sector, particularly, plays an important role. Chlorofluorocarbons (CFCs) and chlorofluorocarbons (HCFCs), compounds used for years as refrigerants, have proven to contribute to the ozone layer destruction. Magnetic refrigeration arises as a promising eco-friendly alternative to the traditional technologies that use harmful substances. Thus, magnetic refrigeration has the potential to reduce the energy consumption in the refrigeration sector and thus become an environmentally sustainable technology, as it has no direct impact during their usage.

The development of this technology contributes to increase the share of clean energy in the total energy consumption, which is directly aligned with different sustainable development goals [30]. The main goal in which this technology has an impact is the thirteenth objective: to take urgent action to combat climate change and its impacts, as magnetic refrigeration is presented as a clean technology that has the potential to substitute part of the polluting conventional systems in the sector. Moving to a more economic dimension, it can also be related in a smaller extent to the ninth goal, in the way of the investment in Research and Development. Magnetic refrigeration technology is a result of the research encouraged to find solutions to environmental challenges and to energy efficiency problems.

References

- [1] Calm, James M. Emissions and environmental impacts from air-conditioning and refrigeration systems. United Kingdom: N. p., 2002. Web. doi:10.1016/S0140-7007(01)00067-6.
- [2] Preserving Montreal Protocol Climate Benefits by Limiting HFCs. By Guus J.M. Velders, A. R. Ravishankara, Melanie K. Miller, Mario J. Molina, Joseph Alcamo, John S. Daniel, David W. fahey, Stephen A. Montza, Stefan reimann.
- [3] Houssef Rafik El-Hana Bouchekara and Mouaz Nahas (2012). Magnetic Refrigeration Technology at Room Temperature, Trends in Electromagnetism - From Fundamentals to Applications, Dr. Victor Barsan (Ed.)
- [4] Yu, BF & Gao, Q & Zhang, Bin & Meng, XZ & Chen, Z. (2003). Review on research of room temperature magnetic refrigeration. International Journal of Refrigeration. 26. 622-636. 10.1016/S0140-7007(03)00048-3
- [5] M. Balli, C. Mahmed, O. Sari, F. Rahali, J. C. Hadorn. Engineering Of The Magnetic Cooling Systems: A Promising Research Axis For Environment And Energy Saving. World Engineers. Convention, Sep 2011, Genève, Switzerland. hal-01185990
- [6] H. N. Kothiya, "A seminar on Magnetic refrigeration," *Department of mechanical engineering - Vivekananda Institution of Technology*, 2014
- [7] "Magnetic cooling" - Refrigeration industry (<https://refindustry.com/articles/articles/magnetic-cooling/>)
- [8] M. Balli, C. Mahmed, O. Sari, F. Rahali, J. C. Hadorn. Engineering Of The Magnetic Cooling Systems: A Promising Research Axis For Environment And Energy Saving. World Engineers' Convention, Sep 2011, Genève, Switzerland. hal-01185990
- [9] B.O. Bolaji, Z. Huan, Ozone depletion and global warming: Case for the use of natural refrigerant – a review, Renewable and Sustainable Energy Reviews, Volume 18, 2013, Pages 49-54, ISSN 1364-0321, <https://doi.org/10.1016/j.rser.2012.10.008>.
- [10] J. Romero Gómez, R. Ferreiro Garcia, A. De Miguel Catoira, M. Romero Gómez, Magnetocaloric effect: A review of the thermodynamic cycles in magnetic refrigeration, Renewable and Sustainable Energy Reviews, Volume 17, 2013, Pages 74-82, ISSN 1364-0321, <https://doi.org/10.1016/j.rser.2012.09.027>.
- [11] Smith, A. Who discovered the magnetocaloric effect?. EPJ H 38, 507–517 (2013). <https://doi.org/10.1140/epjh/e2013-40001-9>

- [12] Luca Granelli. Faculty of Engineering Technology Sustainable Energy Technology Analysis of magnetic pumping for magnetic refrigeration applications. PhD thesis, 2019
- [13] Jeroen Mathijs Boerma. Faculty of Energy, Materials and systems. Pumping of a magnetic fluid by means of an alternating magnetic field; a ferrohydrodynamic model. Bachelor Thesis.
- [14] Mao, L., Elborai, S., He, X., Zahn, M., & Koser, H. (2011). Direct observation of closed-loop ferrohydrodynamic pumping under traveling magnetic fields. *Physical review B*, 84(10), 104431.
- [15] Hegde, B., Dinesh, N.S. Design, development and characterization of variable reluctance ferrofluid pump. *Microsyst Technol* 23, 5023–5040 (2017). <https://doi.org/10.1007/s00542-017-3363-3>
- [16] A. Hatch, A. E. Kamholz, G. Holman, P. Yager and K. F. Bohringer, "A ferrofluidic magnetic micropump," in *Journal of Microelectromechanical Systems*, vol. 10, no. 2, pp. 215-221, June 2001.
- [17] Hertanu, Radu & Olaru, Radu. (2013). A novel minipump actuated by magnetic piston. *Journal of Electrical Engineering*. 61. 148-151.
- [18] Gwan Soo Park and Sang Ho Park, "Design of magnetic fluid linear pump," in *IEEE Transactions on Magnetics*, vol. 35, no. 5, pp. 4058-4060, Sept. 1999, doi: 10.1109/20.800754.
- [19] K. L. Tsai et al., "Magnetic nanoparticle-driven pumping in microchannels," *TRANSDUCERS 2009 - 2009 International Solid-State Sensors, Actuators and Microsystems Conference*, Denver, CO, 2009, pp. 2274-2277, doi: 10.1109/SENSOR.2009.5285889.
- [20] TSSf005.00 Wire Size & Current Rating Guideppt. https://www.jst.fr/doc/jst/pdf/current_rating.pdf
- [21] Block components AWG, Available: <https://docs.rs-online.com/731b/0900766b8121899a.pdf>
- [22] Chapter 8: Magnetical and Electrical Properties. https://www.unf.edu/~michael.lufaso/chem4627/ch8_solid_state.pdf
- [23] "Magnetic susceptibility". *Encyclopedia Britannica*, Inc. 2o December 2006. Available: <https://www.britannica.com/science/magnetic-susceptibility>
- [24] David D. Evans "Calculated Operating Temperatures of Thermally Insulated Electric Cables" National Bureau of Standards. Available: <https://www.govinfo.gov/content/pkg/GOVPUB-C13->

-
- [301a9f4c05b826df45326ea608ad780f/pdf/GOVPUB-C13-301a9f4c05b826df45326ea608ad780f.pdf](https://www.comillas.edu/301a9f4c05b826df45326ea608ad780f/pdf/GOVPUB-C13-301a9f4c05b826df45326ea608ad780f.pdf)
- [25] Khushrushahi, Shahriar & Zahn, Markus. (2020). Understanding Ferrofluid Spin-Up Flows in Rotating Uniform Magnetic Fields.
- [26] PicoTech PicoScope serie 2000 datasheet. Available: <https://www.picotech.com/download/datasheets/PicoScope2200-es.pdf>
- [27] Project Elektronik Teslameter FM 302 for AS-active-probes. Available: <https://www.projekt-elektronik.com/wp-content/uploads/sites/3/data-sheet-Teslameter-FM-302-0204-19.pdf>
- [28] AIM & THURLBY THANDAR INSTRUMENTS LTD. TSX Series. TSX1820. Available on: [http://resources.aimtti.com/manuals/TSX-P Instruction Manual-Iss16.pdf](http://resources.aimtti.com/manuals/TSX-P%20Instruction%20Manual-Iss16.pdf)
- [29] K.A. Gschneidner, V.K. Pecharsky, Thirty years of near room temperature magnetic cooling: Where we are today and future prospects, International Journal of Refrigeration, Volume 31, Issue 6, 2008, Pages 945-961, ISSN 0140-7007, <https://doi.org/10.1016/j.ijrefrig.2008.01.004>. (<http://www.sciencedirect.com/science/article/pii/S0140700708000236>)
- [30] <https://www.un.org/sustainabledevelopment/>

ANNEXES

ANNEX I. Instruments and measuring devices used

1. POWER SUPPLY UNIT

The DC power supply TSX 1820 DC PSU [28] is used as a current source, allowing to regulate the current output in a range of [0 , 20] A with a sensibility of 0.01 A. It has a limited load of 360 W, allowing a maximum voltage of 18 V in the terminals.



Figure 63: Model TSX1820 [28]

Supplier	Model	Current range [A]	Voltage range [V]	Resolution [A] [V]	Current accuracy [A]	Voltage accuracy [V]
AIM & THURLBY THANDAR INSTRUMENTS LTD.	TSX1820	26,3	7,4	0.01	0.5% of reading ± 1 digit	0.2% of reading ± 1 digit

2. OSCILLOSCOPE

The oscilloscope used is PicoScope 2205A. from PicoScope 2000 A Series [26]. It is a small-size compact device that measures inputs of up to 20 A.



Figure 64: PicoScope2205A [26]

Supplier	Model	Input sensitivity[V/div]	Input range [V]	DC accuracy [A]
PicoTech.	PicoScope 2205A	10 mV/div to 4V/div	± 0.05 to ± 20	3% of full scale $\pm 200 \mu\text{V}$

3. TESLAMETER

The magnetic field is measured with the Teslameter FM 302, Projekt Elektronik [27]. The axial probe is introduced in the coil and traverses through the axial direction by means of a motorized positioning system which. The signal is recorded with the oscilloscope which allows to obtain the waveform of the magnetic field induced in the empty coil along the axial position.

Supplier	Model	Probe factor [V/T]	Input range [mT]	Linearity error
Projekt Elektronik	Teslameter FM 302	1	± 20 to ± 2000	$<0.5\% \pm 0.2$ mT

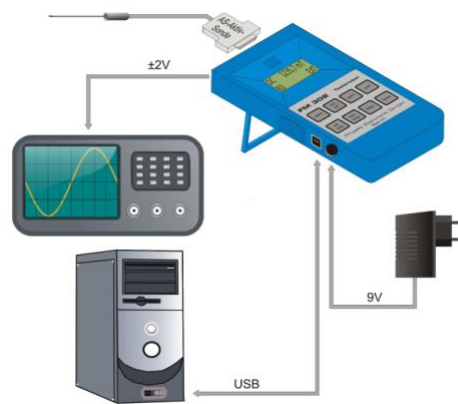


Figure 65: Connection scheme of the teslameter

4. CONFOCAL CHROMATIC SENSOR

The measuring system used consists of a confocal chromatic sensor, which consists of a controller with a white LED light source and a sensor incorporated. The measurement principle works by focusing the polychromatic light beam onto the target surface by means of a multi-lens system that is arranged in such a way that the light is dispersed into different monochromatic lights that are deviated in assigned wavelengths as Figure 66 shows.

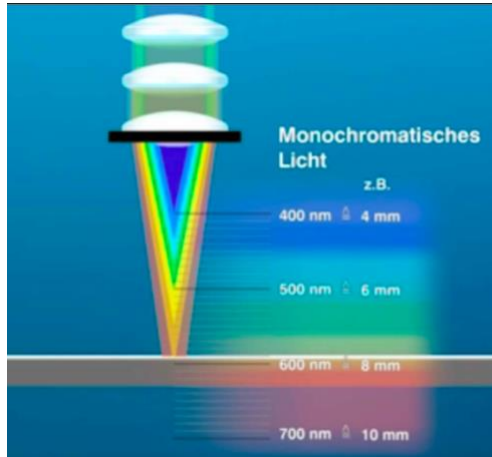


Figure 66: Working principle of the confocal sensor

This way, only the wavelength that reaches the target is reflected, detected by the sensor and evaluated assigning it a distance. In short, it can be considered as a very precise ruler in which the distances are assigned by the different wavelengths dispersed from the source – monochromatic lights.

The sensor used is the model CL-L030 from Keyence, which allows to detect targets within a measuring range of ± 3.7 mm at a reference distance of 30 mm.

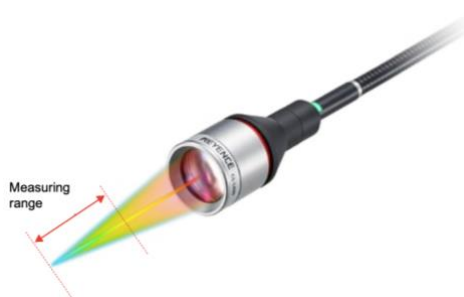


Figure 67: Confocal sensor

Supplier	Model		Start of measuring range [mm]	Measuring range [mm]	Resolution (μm)	Linearity [μm]	Light spot diameter [μm]
Keyence	CL-L	CL-L030	26,3	7,4	0,25 (0,015)	$\pm 0,94$ ($\pm 0,81$)	500

ANNEX II. Experiments conducted

Annex I and II are dedicated to show the appearance of the real set-ups used through this project. This section includes those experiments in which the sensor was used, while next one focuses on the magnetic field built and the solenoids.

1. SELECTION OF THE SENSOR

The sensor utilized in the experiments – which is described in Annex I – was previously tested and compared with others before its selection. In fact, the search for a suitable sensor proved to be a challenging task due to the particular characteristics of the set-up. The objective was to find a very precise measuring system which could monitor the height increase inside the pipe from the top of the tube. The device was required to be small enough to fit into the pipe – of 6 mm of inner diameter – and have a measuring range which could detect the height increases expected in the tube. However, a suitable option could not be found as those two requirements were not compatible. The movement of the fluid was then decided to be measured from the top of the reservoir, assuming equality in the volume displaced in both spots. Different accurate technologies were explored to select the displacement sensor before the experimental research could be started. Most of the options belonged to the ToF (“Time of Flight”) sensors group in which the distance to the target -or displacement of the target- is obtained by measuring the time between the emission and the reception of the light signal. However, only the confocal chromatic technology proved to work on the ferrofluid – which had to be tested as none of them had experience with EFH1.

Within this technology, two different models from separate companies were tested and compared to select the definitive one. The experiments performed for that aimed at

analysing the performance of the sensors in water, introducing different substances to study their sensitivity to concentration, and ferrofluid. Both proved to be suitable for ferrofluid and the model with the best error linearity was chosen

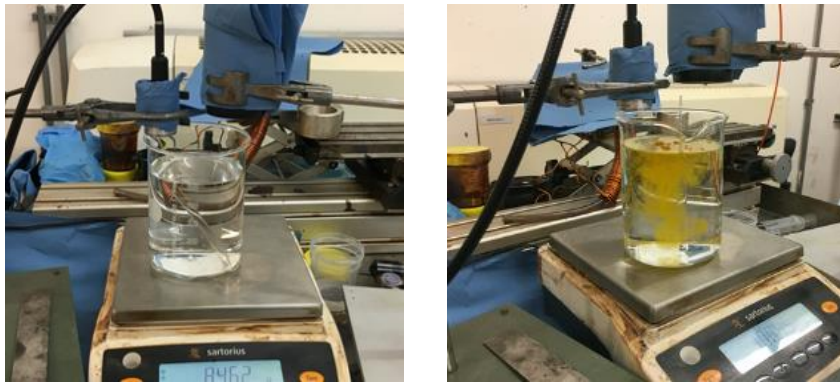


Figure 68: Experiments conducted for selecting a sensor

2. ANALYSIS OF RISING PROCESS. SOLENOID – 1 MM

The pictures included in this section represent the set-up belong to those experiments that make use of the solenoid with 1 mm of wire diameter, which is only tested with the pipe in vertical position (Figure 69). The corresponded experiments are included in Chapter 6 – transient and steady state analysis of the rising process – and chapter 9 – influence of the input-current shape.

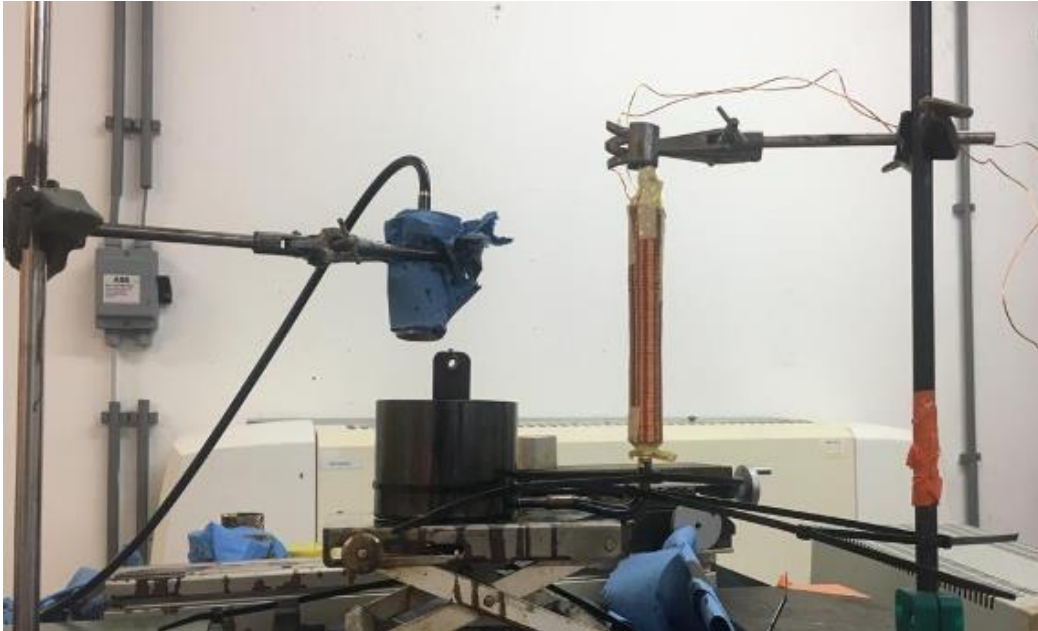


Figure 69: Set-up with the pipe in vertical position. Solenoid 1 mm

The different heights at which the fluid is positioned respect to the coil are represented in Figure 70. The reservoir is filled up to the lowest point from the set of trials – at -12 mm from the bottom of the coil – and marked in the plastic tube as a reference for the next ones. From then on, the heights for next trials are set with the help of the sensor, which displays the actual level of the fluid in the reservoir, allowing to accurately fill it up to the next point. Of course, the level of the pipe is the same of that of the reservoir as the fluid is at rest.

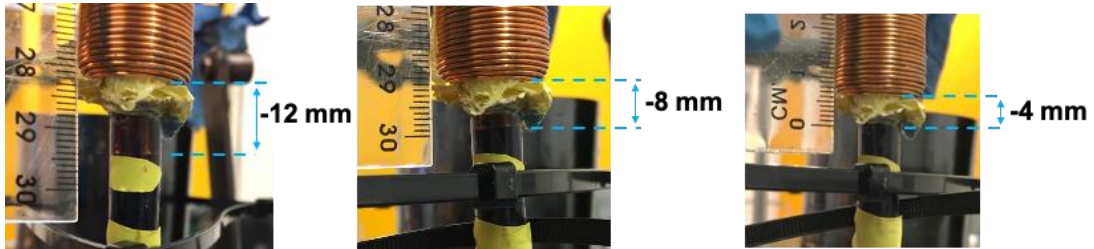


Figure 70: Different initial levels of the fluid respect to the solenoid

3. ANALYSIS OF THE RISING PROCESS. SOLENOID – 0.8 MM

The set-ups shown below belong to the experiments included in chapter 7 and 8, which are focused on the influence of the inclination of the pipe (Figures 71 and 72) and the effect of temperature respectively.

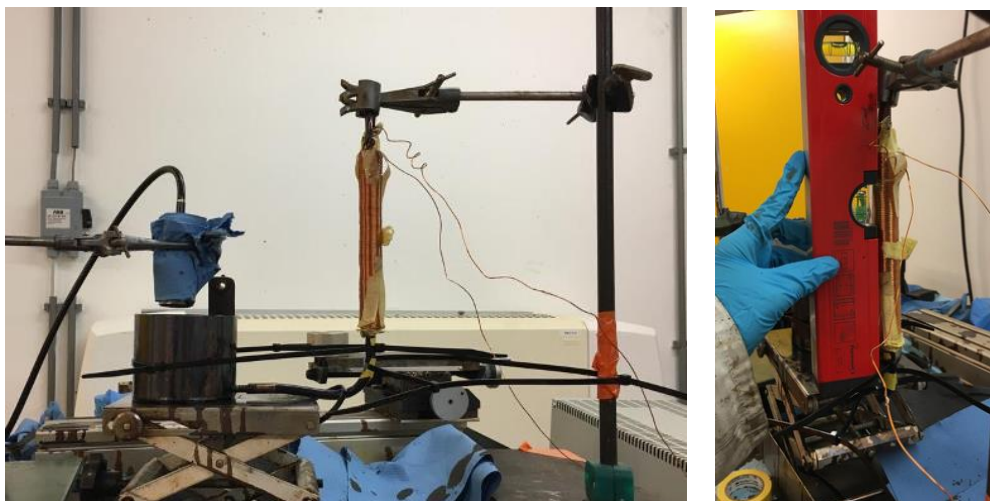


Figure 71: Set-up with the pipe in vertical position. Solenoid 0.8 mm

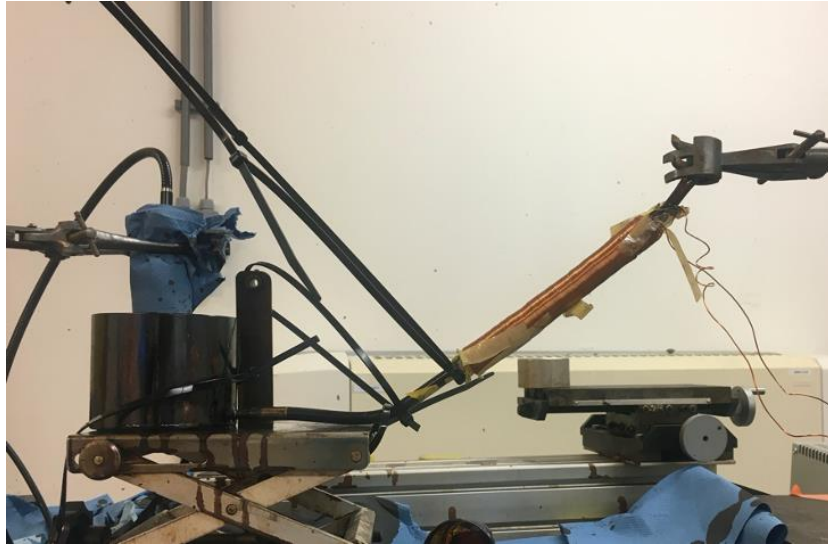


Figure 72: Set-up with the pipe in inclined position. Solenoid 0.8 mm

The selection of the different heights at which the fluid rest in each experiment is the same of that described in the last section, being slightly different for the inclined pipe configuration. As the distances between trials are taken along the pipe, the corresponding height steps do not match with those happening in the reservoir.

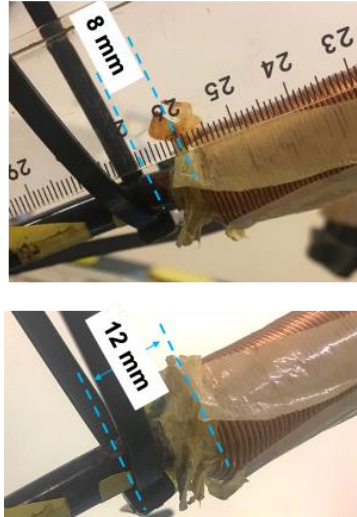


Figure 73: Initial levels of ferrofluid. Pipe in inclined position. Solenoid 0.8 mm

ANNEX III. Magnetic field measurement experiment and construction of the solenoids

This section is dedicated to the building of the coils. Only two first of the three solenoids represented (Figure X and X) are actually used in the experiments.

1. CONSTRUCTION OF THE SOLENOIDS

Figure X depicts how the solenoids were built in a solenoid machine, in order to induce a magnetic field as uniform as possible.



Figure 74: Winding process of the solenoids

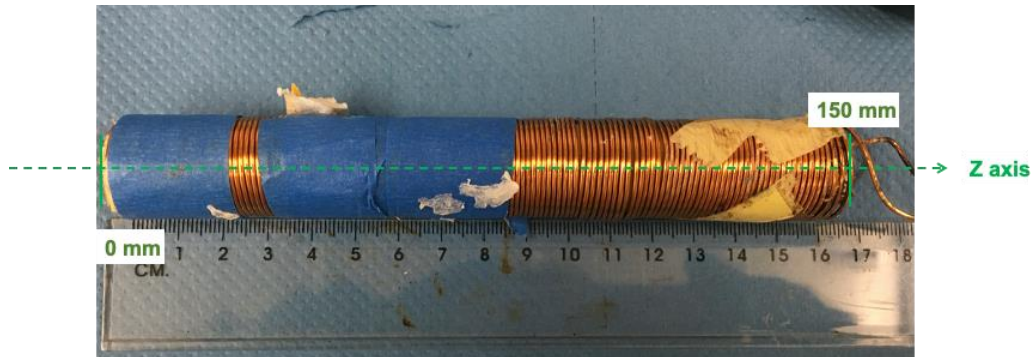


Figure 75: Solenoid 1 mm. 6 layers. 15 cm

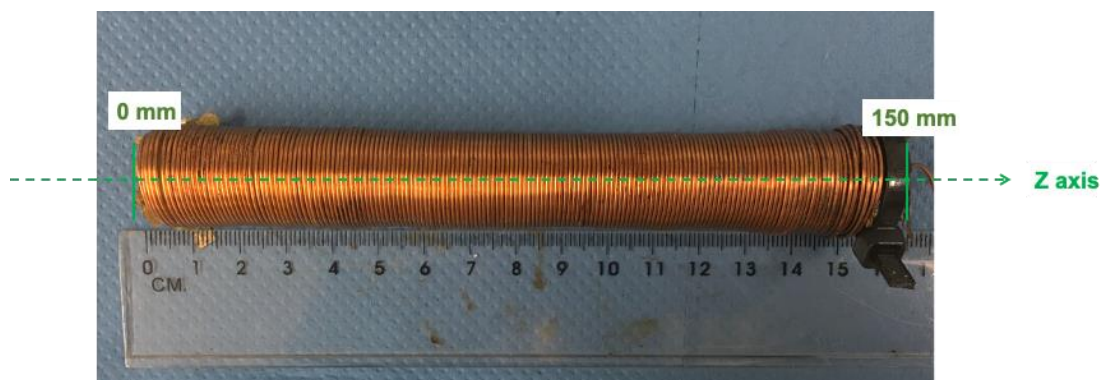


Figure 76: Solenoid 0.8 mm. 6 layers. 15 cm

On the other hand, the coil from Figure 77 is manually wound for the magnetic pump experiments, as it has a higher section.



Figure 77: Solenoid 2 mm. 3 layers. 15 cm

2. MAGNETIC FIELD MEASUREMENT

The magnetic field on axis is measured for the three solenoids. For that, a set-up like the one shown in Figure 78 is built to introduce the axial probe of the teslameter inwards the coil, with the help of a motorized positioning system that is moved in two axes.

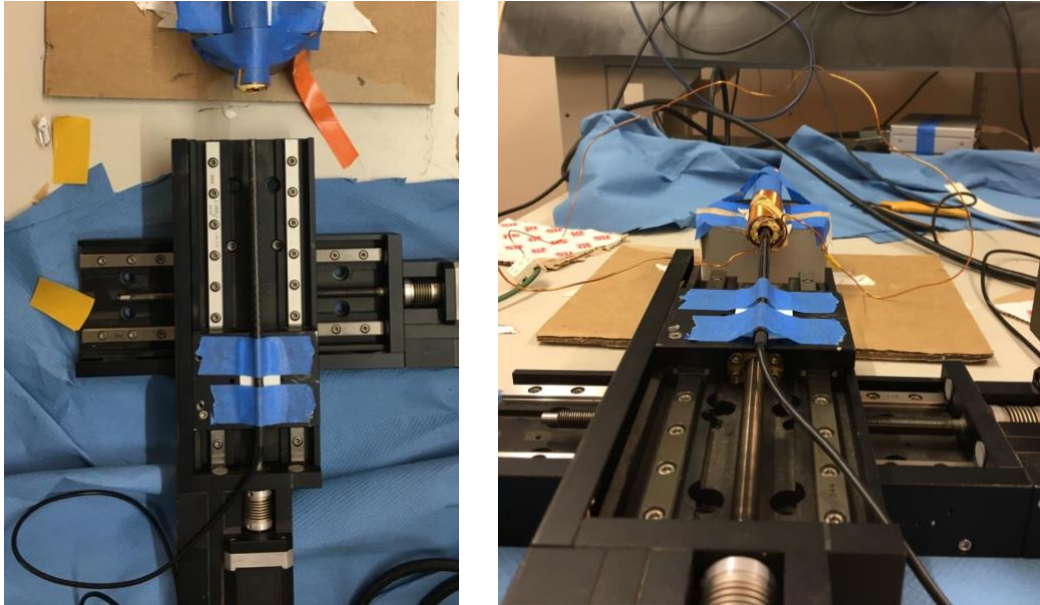


Figure 78: Measuring set-up

ANNEX IV. Experimental results

These following sections present the results obtained from the whole set of trials of the experiments. First one is dedicated to the 1 mm solenoid experiments. Figures from 79 to 83 show the height increase in the pipe at the different levels for the range of currents used. Figure 84 and 85 show those results obtained in the experiment from chapter 9. The second section present the height increase obtained when using the 0.8 mm solenoid, both with the pipe in vertical and inclined position. Lastly, third fourth and fifth sections present the results obtained from the magnetic field measurement for each one of the solenoids.

1. RISING PROCESS – SOLENOID 1 MM.

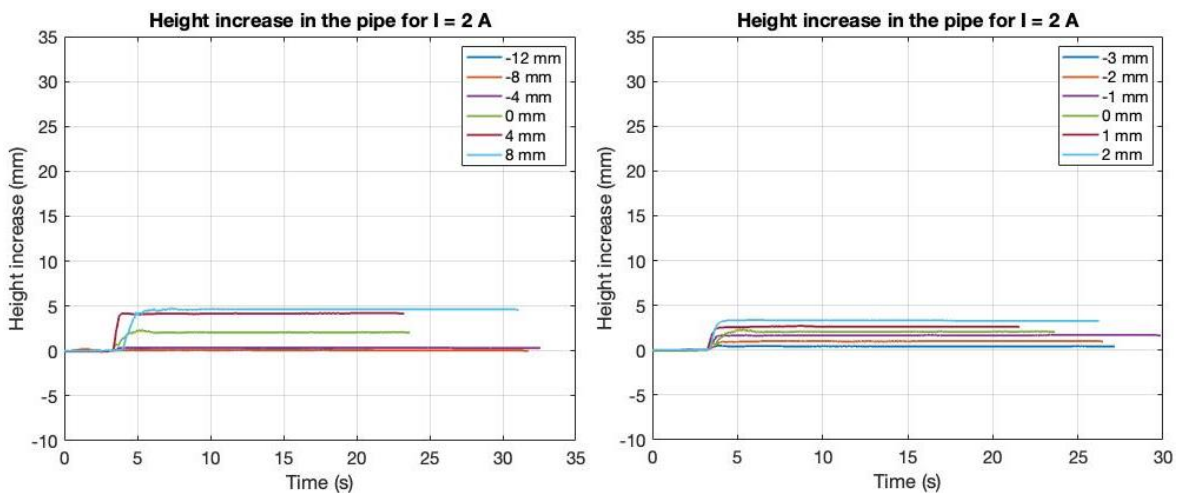


Figure 79: Height increase in the pipe for $I = 2 A$

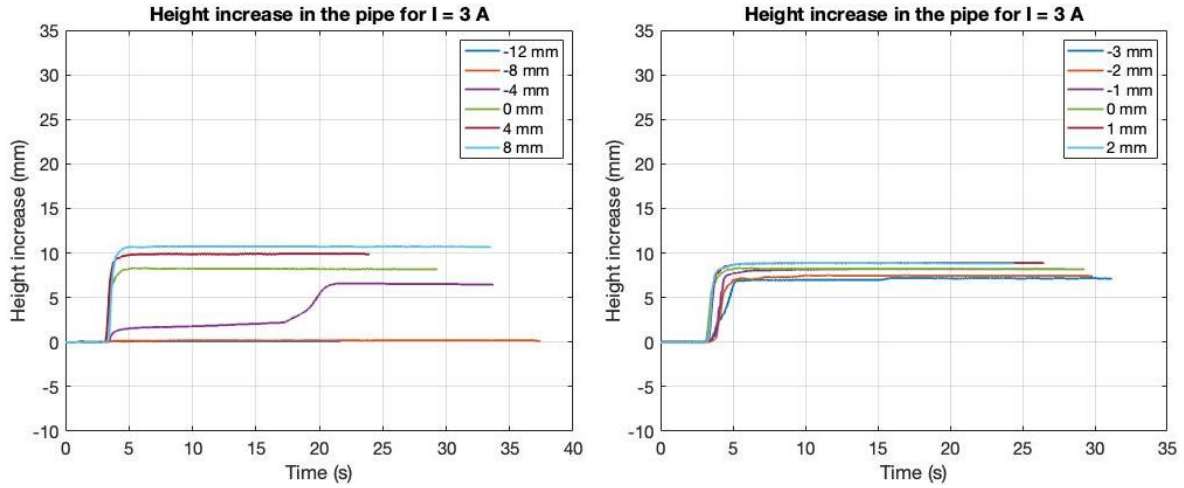


Figure 80: Height increase in the pipe for $I = 3 A$

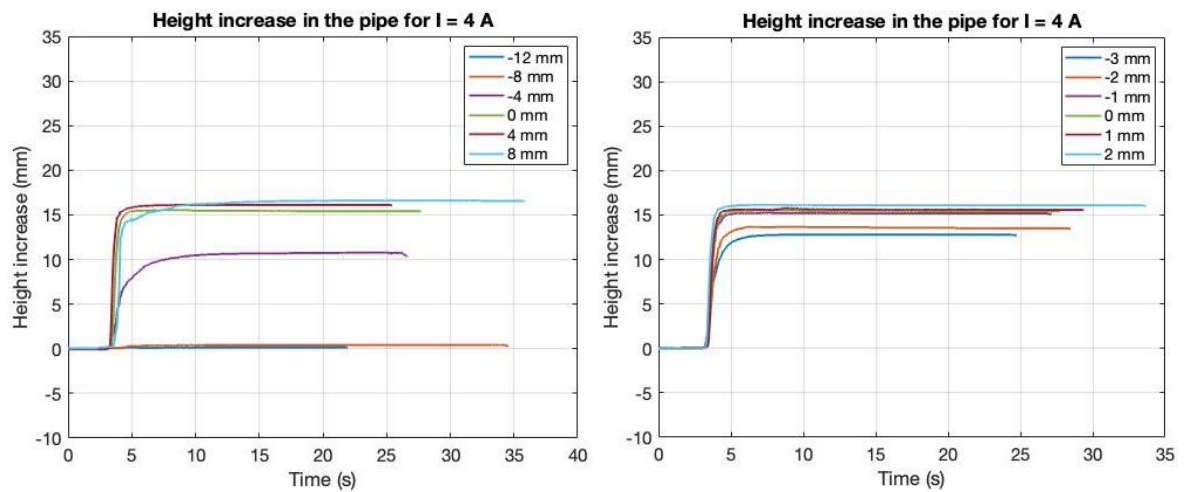


Figure 81: : Height increase in the pipe for $I = 4 A$

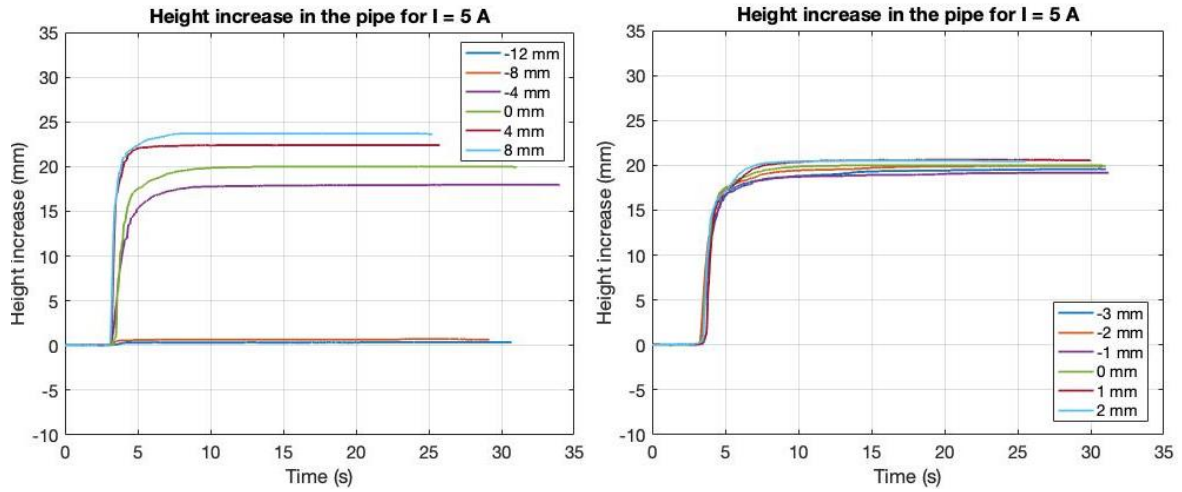


Figure 82: : Height increase in the pipe for I = 5 A

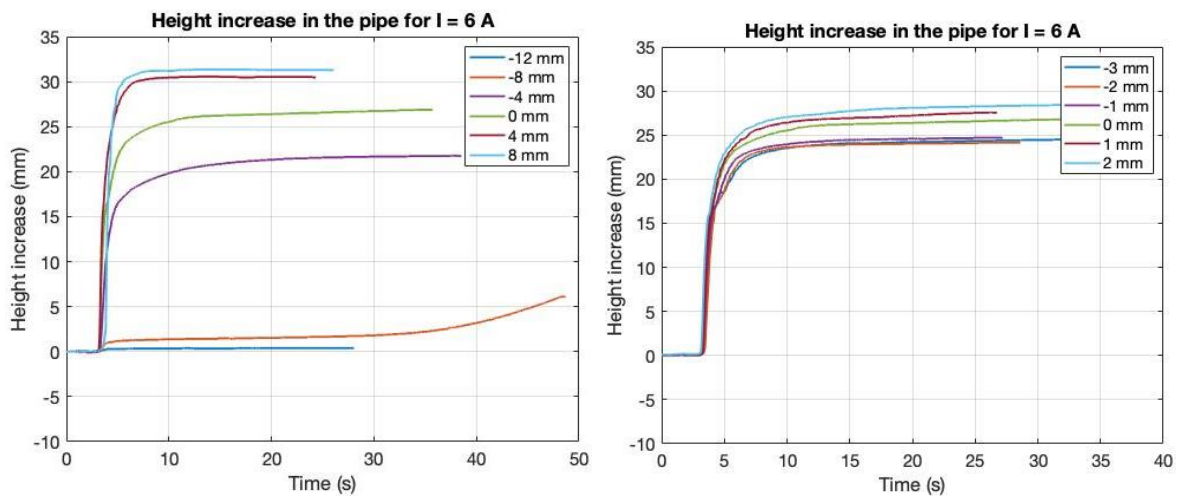


Figure 83: : Height increase in the pipe for I = 6 A

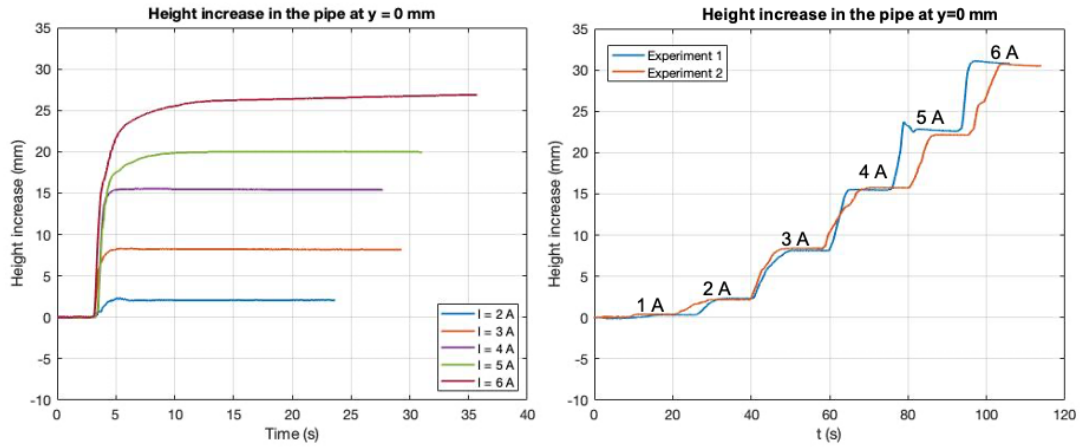


Figure 84: Experiment conducted in Chapter 9. Current input at intervals. The experiment is repeated twice in terms of repeatability

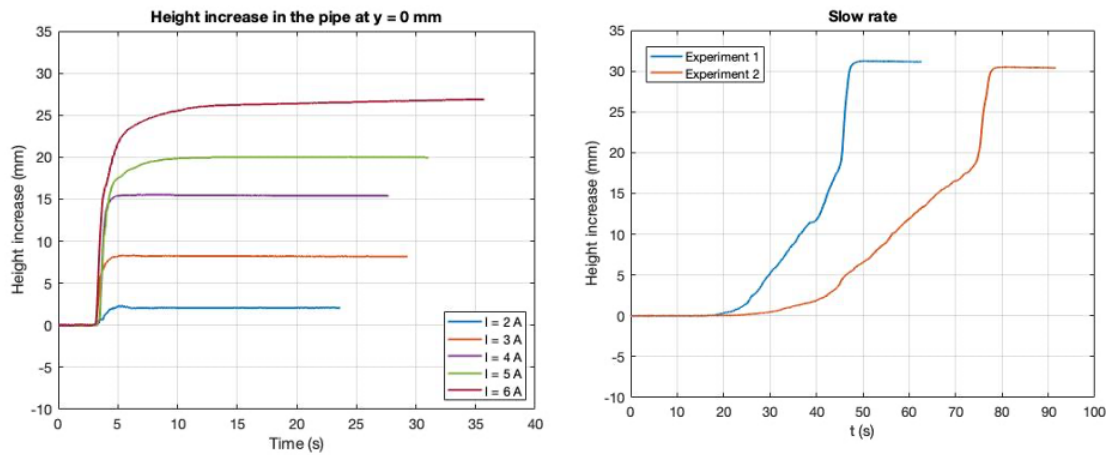


Figure 85: Experiment conducted in Chapter 9. Current input at continuous input. The experiment is repeated twice in terms of repeatability

2. RISING PROCESS – SOLENOID 0.8 MM.

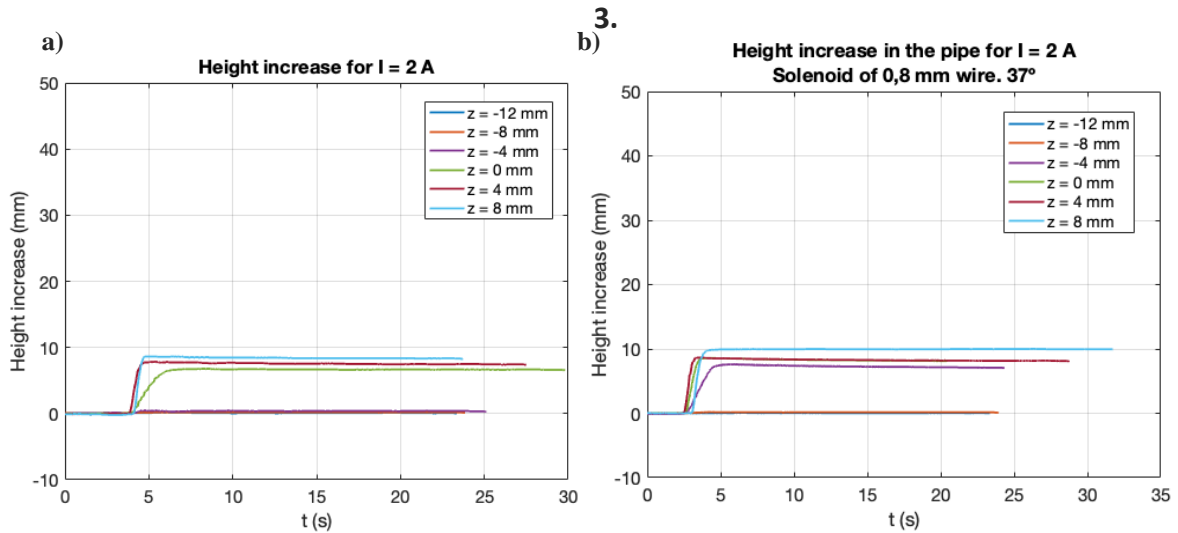


Figure 86: Height increase in the pipe for $I = 2\text{ A}$. a) Pipe in 90° b) Pipe in 37°

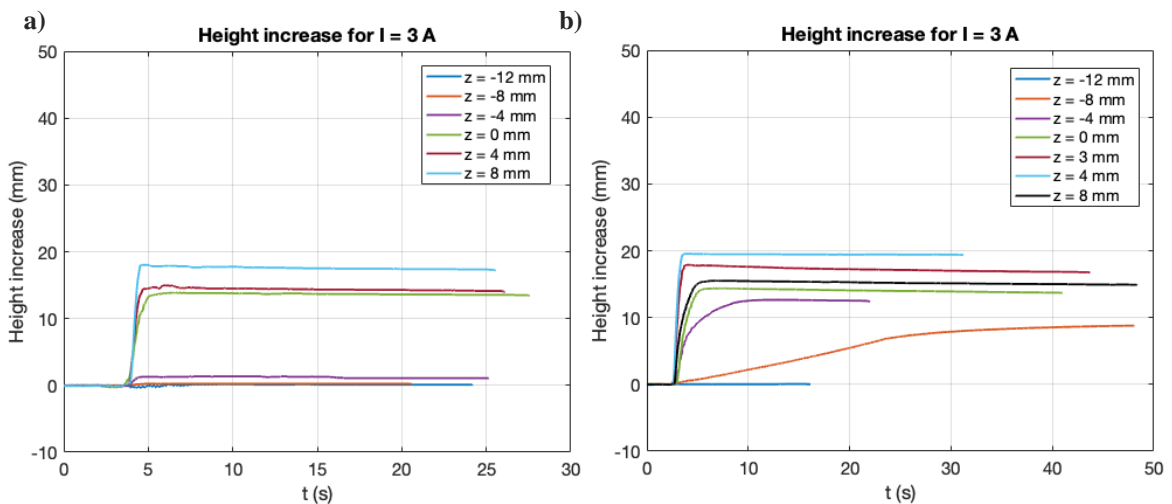


Figure 87: Height increase in the pipe for $I = 3\text{ A}$. a) Pipe in 90° b) Pipe in 37°

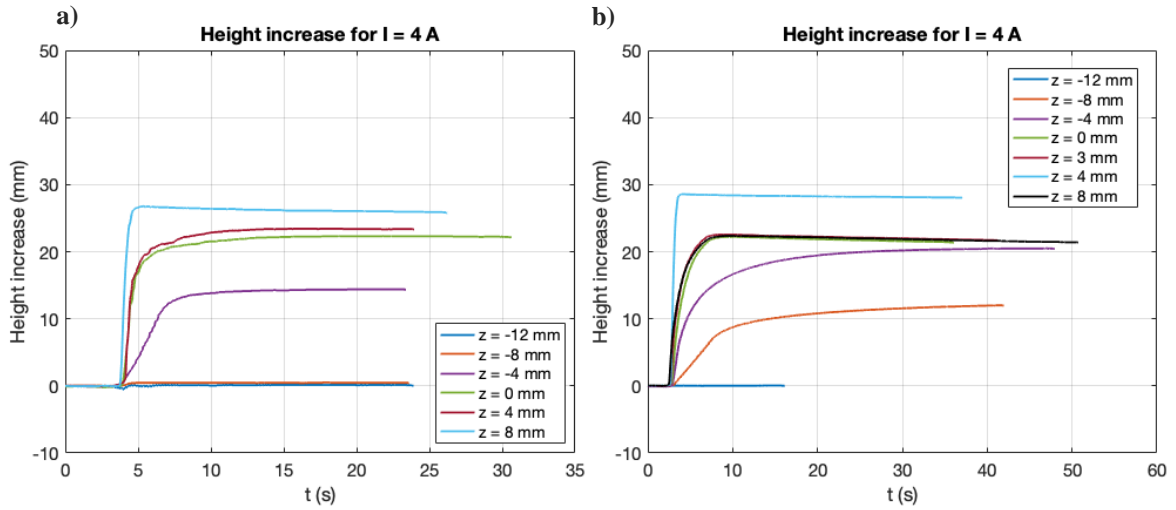


Figure 88: Height increase in the pipe for $I = 4\text{ A}$. a) Pipe in 90° . b) Pipe in 37°

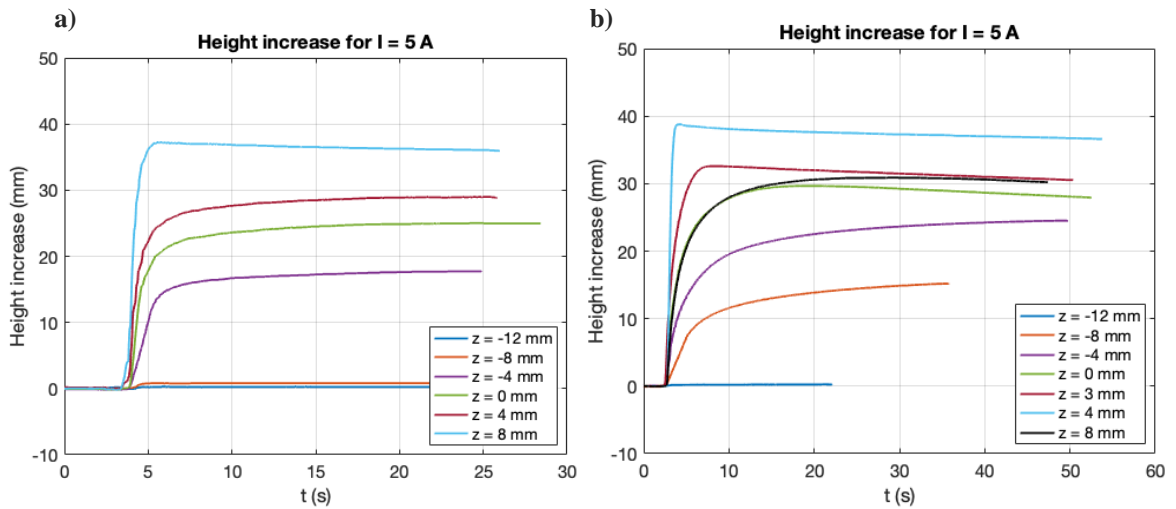


Figure 89: Height increase in the pipe for $I = 5\text{ A}$. a) Pipe in 90° . b) Pipe in 37°

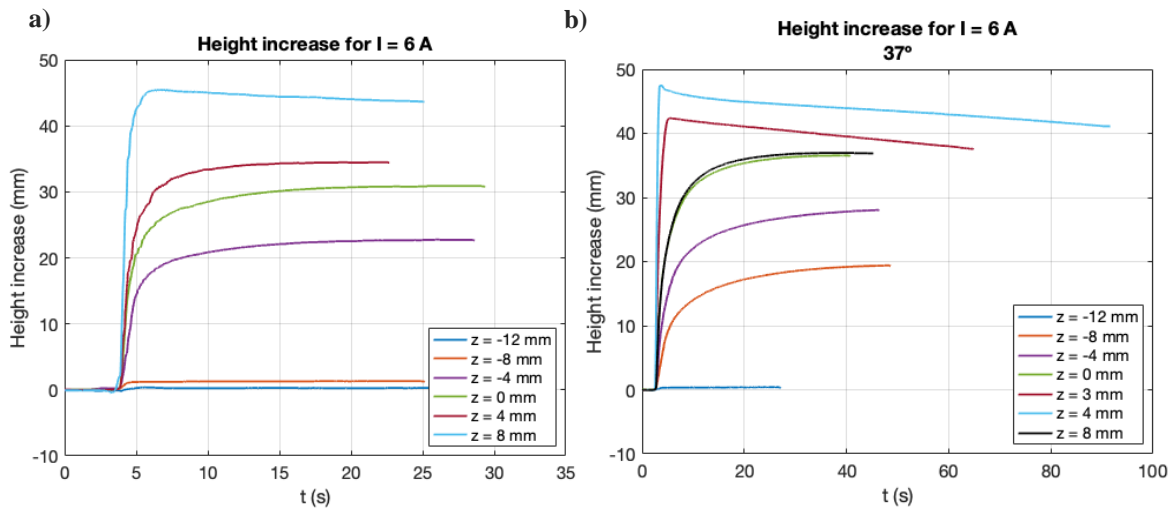


Figure 90: Height increase in the pipe for $I = 6\text{ A}$. a) Pipe in 90° . b) Pipe in 37°

4. MAGNETIC FIELD – SOLENOID 1 MM.

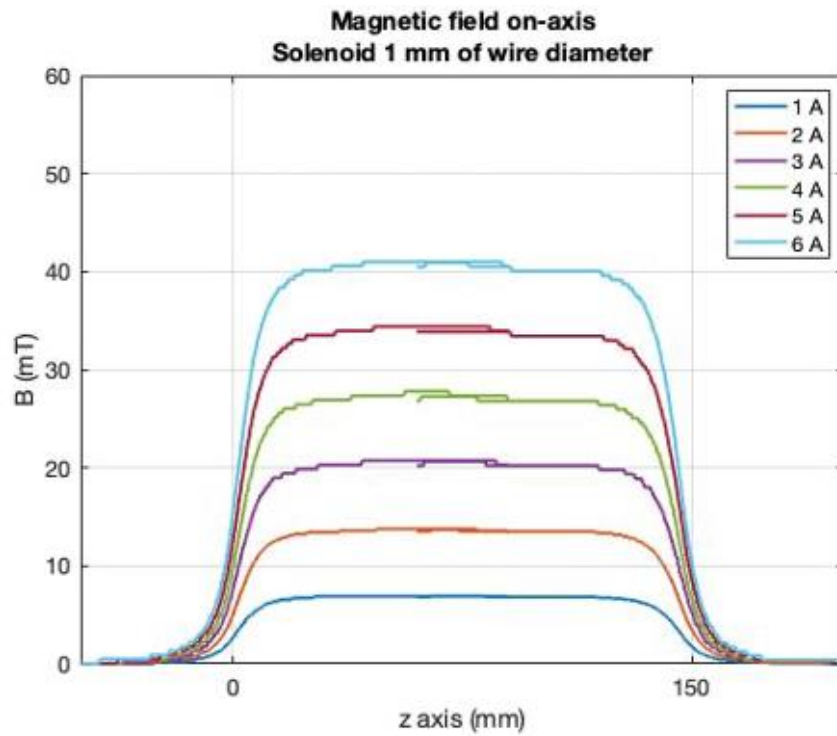


Figure 91: Measured magnetic field on- axis. Solenoid 1 mm

5. MAGNETIC FIELD – SOLENOID 0.8 MM.

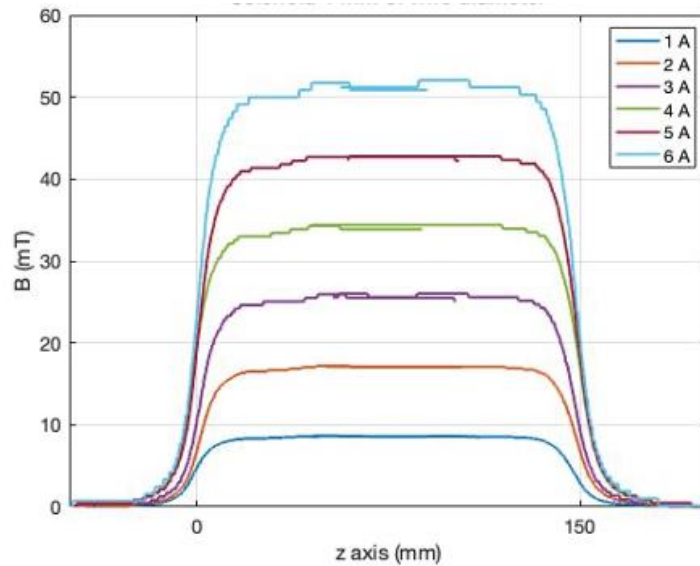


Figure 92: Measured magnetic field on- axis. Solenoid 0.8 mm

6. MAGNETIC FIELD – SOLENOID 2 MM.

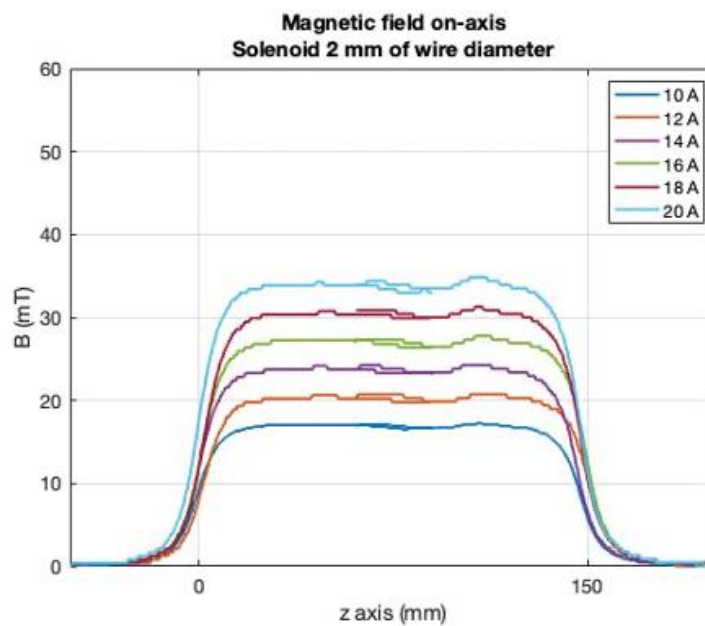


Figure 93: Measured magnetic field on- axis. Solenoid 2 mm

ANNEX V. Error treatment

It is assumed a certain error for the results presented. The following section has been included in order to quantify it for the different experiments realized. The uncertainty of results comes, on one hand, from the precision of the measuring instrumentation employed, which is a provided value and can be easily quantified. On the other, there is the human error assumed while taking the measurements. The uncertainty associated to them is to be estimated.

When a certain value is obtained from other measurements, the total interval of error is calculated in function of the influence – weight – that each measurement has on the final value. Thus, given a magnitude X dependant on U_i variables:

$$\alpha(X) = \sum^i \left| \frac{\partial X}{\partial U_i} \right| \alpha(U_i)$$

where X is the dependent magnitude, U_i the measurements on which X depends and $\alpha(X)$ and $\alpha(U_i)$ the maximum error associated. This way, the expression assume that all the measurements can have their maximum error at the same time. It is applied on the obtention of the height increase in the pipe and the magnetic field, which are expressed in function of different measures. In the case of magnitudes which has been directly measured, the precision of the measuring device used is taken. The human error, on the other hand, is assigned when it comes to reading of measurements – i.e. reading from a calliper. Others, however, are owed to inaccuracies in the experimental set-up. The latter, in fact, has had a significant influence in some of the experiments, where the position of the experiment was not fully perpendicular to the liquid surface and higher distances were measured.

1. RISING PROCESS – SOLENOID 1 MM.

The height increase in the pipe is obtained from the following expression – see chapter 4.

$$\Delta h \text{ [mm]} = \Delta h_B \text{ [mm]} \frac{S_B \text{ [mm}^2\text{]}}{S_A \text{ [mm}^2\text{]}} \sin \theta \text{ [}^\circ\text{]}$$

where Δh_B is the displacement recorded by the confocal sensor, θ is the inclination of the rising pipe – with respect to the horizontal plane – and S_B and S_A are the sections of the reservoir and the pipe respectively. The maximum error is calculated according to the relative weight that each one of the factors have in the result.

$$\alpha(\Delta h) = \left| \frac{\partial \Delta h}{\partial \Delta h_B} \right| \alpha(\Delta h_B) + \left| \frac{\partial \Delta h}{\partial d_B} \right| \alpha(d_B) + \left| \frac{\partial \Delta h}{\partial \theta} \right| \alpha(\theta)$$

where the maximum error considered for each one is given in ANNEX I.

The results for which the range of error is calculated belong to the experiment conducted in chapter 6, as they are considered the most reliable ones in a quantitatively way.

z [mm]	I = 2 A			I = 3 A			I = 4 A		
	Δh [mm]	$\pm \varepsilon(\Delta h)$ [%]	$\pm \alpha(\Delta h)$ [mm]	Δh [mm]	$\pm \varepsilon(\Delta h)$ [%]	$\pm \alpha(\Delta h)$ [mm]	Δh [mm]	$\pm \varepsilon(\Delta h)$ [%]	$\pm \alpha(\Delta h)$ [mm]
-12	0,0401	4,73E+02	0,1895	0,1003	1,90E+02	0,1909	0,1606	1,20E+02	0,1922
-8	0,0401	4,73E+02	0,1895	0,1606	1,20E+02	0,1922	0,3612	5,45E+01	0,1967
-4	0,3613	5,44E+01	0,1967	6,5828	5,09E+00	0,3351	10,6970	3,99E+00	0,4266
-3	0,4616	4,31E+01	0,1989	7,2451	4,83E+00	0,3498	12,8444	3,69E+00	0,4743
-2	1,0235	2,07E+01	0,2114	7,3856	4,78E+00	0,3529	13,6071	3,61E+00	0,4913
-1	1,6056	1,40E+01	0,2244	8,1683	4,53E+00	0,3703	15,1725	3,47E+00	0,5261
0	2,1073	1,12E+01	0,2355	8,2686	4,51E+00	0,3725	15,4133	3,45E+00	0,5314
1	2,5689	9,57E+00	0,2458	8,8306	4,36E+00	0,3850	15,5137	3,44E+00	0,5337
2	3,2914	7,96E+00	0,2619	8,8908	4,35E+00	0,3864	16,1358	3,39E+00	0,5475
4	4,2146	6,70E+00	0,2824	9,8140	4,15E+00	0,4069	16,1158	3,39E+00	0,5471
8	4,6360	6,29E+00	0,2918	10,6368	4,00E+00	0,4252	16,4971	3,37E+00	0,5555

Distance to coil [mm]	$I = 5 A$			$I = 6 A$		
	Δh [mm]	$\pm \varepsilon(\Delta h)$ [%]	$\pm \alpha(\Delta h)$ [mm]	Δh [mm]	$\pm \varepsilon(\Delta h)$ [%]	$\pm \alpha(\Delta h)$ [mm]
-12	0,3010	6,49E+01	0,1953	0,4014	4,92E+01	0,1976
-8	0,6824	2,99E+01	0,2038	5,9205	5,41E+00	0,3203
-4	17,8417	3,28E+00	0,5854	21,6951	3,09E+00	0,6711
-3	19,4674	3,19E+00	0,6216	24,3442	3,00E+00	0,7301
-2	19,8286	3,18E+00	0,6296	24,0031	3,01E+00	0,7225
-1	19,0058	3,22E+00	0,6113	24,7055	2,99E+00	0,7381
0	19,9892	3,17E+00	0,6332	26,7526	2,93E+00	0,7836
1	20,4909	3,14E+00	0,6444	27,3948	2,91E+00	0,7979
2	20,5110	3,14E+00	0,6448	28,0972	2,90E+00	0,8135
4	22,3574	3,07E+00	0,6859	30,5256	2,84E+00	0,8675
8	23,6819	3,02E+00	0,7153	31,2481	2,83E+00	0,8836

2. MAGNETIC FIELD.

The magnetic field induced in the coil on the axis is measured making use of a Teslameter – measuring device which measures the magnetic field induction in a non-magnetic medium as the air – and an oscilloscope. The probe of the device is placed on a motorized positioning system which is moved along the axis from a certain distance, recording the field.

As different measuring devices are involved in the obtention of the magnetic field, the precision is calculated as:

$$\varepsilon(B) = \varepsilon_{Oscilloscope} + \varepsilon_{Teslameter} + \varepsilon_{DC Power Supply}$$

where ε represents the percentage of error assumed from each measurement:

1.1. Solenoid 1 mm

<i>Solenoid: 1 mm of wire diameter, 6 layers</i>						
<i>I [A]</i>	$\pm \epsilon_{DC\ Power\ Supply} [\%]$	$\pm \epsilon_{Oscilloscope} [\%]$	$\pm \epsilon_{Teslameter} [\%]$	<i>*B [mT]</i>	$\pm \epsilon(B) [\%]$	$\pm \alpha(B)$
1	1,50	1,16	3,40	6,90	6,05	0,42
2	1,00	1,01	1,95	13,77	3,97	0,55
3	0,83	1,54	1,46	20,75	3,84	0,80
4	0,75	1,15	1,22	27,80	3,12	0,87
5	0,70	0,93	1,08	34,40	2,71	0,93
6	0,67	0,78	0,99	41,01	2,43	1,00

1.2. Solenoid 0.8 mm

<i>Solenoid: 0.8 mm of wire diameter, 6 layers</i>						
<i>I [A]</i>	$\pm \epsilon_{DC\ Power\ Supply} [\%]$	$\pm \epsilon_{Oscilloscope} [\%]$	$\pm \epsilon_{Teslameter} [\%]$	<i>*B [mT]</i>	$\pm \epsilon(B) [\%]$	$\pm \alpha(B)$
1	1,50	0,93	2,82	8,61	5,25	0,45
2	1,00	0,82	1,67	17,04	3,49	0,60
3	0,83	1,25	1,28	25,50	3,37	0,86
4	0,75	0,94	1,09	33,88	2,78	0,94
5	0,70	0,75	0,97	42,68	2,42	1,03
6	0,67	1,19	0,89	51,84	2,74	1,42

1.3. Solenoid 2 mm

<i>Solenoid: 2 mm of wire diameter, 3 layers</i>						
<i>I [A]</i>	$\pm \epsilon_{DC\ Power\ Supply} [\%]$	$\pm \epsilon_{Oscilloscope} [\%]$	$\pm \epsilon_{Teslameter} [\%]$	<i>*B [mT]</i>	$\pm \epsilon(B) [\%]$	$\pm \alpha(B)$
10	0,60	0,82	1,67	17,04	3,09	0,53
12	0,58	1,61	1,51	19,78	3,71	0,73
14	0,57	1,34	1,34	23,75	3,26	0,77
16	0,56	1,17	1,23	27,27	2,97	0,81
18	0,56	1,07	1,17	29,91	2,79	0,83
20	0,55	0,94	1,09	33,88	2,58	0,87

*B refers to the constant value in the centre of the solenoid

ANNEX VI.

17.3.35

$$E(m) = [1 + a_1 m_1 + a_2 m_1^2] + [b_1 m_1 + b_2 m_1^2] \ln(1/m_1) + \epsilon(m)$$

$$|\epsilon(m)| < 4 \times 10^{-5}$$

$a_1 = .46301\ 51$	$b_1 = .24527\ 27$
$a_2 = .10778\ 12$	$b_2 = .04124\ 96$

17.3.36

$$E(m) = [1 + a_1 m_1 + \dots + a_4 m_1^4] + [b_1 m_1 + \dots + b_4 m_1^4] \ln(1/m_1) + \epsilon(m)$$

$$|\epsilon(m)| < 2 \times 10^{-8}$$

$a_1 = .44325\ 141463$	$b_1 = .24998\ 368310$
$a_2 = .06260\ 601220$	$b_2 = .09200\ 180037$
$a_3 = .04757\ 383546$	$b_3 = .04069\ 697526$
$a_4 = .01736\ 506451$	$b_4 = .00526\ 449639$

Figure 94: Expression for $E(k)$ by polynomial approximation

17.3.33

$$K(m) = [a_0 + a_1 m_1 + a_2 m_1^2] + [b_0 + b_1 m_1 + b_2 m_1^2] \ln(1/m_1) + \epsilon(m)$$

$$|\epsilon(m)| \leq 3 \times 10^{-5}$$

$a_0 = 1.38629\ 44$	$b_0 = .5$
$a_1 = .11197\ 23$	$b_1 = .12134\ 78$
$a_2 = .07252\ 96$	$b_2 = .02887\ 29$

17.3.34

$$K(m) = [a_0 + a_1 m_1 + \dots + a_4 m_1^4] + [b_0 + b_1 m_1 + \dots + b_4 m_1^4] \ln(1/m_1) + \epsilon(m)$$

$$|\epsilon(m)| \leq 2 \times 10^{-8}$$

$a_0 = 1.38629\ 436112$	$b_0 = .5$
$a_1 = .09666\ 344259$	$b_1 = .12498\ 593597$
$a_2 = .03590\ 092383$	$b_2 = .06880\ 248576$
$a_3 = .03742\ 563713$	$b_3 = .03328\ 355346$
$a_4 = .01451\ 196212$	$b_4 = .00441\ 787012$

Figure 95: Expression for $K(k)$ by polynomial approximation